A PRELIMINARY SIZING TOOL FOR MINIMUM WEIGHT AIRCRAFT WINGBOX STRUCTURAL DESIGN

A THESIS SUBMITTED TO
THE GRADUATE SCHOOL OF NATURAL AND APPLIED SCIENCES
OF
MIDDLE EAST TECHNICAL UNIVERSITY

BY

MESUT MERT

IN PARTIAL FULFILLMENT OF THE REQUIREMENTS
FOR
THE DEGREE OF MASTER OF SCIENCE
IN
AEROSPACE ENGINEERING

SEPTEMBER 2018

Approval of the thesis:

A PRELIMINARY SIZING TOOL FOR MINIMUM WEIGHT AIRCRAFT WINGBOX STRUCTURAL DESIGN

submitted by **MESUT MERT** in partial fulfillment of the requirements for the degree of **Master of Science in Aerospace Engineering Department, Middle East Technical University** by,

Prof. Dr. Halil Kalıpçılar _____
Dean, Graduate School of **Natural and Applied Sciences**

Prof. Dr. Ozan Tekinalp _____
Head of Department, **Aerospace Engineering**

Prof. Dr. Altan Kayran _____
Supervisor, **Aerospace Engineering Dept., METU**

Examining Committee Members:

Assoc. Prof. Dr. Demirkan Çöker _____
Aerospace Engineering Dept., METU

Prof. Dr. Altan Kayran _____
Aerospace Engineering Dept., METU

Assoc. Prof. Dr. Ercan Gürses _____
Aerospace Engineering Dept., METU

Asst. Prof. Dr. Tuncay Yalçınkaya _____
Aerospace Engineering Dept., METU

Prof. Dr. Erdem Acar _____
Mechanical Engineering Dept., TOBB
University of Economics and Technology

Date**:** 07/09/2018

I hereby declare that all information in this document has been obtained and presented in accordance with academic rules and ethical conduct. I also declare that, as required by these rules and conduct, I have fully cited and referenced all material and results that are not original to this work.

Name, Last name : Mesut Mert

Signature :

ABSTRACT

A PRELIMINARY SIZING TOOL FOR MINIMUM WEIGHT AIRCRAFT WINGBOX STRUCTURAL DESIGN

Mert, Mesut

M.Sc, Department of Aerospace Engineering

Supervisor: Prof. Dr. Altan Kayran

September 2018, 211 Pages

This thesis presents a preliminary structural sizing tool for the design of aircraft wingbox structures. The primary goal is to obtain the least possible structural weight for a metallic wingbox by using the thin walled multi-cell box beam methods in the literature as part of an iterative process. An automatized tool based on simple and quick approximate methods is created to take advantage in the preliminary stages of design when several possible structural alternatives are being investigated.

Airfoil data, material properties, wing geometry and layout (chord, span, taper, spar locations, stringer locations, rib locations, etc.) are the user inputs for the generated tool. Internal loads are then obtained by integrating the external loads along the wing span. Corresponding failure criteria of the structural elements are checked to have a marginal structural sizing for light-weight design.

Different internal load distribution methods are used for the subsonic and the supersonic air vehicles. For subsonic wings, internal load redistribution after skin local buckling is also covered. A new method, offering consecutive application of linear static finite element analysis to approximate the post-buckling load redistribution, is introduced within this thesis. The offered method is validated by a comparison with nonlinear finite element analysis.

Keywords: Preliminary Structural Sizing, Wingbox Design, Post-buckling Load Redistribution, Finite Element Method

ÖZ

MİNİMUM AĞIRLIKLI UÇAK KANAT KUTUSU YAPISAL TASARIMI İÇİN BİR ÖN BOYUTLANDIRMA ARACI

Mert, Mesut

Yüksek Lisans, Havacılık ve Uzay Mühendisliği Bölümü

Tez Yöneticisi: Prof. Dr. Altan Kayran

Eylül 2018, 211 Sayfa

Bu tez, uçak kanat kutusu yapıları için bir ön boyutlandırma aracı sunmaktadır. Ana amaç, metalik bir kanat kutusu için literatürdeki ince cidarlı yapı metotlarını tekrarlı olarak kullanarak mümkün olan en düşük ağırlığı elde etmektir. Olası birçok yapısal alternatifin araştırıldığı ön boyutlandırma sürecinde kullanılabilecek; sade ve hızlı metotlara dayanan bir araç geliştirilmiştir.

Kanat profili, malzeme özellikleri, geometrik özellikler ve yerleşim (kanat kordu, kanat açıklığı, koniklik, kiriş ve kaburga konumları vs.) geliştirilen araç için kullanıcı tarafından girilmektedir. Daha sonra harici yükler kullanılarak kanat boyunca iç yük hesabı yapılmaktadır. Hafif bir tasarım için yapısal elemanlar, ilgili göçme kıstasları ile kontrol edilmektedir.

İç yük dağılımları ses altı ve ses üstü araçlar için ayrı yöntemlerle elde edilmektedir. Ses altı kanatlar için kabuk lokal burkulması sonrası iç yükün yeniden dağılımı da bu çalışmada ele alınmıştır. Doğrusal sonlu eleman analizinin tekrarlı olarak kullanılmasıyla, burkulma sonrası iç yük dağılımını elde etmeyi amaçlayan yeni bir yöntem bu tez kapsamında sunulmaktadır. Sunulan yeni yöntem, doğrusal olmayan sonlu eleman analizleriyle karşılaştırma yapılarak doğrulanmaktadır.

Anahtar Kelimeler: Ön Yapısal Boyutlandırma, Kanat Kutusu Tasarımı, Burkulma Sonrası Yükün Yeniden Dağılımı, Sonlu Elemanlar Metodu

To the Year 2013

ACKNOWLEDGEMENTS

First and foremost, I would like to express my deepest gratitude to my supervisor Prof. Dr. Altan Kayran for his guidance, support, and patience. I also thank to the jury members Assoc. Prof. Dr. Demirkan Çöker, Assoc. Prof. Dr. Ercan Gürses, Asst. Prof. Dr. Tuncay Yalçınkaya, and Prof. Dr. Erdem Acar for their constructive criticism and suggestions.

I owe many thanks to Ali Can Arık for his wisdom and friendship. This thesis would not have been completed without his contribution.

I am indebted to Burak Ay of Turkish Aerospace Industries for his support and understanding throughout both this work and my entire engineering career. I would also like to thank Barış Gider, İnanç Gürbüz, Tuğba Öztürk, Ozan Adıgüzel, Osman Aksöz, Naz Tuğçe Öveç, and Sogand Yousefbeigi for their support.

I am grateful to Burcu Şayin for the inspiring conversations over this thesis. She always helped by asking the right questions.

I owe also a great deal to my family for their unconditional love and infinite support.

Finally, my greatest thanks go to my dearest comrade and beloved fiancée Meltem Al for the years we stood together to create, grow, and preserve our flame.

TABLE OF CONTENTS

LIST OF TABLES

TABLES

LIST OF FIGURES

FIGURES

LIST OF ABBREVIATIONS

CHAPTER 1:

MDO	Multi-disciplinary Optimization
CAD	Computer Aided Design
FEM	Finite Element Method
CG	Center of Gravity
OML	Outer Mold Line
FEA	Finite Element Analysis
BDF	Bulk Data File (NASTRAN Input File)
PCL	PATRAN Command Language

CHAPTER 2:

ESDU	Engineering Sciences Data Unit
A	Aspect ratio
a_1	lift curve slope [rad^{-1}]
C_L	lift coefficient
C_{LL}	local lift coefficient
C_{Lspr}	lift coefficients specified in input
C_m	pitching moment coefficient about wing apex, based on $\bar{c}$

C_{mL} local pitch moment coefficient about local quarter-chord point, based on c, positive leading edge up

c local chord [m]

$\bar{c}$ geometric mean chord [m]

c_0 root chord [m]

c_i chord at crank [m]

c_{Ms1} chord at first outboard collocation station [m]

c_t tip chord [m]

Λ_n sweep of nth-chord line of straight-tapered planform [deg]

Λ_0 leading edge sweep of straight-tapered planform [deg]

CHAPTER 3:

V Vertical Shear Load

q Shear Flow

Q First Moment of Area

A Cross sectional flange area

a Long dimension of plate

b Short dimension of plate (loaded edge)

E Elasticity modulus

k_c Compressive buckling coefficient

k_s Shear buckling coefficient

k_b	Bending buckling coefficient
σ_c	Compressive stress
σ_{cr}	Compressive buckling strength
σ_b	Bending stress
$\sigma_{b.cr}$	Buckling stress under bending
σ_{st}	Axial stress in stiffener
t	Design skin panel thickness
τ	Shear stress
τ_{cr}	Shear buckling strength
v	Poisson's ratio
F_{cy}	Compression yield strength
F_{tu}	Tensile ultimate strength
F_{ty}	Tensile yield strength
UF	Ultimate factor

CHAPTER 4:

NACA	National Advisory Committee for Aeronautics

CHAPTER 5:

A	Cross sectional flange area
a	Long dimension of plate

b	Short dimension of plate (loaded edge)
E	Elasticity modulus
k_c	Compressive buckling coefficient
k_s	Shear buckling coefficient
σ_c	Compressive stress
σ_{cr}	Compressive buckling strength
σ_{st}	Axial stress in stiffener
t	Design skin panel thickness
t_{eq}	Equivalent skin panel thickness
τ	Shear stress
τ_{cr}	Shear buckling strength
v	Poisson's ratio
w	Effective width of the buckled panel

CHAPTER 1

INTRODUCTION

1.1 Motivation of the Thesis

Preliminary design methods of airframe structures have always been explored within the scope of development programs. Although the word “preliminary” sounds uncomplicated, the work can be very tough and complex when various disciplines collaborate to create something from scratch. Early design phases are always hard to process because engineers have no mature design criteria and constraints in hand. Even customer requirements can be uncertain in the beginning of the design process. Sobieszczanski-Sobieski [1] built a typical design paradox, which clearly shows the trouble engineers have for new designs. Up to mid-preliminary level, knowledge about design does not increase significantly, as illustrated in Figure 1-1.

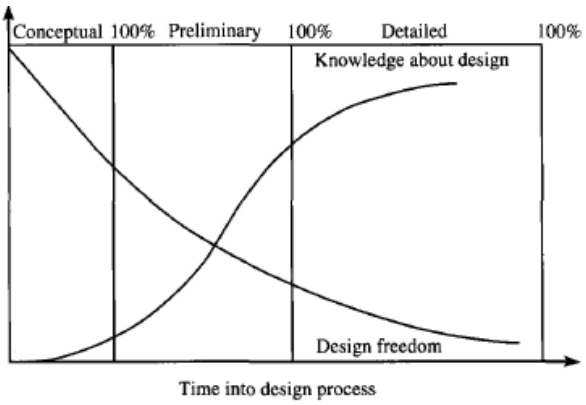

Figure 1-1 Design Paradox of Typical Products [1]

Another important remark is the huge freedom to design with a very small amount of knowledge. This freedom creates the need for a very careful consideration of all disciplines. Therefore, all engineering groups have to make certain assumptions and these assumptions should be aligned with each other.

To maintain the harmony between different disciplines, major aerospace companies have in-house multi-disciplinary tools and methods and they spend extensive time and workforce for their conceptual and preliminary design environments. Depending on the scope and extent of their design environment, companies can prefer to keep their preliminary approach until the detail design starts.

One example for in-house structural sizing software is the ECLIPSE code developed within BAE Systems and used to size Eurofighter Typhoon [2]. Etheridge [2] defines the principle of this tool as using finite element results for the determination of cross-sectional properties to have minimum structural mass while satisfying the design criteria. Finite element model is repeatedly updated until convergence is reached. ECLIPSE utilizes NASTRAN for strength and stability checks. It also has the capability to size for aeroelasticity and deflection.

Another example is the application of multi-disciplinary optimization (MDO) to structural design for a future project called N+2, which is funded by NASA. Chen et al. [3] describes the complete process starting with the outer geometry, continuing with the structural and aero meshing, making use of trim analysis and obtains a load distribution, and finally running an optimizer to achieve minimum weight. Details of ECLIPSE and N+2 environments, as well as many other applications, are further explained in the literature survey section of this thesis. In this stage, there is enough evidence to state that a typical preliminary structural design workflow consists of:

- the usage of the external geometry as an input,
- preliminary structural layout generation, in which main structural members are located into the vehicle with an experience-based approach,

- finite element mesh generation,
- utilization of preliminary loading conditions,
- finite element analysis to solve for internal loads,
- sizing of structural elements,
- iterations to converge the design

It should be noted these are very simplified general expressions common in many preliminary design approaches. To be more precise, the main idea is to start in a CAD environment, then use a finite element pre-processor, a finite element solver, and an optimizer. In addition, this multi-step approach requires failure analyses to be integrated to the commercial software, which is achieved by coding in the available failure methods.

It is clear that a multi-disciplinary approach to preliminary design is very expensive in terms of both labor and software usage. This is normal when the scope and capability of advanced MDO processes are considered. The motivation of this study is to offer a simpler preliminary structural sizing method and tool for the design of aircraft wingbox structures. The main idea is not to replace the advanced and comprehensive MDO environments. This study offers a much faster approach, which obtains the least possible structural weight for a metallic wing box by using thin walled multi-cell box beam methods. The tool is based on simple and approximate methods, which can be very useful in the very early stages of aircraft development programs when several structural layout alternatives are investigated.

This study, as well as most other studies in the literature, deals with the wing design because it is the most important activity in aircraft development. An advantage with the wing structures is the freedom to define the number and locations of structural elements. Fuselage structural layouts, in contrast, are generally constrained by the aircraft systems. For instance, when the engines, landing gears, weapon bays, cockpit and firewalls are located into the fuselage, number and location of the fuselage

frames are almost complete. Airfoil structures (wings and tails) consist of fewer systems, which results in a domain which the engineers can use to their advantage to have lighter structures.

1.2 Scope of the Thesis

The objective of this thesis is to develop a preliminary sizing tool to carry out the initial sizing of the primary structure of a cantilever aircraft wing with known outer geometry. Preliminary sizing tool works on a specified layout of structural elements. In other words, locations of spars, stringers, and ribs are assumed determined beforehand. Specified layout may either be a result of an early structural optimization process or some design limitations due to manufacturing, installation of landing gears, placement of fuel tanks, etc. Most of the time, structural layout generation is based on previous experiences and competitors. Layout optimization is not preferred because there would not be so many feasible layout candidates in a real-life application. It is faster and cheaper to choose from a few educated guesses with the help of a sizing tool.

The initial input of the generated tool is wing outer geometry. Root and tip chord lengths, taper ratio and wing half span are the first set of data that specifies outer geometry together with airfoil information. Airfoil data is usually given in a universal standard that represents the upper and lower sides of the airfoil in two sets of points going from zero to one along airfoil chord.

Next step is the determination of structural members. Numbers and locations of structural members (spars, stringers, and ribs) are specified to have the interior wing geometry. Locations of spars, upper stringers, and lower stringers are represented in percentages such that airfoil leading edge is 0% and trailing edge is 100%. Likewise, ribs are located on wing using the distance from wing root in percentage of wing semi span.

The main goal is to size the sections (single or multi-cell boxes) of the wing by finding reasonable values for

- Spars (Thicknesses of spar webs, areas of spar flanges)
- Upper and lower skin thicknesses
- Ribs (Rib web thicknesses, rib upper and lower flange areas, rib front and rear flange areas)
- Stringer areas

Areas of stringers, areas of spar flanges, and thicknesses are kept constant within a section of wing and they are changed discretely from tip to root.

The tool does not select the materials. Materials of spars, stringers, ribs, and skins are from available common aerospace metals and are entered as inputs to the tool. Material mechanical properties and allowable stresses are used for the sizing.

The tool is based on a classical wing structural analysis methodology based on the calculation of the internal load distribution on a multi-cell box through hand calculations. The theory behind the structural idealization is a common and reliable theory, which is based on the assumption that the wing is a closed box beam with axial stiffness, bending stiffness and torsional stiffness.

Second part of the study is allocated to the post-buckling load redistribution phenomenon. It is essential to understand this behavior because it is one the most important weight saving opportunities especially for subsonic wings. Within the generated sizing tool, the user has the option to allow elastic buckling of skins before the limit load is reached. Therefore, load distribution after buckling is also examined within this thesis. This study offers a rapid method to calculate the internal loads using iterative application of linear static finite element analysis. Local buckling of panels and load redistribution is based on traditional effective width method that is applicable for compressive post-buckling of stiffened panels. Comparison of the developed method to geometric nonlinear finite element analysis is also demonstrated with a FEM based validation in the corresponding chapter.

1.3 Literature Survey

Structural design at the preliminary design stage of aircraft programs has been widely explored in aerospace literature. There is a large variety of preliminary design approaches in the history whereas the philosophies of recent studies have many things in common. The common steps in a typical preliminary structural design workflow have already been introduced in the motivation section of this chapter. This section has a more detailed look into the design workflows created within the last couple of decades. Recent studies are investigated to demonstrate the sophisticated stage preliminary approaches have reached so far.

Among one of the most recent studies on this subject, Eldred et al. [4] described the way of implementing structural analysis to NASA's previously developed conceptual design process. This study aimed to apply structural analysis to supersonic aircraft design candidates to evaluate the internal structure in terms of weight, CG, structural material selection, and its response to outer mold line changes. For this purpose, OML geometry creation, predefined inner structure layout, meshing, load case creation, and static sizing are handled in an automated way. Figure 1-2 and Figure 1-3 show the flow charts of this process. In-house and commercial software used for each step are also shown under each block. It is noted that a sizing software is utilized in addition to common CAD and FEA software. This fast and automated process makes it possible to study the structures of all candidate concepts.

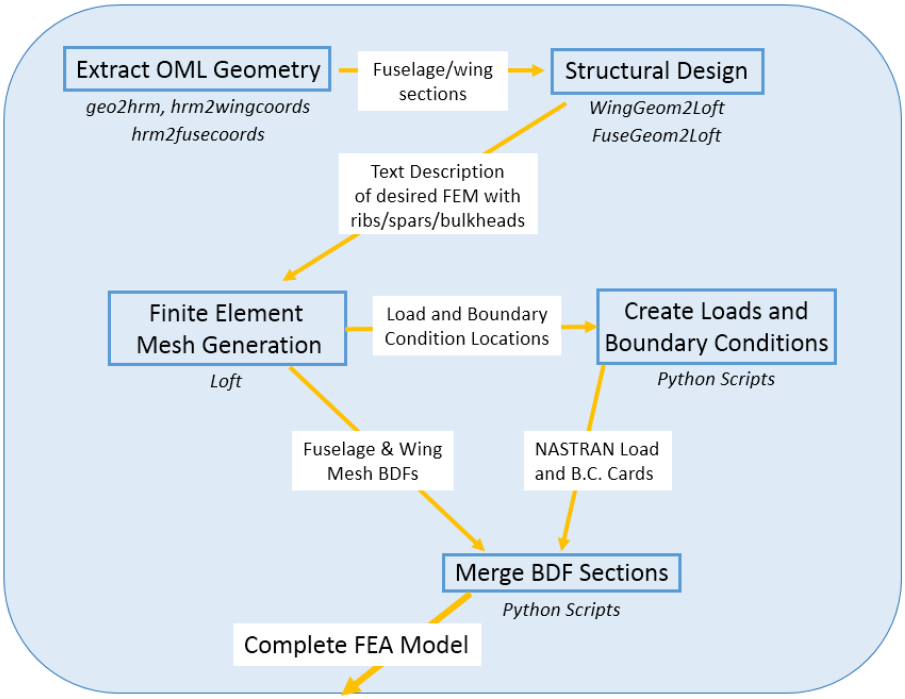

Figure 1-2 Finite Element Model Creation Flow Chart [4]

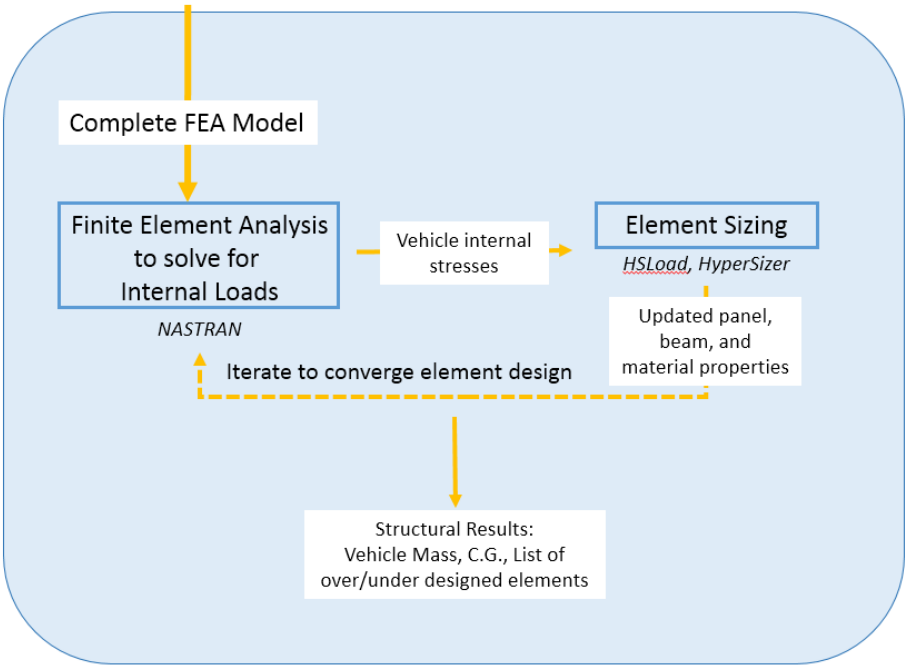

Figure 1-3 Finite Element Model Sizing Flow Chart [4]

Chen et al. [3] carried out another multidisciplinary study for a future supersonic transport program funded by NASA. As already stated in the motivation section of this thesis, Chen's process was tested within the N+2 supersonic program. Figure 1-4 shows the complex flowchart of N+2 structural analysis process.

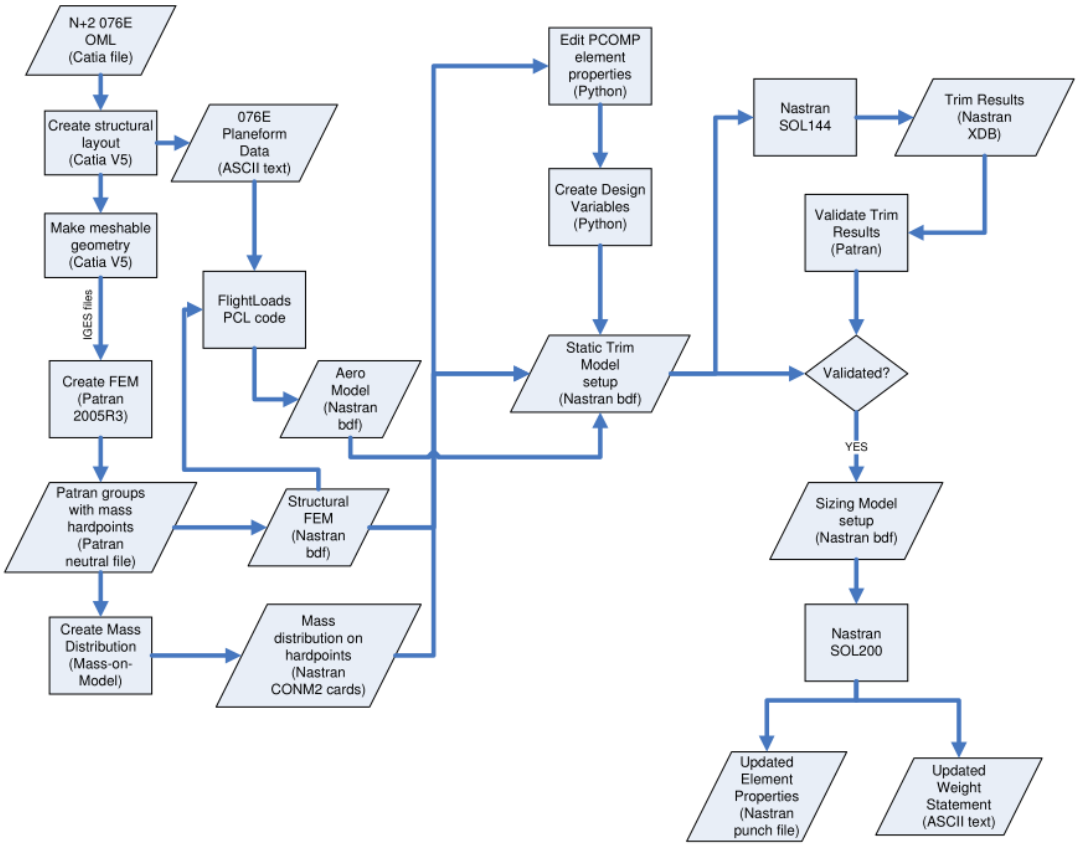

Figure 1-4 N+2 Program Structural Analysis Flow Chart [3]

It is seen that this process starts with the creation of structural layout in CAD environment. Meshable geometry is exported from CAD environment, then meshed manually, which is stated as a drawback of this work. This study also utilizes trim analysis in order to obtain flight loads for specific maneuvers. At the final step, an optimization code is used to minimize the weight by using finite element properties as design variables. Many steps within the flow chart are automated using some in-house codes, whereas some parts still have to be linked manually. At the end of this

study, sizing was performed with both strength and flutter constraints and resulting weights were compared.

ECLIPSE tool [2], which was already introduced in the motivation section of this chapter, is another example to advanced in-house company tools for preliminary structural design. The tool works on a structural mesh and uses an evolutionary structural optimization process such that some portion of the thinnest elements are removed from the finite element model after first sizing. After the removal of the thinnest elements, resulting new model is reanalyzed until the predefined number of iterations is reached. Figure 1-5 shows the evolutionary strength optimization approach by ECLIPSE software within British Aerospace Systems.

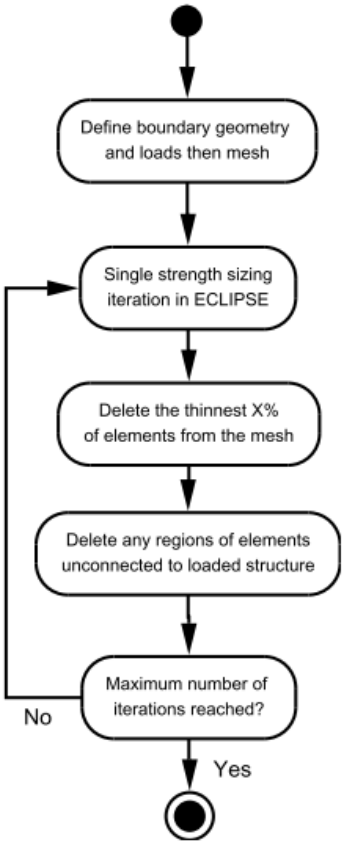

Figure 1-5 ECLIPSE approach to structural sizing [2]

In addition to in-house tools owned by major aerospace companies, commercial software companies also have been seeking to offer solutions for preliminary structural design in recent years. For instance, Kumar A and Mariayyah [5] offered a multidisciplinary wing design process for a typical low aspect ratio wing. For that purpose, they combined a workflow integrator software called Isight to CAD and FEA environment. They aimed to solve the multi-objective optimization problem of maximizing the lift to drag ratio and minimizing the weight. Figure 1-6 shows the flow chart they formed for this purpose.

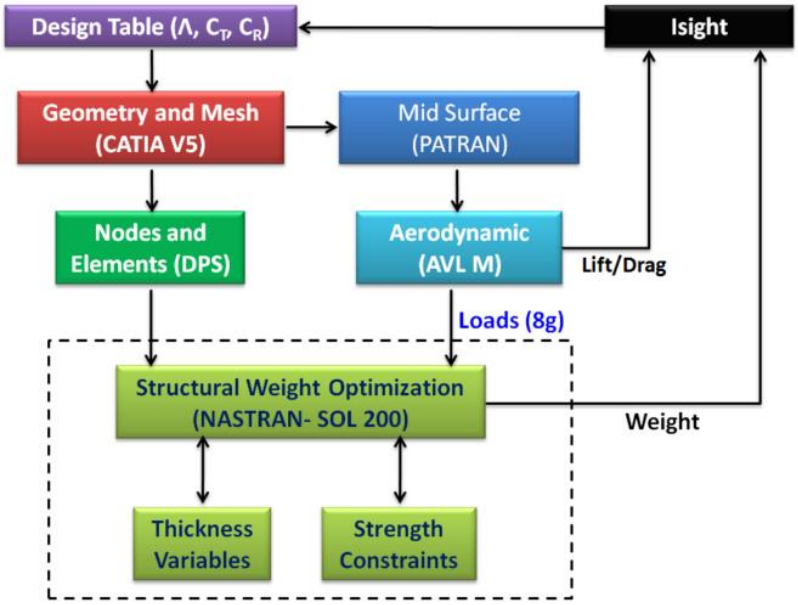

Figure 1-6 Optimization Flow Chart by Kumar A and Mariayyah [5]

Aerodynamic analysis and structural analysis are utilized as two separate sub-flows as shown in Figure 1-6. Interactions between the blocks, i.e. CAD, FEA and optimization software, are achieved by the capability of the workflow integrator software and in-house coding.

Another commercial software used for the wingbox preliminary design was evaluated within the study of Ainsworth et al. [6]. HyperSizer, which is a commercial structural analysis and sizing software, was used for a trade study

between various stiffened panel concepts. Wingbox structure of a commercial aircraft is used for assessment. The sizing software has the ability to extract the finite element internal loads. It also has many failure theories encoded so that it can perform structural analysis for both strength and stability for stiffened panels. At the end of Ainsworth's study, various panel concepts for both metallic and composite structures are compared.

As already mentioned within the scope section of this thesis, post-buckling behavior of stiffened panels is investigated because this phenomenon is essential for wing design especially for subsonic vehicles. A comprehensive survey is made for studies on the post-buckling and global buckling of stiffened panels. Within the last decades, several researches have been carried out with the help of finite element applications and/or test correlations.

A buckling analysis of a hat-stiffened panel under uniaxial compression was presented by Ko and Jackson [7]. It was demonstrated that the global buckling load is much higher than the local buckling load. They used finite element predictions and verified them by test data. Ko and Jackson [8] also analyzed the same panel under uniform shear with finite element analysis. Local buckling loads showed agreements with experiments and finite element techniques in both studies.

Lynch and Sterling [9] presented a finite element methodology for the compressive post-buckling analysis. They compared the test data to the results of several different finite element modeling approaches for skin-stringer interfaces. Required mesh density to accurately capture buckling modes was also determined. Heitmann and Horst [10] proposed a semi-empirical method to obtain the effective skin stiffness in the post-buckled range. They reached a fast, quasi nonlinear finite element analysis using that method for combined compression and shear.

Van der Veen and Coatta [11] used the post-buckling load redistribution phenomenon on panels made from new metal alloys. By utilizing new high damage tolerant skins and high strength stiffeners, they increased the panel buckling

performance and proposed keeping stringer pitches at economic levels. Collier and Yarrington [12] presented a method for industry usage to obtain internal load redistribution by an iterative convergence in buckling parameters. Their method was implemented into the HyperSizer® software.

1.4 Organization of the Thesis

Chapter 1 introduces the thesis. Literature review and the motivation of present work are covered.

Chapter 2 outlines the load generation procedures for both supersonic and subsonic wings. One of the most essential steps for preliminary wingbox structural sizing is the approach taken for the loading of wing. Two approaches followed in this thesis, namely, the lifting surface theory and Schrenk's approximation method are introduced in Chapter 2. Sample load generation study is also included in this part.

Chapter 3 shows the methodology of this work. Traditional strength and stability methods are covered. Design strategy, simplifications and assumptions are explained in detail. Overall design strategy and steps are presented.

Chapter 4 includes the case study results. The tool developed for this thesis was used for the sizing of three different wingbox configurations. The design exploration studies and the final weights are all provided in Chapter 4.

Post-buckling load redistribution study is shown in Chapter 5. The methodology to calculate the effective width of skin panels and internal loads through the iterative application of the linear static finite element analysis is offered in this section. FEM validation with a geometric nonlinear finite element solver is also explained in Chapter 5.

Finally, Chapter 6 emphasizes the remarks, conclusions, and possible future studies.

CHAPTER 2

EXTERNAL AND INTERNAL LOAD CALCULATION FOR PRELIMINARY DESIGN

Selection of loading method is important for the preliminary design. Loading is the most essential input that affects the sizing and weight of the wingbox structure. Therefore, careful consideration should be given to loads calculations.

Maneuvers, landing, buffet, control surface deflections, impacts (bird strike), high local loads due to engine or weapon attachments are the main sources of aircraft wing loading. However, at the early design phases, there is generally no or little information about the entire aircraft, which makes it very difficult to calculate the true loads coming from different sources. Symmetric pull-up maneuver with maximum positive load factor is generally chosen as the only load case for preliminary design phase. This may be perceived as a very cruel assumption at the first glance, but the goal is not to achieve the most reliable results at the first sizing loop; main aim is to compare candidate designs with each other. Therefore, any valid approach for the loading can work at this stage of wingbox design, as long as the same approach is implemented to all candidate designs.

This chapter deals with the distribution of loads along the aircraft wing. Two common methods widely used for subsonic and supersonic wing loading are examined.

2.1 Subsonic Wing Loads

For subsonic wing loading, ESDU 95010 Computer program for estimation of spanwise loading of wings with camber and twist in subsonic attached flow [13] is used. This computer program is called as ESDUpac A9510 and is attached to ESDU 95010 report. It is based on a method called as the subsonic lifting-surface theory derived by Multhopp [14]. User can get the spanwise load distribution of local lift and pitching coefficients out of the program. Wing incidence, camber, and twist effects can be taken into account for calculations. The program can handle tapered and cranked wings and has specific text-based input and output file formats, which are explained in detail within the example studies in this thesis.

ESDUpac A9510 is selected to estimate the subsonic loads for this thesis because it is based on an old and valid method that has been widely used in aircraft design literature. Detailed correlation studies and applicability limitations of this method are provided in a separate data sheet, ESDU 83040 [15].

The preliminary design tool, which is developed in MATLAB environment for this thesis, integrates the utilization of ESDUpac A9510 in a fully automated way. The tool generates the A9510 input file by extracting the necessary information from the main input file. It then sends the input file to A9510. The tool checks for all limitations and constraints defined in the method and it reports any errors and/or warnings. After the execution of A9510, the tool parses the output file to obtain the local overall lift and pitching moment coefficients. While keeping the ESDUpac A9510 input and output files for reference, the tool returns to its own environment after the load calculation is finished.

ESDUpac A9510 input format and input list, restrictions, and outputs are examined in the following sections.

2.1.1 ESDUpac A9510 Restrictions

Although most practical wing planforms obey the following restrictions, these conditions still need to be checked before the execution of A9510 program. It is

imposed that for straight-tapered planforms, following restrictions have to be met [13]:

- Restriction 1

$$0 \le \beta A \le 12 \tag{2.1}$$

where A is the aspect ratio, which is derived from wing span and wing area, and β stands for the compressibility parameter and equals to

$$\beta = (1 - M^2)^{1/2} \tag{2.2}$$

where M stands for the Mach number.

- Restriction 2

$$A \tan \Lambda_{1/2} \le 6 \tag{2.3}$$

where $\Lambda_{1/2}$ is the sweep angle of mid chord line.

- Restriction 3

This is a simple check on the taper ratio λ and is given by:

$$0 \le \lambda \le 1 \tag{2.4}$$

- Restriction 4

$$A \tan \Lambda_{1/2} \ge -2\left(\frac{1-\lambda}{1+\lambda}\right) \tag{2.5}$$

- Restriction 5

$$\tan^{-1}\left[\frac{A \tan \Lambda_{1/2}}{\beta A}\right] \ge -20° \tag{2.6}$$

The preliminary design tool developed for this thesis checks all these and warns the user before terminating the process if any of the constraints is violated.

2.1.2 ESDUpac A9510 Input File

It is important to understand the input format of A9510 program. Input parameters are listed in Table 2-1. Detailed explanations and some remarks are provided at the end of the table.

Table 2-1 ESDUpac A9510 Input List

Entry #	Condition (if exists)	Input	Remark
1			*text*
2			*text*
3			*text*
4		N_{Ms}, N_{Mc}	*Integers. Number of spanwise and chordwise Multhopp collocation stations.*
5		N_L	*Number of loading type.* $1 \leq N_L \leq 3$
6		$\{L_m\}$	*Defines loading type* *1 Loading due to incidence* *3 Loading due to camber* *4 Loading due to twist*
7		N_M	*Number of Mach numbers.* $1 \leq N_M \leq 20$
8		M_l	*Values of Mach numbers.* $0 \leq M_l \leq 1$
9		N_o	*Number of spanwise stations for output.* $1 \leq N_o \leq 40$
10		η_{oi}	*Dimensionless values of spanwise stations for output*
11		**P**	*Selects calculation mode.* *P = 0 Separate spanwise loadings only.* *P = 1 Also calculates total loading for specified angles of incidence* α_{spr}. *P = 2 Also calculates total loading for specified values of overall lift coefficient* C_{Lspr}
C1	If P = 1 or 2	N_{sp}	*Number of specified values of* α_{spr} *or* C_{Lspr}
C2	If P = 1	α_{spr}	*Specified incidences for loading calculation (deg)*
	If P = 2	C_{Lspr}	*Specified overall lift coefficients for loading calculation*
12		N_k	*Number of cranks in wing;* $0 \leq N_k \leq 13$ $N_k = 0$ → *straight-tapered planform.*
C3	If N_k=0	**A**	*Aspect ratio*
C4		λ	*Taper ratio*
C5		Λ_n	*Sweep of* n^{th}*-chord line*
C6		**n**	*Chord line identifier*

C7	If $N_k \geq 1$	**Units**	*Integer. 1 = SI units (m), 2 = British units (ft).*
C8		s_i	*Spanwise stations for cranked wing*
C9		x_i	*Streamwise co-ordinates of wing leading edge at spanwise stations s_i*
C10		c_i	*Chords for cracked wing at spanwise stations s_i*
C11	If {L_m} contains 3 (camber data)	N_{sC}	*Number of spanwise stations η_{ci} for camber input. $2 \leq N_{sC} \leq 20$*
C12		η_{ci}	*Dimensionless values of spanwise stations for camber input, from tip to root, as fraction of semi-span*
C13		N_{cCi}	*Number of chordwise stations for camber input at η_{ci}*
C14		ξ_{Ci1} ζ_{Ci1}	*N_{cCi} pairs* . . . *Repeat N_{sC} times*
C15	If {L_m} contains 4 (twist data)	N_{sT}	*Number of spanwise stations for twist input $2 \leq N_{sT} \leq 20$*
C16		η_{T1} α_{T1}	*N_{sT} pairs* . .

Entries 1 to 3 are text inputs used to define the study.

Entry 4 defines Multhopp collocation stations. ESDU 95010 data sheet [13] has a detailed study on the selection of these parameters. Many correlation studies were carried out to select these parameters. At the end, with N_{Ms} = 33 and N_{Mc} = 3, good correlations were achieved [13], while the following restriction is satisfied:

$$\beta^{-1} \tan \Lambda_0 < 4 \tag{2.7}$$

There is also a statement in the same data sheet that N_{Mc} should be increased to 5 for $\beta A \geq 2$. Developed tool for this thesis makes the necessary check to decide on the number to be used for N_{Mc} parameter. In other words, the tool can increase N_{Mc} to 5 once the check on βA value meets the certain condition.

Entry 5 is the number of loading types. As already stated, ESDUpac A9510 can distribute the load due to incidence, due to camber, and due to twist. Selection of multiple loadings is possible.

Entry 6 stands for a vector that is dependent on Entry 5 and contains the number corresponding to loading types. Number of loadings and loading types (Entries 5 and 6) are first defined in the main tool input and is taken to ESDU input automatically.

Entry 7 and Entry 8 are the number and values of Mach numbers used in the load cases, respectively. Since the preliminary sizing case occurs with the critical (dive) speed, A9510 program runs for a single speed, which is a user input to the main tool.

Entry 9 and Entry 10 stand for the spanwise stations for output. The output is generally taken at around 20 equally spaced positions along the span. In addition, the tool developed for this thesis adds all rib stations to this list of spanwise stations for output. It should be noted that the number of output stations should not exceed 40. The main tool also checks for the number of output stations and warns the user if it exceeds 40.

Entry 11 selects the calculation mode. Although ESDUpac A9510 gives the opportunity to calculate the loading for specified lift coefficient, incidence angle is more important for the purposes of this thesis. The angle corresponding to the speed specified in Entry 8 is calculated in this step. Then, the tool writes the value of the calculated incidence angle to A9510 input file for C1 and C2 entries.

Entry 12 is the number of cranks in the wing. ESDUpac A9510 makes it possible to calculate loads for cranked wings. If there are no cranks, essential geometric parameters such as the aspect ratio, taper ratio, and sweep angle are required for entries C3 to C6. If there are cranks in the wing, then entries C7 to C10 are used to define the cranked wing geometry.

Conditional entries C11 to C14 stand for the camber definition. ESDUpac A9510 also allows for changing camber definitions through the span. Camber data is listed as pairs in A9510 program input.

Finally, conditional entries C15 and C16 are used for the twist definition.

2.1.3 ESDUpac A9510 Output

A9510 program output contains a list of local lift and pitching moment coefficients corresponding to spanwise positions. The tool developed for this thesis automatically reads the output file, extracts the local coefficients, and then calculates the shear force, bending moment, and pitching moments at each station along the span. Calculated wing loads are taken into MATLAB environment to be used for sizing.

2.1.4 Sample Load Calculation for a Subsonic Wing

Sample load calculation for the wing of a turboprop trainer making a symmetric pull-up maneuver is provided in this section. For illustration purposes, Pilatus PC-21 advanced trainer aircraft is selected. Table 2-2 shows some important performance characteristics and geometric information of PC-21, which are used for ESDUpac A9510 input generation.

Table 2-2 Pilatus PC-21 Aircraft Information [16]

Wing Span, b	9.11 m
Wing Projected Area, S_w	15.22 m^2
Maximum Operating Mach Number, M	0.72
Maximum Positive Load Factor, n	+8.0 g
Maximum Take-off and Landing Weight, W	3100 kg

In addition to the above data, some assumptions are made for the missing geometric properties of the wing. Assumed values for the root and tip chord lengths, leading edge and mid-chord line sweep angles are listed in Table 2-3.

Table 2-3 Assumed Geometric Values

Root Chord Length, c_{root}	2258 mm
Tip Chord Length, c_{tip}	1085 mm
Leading Edge Sweep Angle (Λ_0)	12°
Sweep Angle of the Mid Chord Line ($\Lambda_{1/2}$)	5°

It should be noted that the assumed parameters are not provided in the official documentation of the PC-21 aircraft. These values are just extracted from the top and bottom view 2-dimensional drawings of the PC-21 aircraft, which is shown in Figure 2-1. Although the assumed values may not be precise, they provide sufficient accuracy for the sample load generation study in this section. The region enclosed with red dotted lines is used as the wing planform shape to obtain the assumed geometric values.

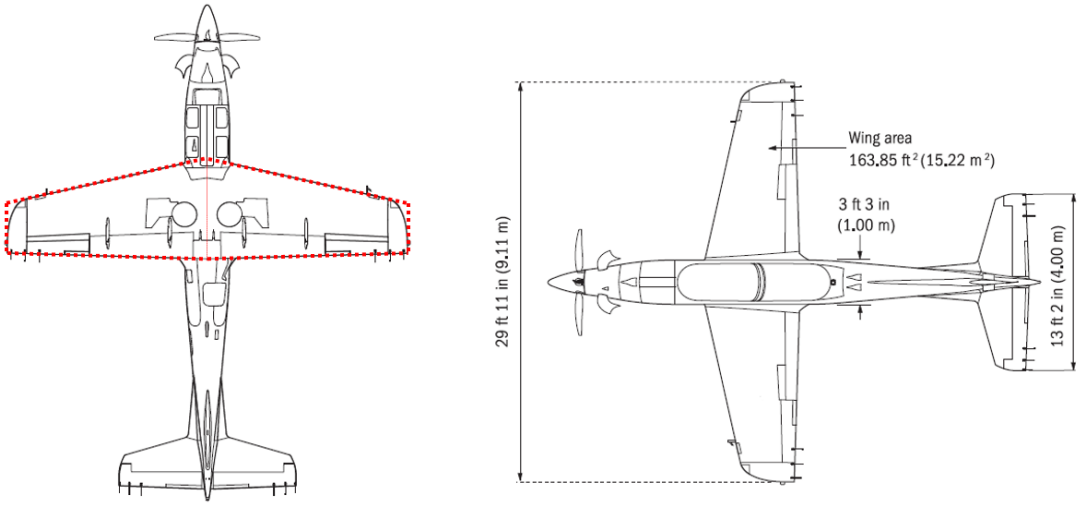

Figure 2-1 PC-21 Bottom and Top View Drawings [16]

Finally, NACA 2412 airfoil was selected to account for the camber effect on the wing loading. The real airfoil shape of PC-21 wing is not provided in the official document. NACA 2412 is used because it is a common airfoil that can be helpful for illustration purposes.

2.1.4.1 Restrictions Check

Restrictions provided in section 2.1.1 are checked to see whether the PC-21 wing planform is suitable for ESDUpac A9510 or not.

- Restriction 1

In order to check this restriction, aspect ratio (A) and the compressibility parameter (β) are to be obtained first.

$$A = \frac{b^2}{S_w} = 5.45 \tag{2.8}$$

$$\beta = (1 - M^2)^{1/2} = 0.69 \tag{2.9}$$

Therefore,

$$\beta A = 3.78 \tag{2.10}$$

which is greater than 0 and smaller than 12, as imposed by restriction 1. Thus, the first condition is satisfied.

- Restriction 2

$$A \tan \Lambda_{1/2} = 0.48 \tag{2.11}$$

which is smaller than 6. The second criterion is satisfied.

- Restriction 3

Taper ratio is the ratio of the tip chord length to the root chord length. It is calculated by the following equation.

$$\lambda = \frac{c_{tip}}{c_{root}} = 0.48 \tag{2.12}$$

which satisfies the third condition.

- Restriction 4

$$-2\left(\frac{1-\lambda}{1+\lambda}\right) = -0.70 \tag{2.13}$$

Above parameter is smaller than the one found in equation (2.11). Therefore, condition 4 is also satisfied.

- Restriction 5

$$\tan^{-1}\left[\frac{A\tan\Lambda_{1/2}}{\beta A}\right] = 7.19° \tag{2.14}$$

Condition 5 is also satisfied as the calculated value is greater than -20°.

Consequently, it is clearly seen that the wing planform obeys all the restrictions imposed by A9510 program. Therefore, the input file can be created for the load generation.

2.1.4.2 Input File

The input file generated for the sample study is explained in detail in this section.

Entries 1 to 3 introduce the study:

```
1  TEXT1 ESDU 95010
2  TEXT2 Sample Load Generation Study
3  TEXT3 PC21 Aircraft with NACA 2412 Airfoil
```

Entry 4 defines Multhopp collocation stations. Criteria given in section 2.1.2 are used to determine N_{Ms} and N_{Mc} values. First check is made using equation (2.7):

$$\beta^{-1}\tan\Lambda_0 = 0.31 \tag{2.15}$$

The above value is smaller than 4. Therefore, it is decided that N_{Ms} = 33 is suitable for this planform.

Another check is made to determine N_{Mc} parameter. Since the βA value, which is already calculated in equation (2.10), is greater than 2, N_{Mc} is increased from 3 to 5. Hence, entry 4 of the input file is as follows:

```
4   33 5
```

Entry 5 and entry 6 stand for the number and types of the loading, consecutively. Loading due to incidence and camber is investigated in this study:

```
5   2
6   1 3
```

Entries 7 and 8 define the Mach number:

```
7   1
8   0.72
```

Entry 9 and Entry 10 stand for the spanwise output stations. 22 stations along the wing span are selected for this study:

```
9   22
10  0 0.05 0.1 0.15 0.2 0.25 0.3 0.35 0.4 0.45 0.5 0.55 0.6 0.65
    0.7 0.75 0.8 0.85 0.9 0.95 0.98 0.9999
```

Entry 11 selects the calculation mode. In this step, calculation of the total loading for a specified value of overall lift coefficient is needed. The tool developed for this thesis makes the following calculation to obtain the C_{Lspr} value. Simple definition of the lift is used here. Aircraft weight with maximum positive load factor is considered to solve for the lift coefficient.

$$L = nW \tag{2.16}$$

where n is the maximum load factor, which is equal to +8g, and W is the aircraft weight, 3100 kg.

From the general lift formula:

$$L = nW = 0.5\rho_{\infty}V_{\infty}^{2}S_{w}C_{L} \tag{2.17}$$

where air density, ρ_∞ = 1.225 kg/m^3 at sea level and

$$V_\infty = Ma_\infty = 244.8\ m/s$$

Solving for C_L in equation (2.17);

$$C_L = 0.4355$$

Calculated lift coefficient is placed into the A9510 program input file as the C_{Lspr} value:

```
11  2
12  1
13  0.4355
```

Since there are no cranks in the PC-21 wing, entry 12 (line 14) is zero. Conditional entries C3 to C6 are defined through lines 15 to 18. Aspect ratio, taper ratio, and leading edge sweep angle are specified in these entries:

```
15  5.45
16  0.48
17  12
18  0
```

Next step is the camber input. Conditional entries C11 to C14 stand for the camber definition. The camber data is provided at the root and the tip sections of the wing. It is assumed that the camber does not change along the span. Therefore, same list is valid for both ends of the wing. Camber line definition is made using the airfoil data. It should be noted that the airfoil data is an input to the main tool developed for this thesis and it is used to determine the wing box geometry. Upper and lower curves which define NACA 2412 airfoil is provided in Table 2-4.

Table 2-4 Airfoil Data (NACA 2412)

Upper		Lower	
0	0	0	0
0.0125	0.0215	0.0125	-0.0165
0.025	0.0299	0.025	-0.0227
0.05	0.0413	0.05	-0.0301
0.075	0.0496	0.075	-0.0346
0.1	0.0563	0.1	-0.0375

0.15	0.0661	0.15	-0.041
0.2	0.0726	0.2	-0.0423
0.25	0.0767	0.25	-0.0422
0.3	0.0788	0.3	-0.0412
0.4	0.078	0.4	-0.038
0.5	0.0724	0.5	-0.0334
0.6	0.0636	0.6	-0.0276
0.7	0.0518	0.7	-0.0214
0.8	0.0375	0.8	-0.015
0.9	0.0208	0.9	-0.0082
0.95	0.0114	0.95	-0.0048
1	0.0013	1	-0.0013

In addition to the above data, maximum camber, maximum camber position, and the thickness parameters are provided for NACA 2412 airfoil:

Table 2-5 Additional Airfoil Information

Max Camber, *MC* (%)	2
Max Camber Position, *MCP* (%)	40
Thickness (%)	12

The equation for camber line is provided in two sections. For the front side of the *MCP* ($0 \le x < MCP$):

$$y_c = \frac{MC}{MCP^2}\left(2 \cdot MCP \cdot x - x^2\right) \tag{2.18}$$

For the aft side of the *MCP* ($MCP \le x \le 1$)

$$y_c = \frac{MC}{(1-MCP)^2}\left(1 - 2 \cdot MCP + 2 \cdot MCP \cdot x - x^2\right) \tag{2.19}$$

where x stands for the chord station from 0 to 1.

Camber line is obtained using Equations (2.18) and (2.19). The input file is finished with the addition of the camber data. Table 2-6 shows the complete input file sent to A9510 program.

Table 2-6 ESDUpac A9510 Input File for the Sample Problem

```
1   TEXT1 ESDU 95010
2   TEXT2 Sample Load Generation Study
3   TEXT3 PC21 Aircraft with NACA 2412 Airfoil
4   33 5
5   2
6   1 3
7   1
8   0.72
9   22
10  0 0.05 0.1 0.15 0.2 0.25 0.3 0.35 0.4 0.45 0.5 0.55 0.6 0.65
    0.7 0.75 0.8 0.85 0.9 0.95 0.98 0.9999
11  2
12  1
13  0.4355
14  0
15  5.45
16  0.48
17  12
18  0
19  2
20  1
21  18
22  0       0.0000
23  0.0125  0.0012
24  0.025   0.0024
25  0.05    0.0047
26  0.075   0.0068
27  0.1     0.0088
28  0.15    0.0122
29  0.2     0.0150
30  0.25    0.0172
31  0.3     0.0188
32  0.4     0.0200
33  0.5     0.0194
34  0.6     0.0178
35  0.7     0.0150
36  0.8     0.0111
37  0.9     0.0061
38  0.95    0.0032
39  1       0.0000
40  0
41  18
42  0       0.0000
43  0.0125  0.0012
44  0.025   0.0024
45  0.05    0.0047
46  0.075   0.0068
47  0.1     0.0088
48  0.15    0.0122
49  0.2     0.0150
50  0.25    0.0172
51  0.3     0.0188
52  0.4     0.0200
```

```
53  0.5     0.0194
54  0.6     0.0178
55  0.7     0.0150
56  0.8     0.0111
57  0.9     0.0061
58  0.95    0.0032
59  1       0.0000
```

2.1.4.3 Output File

ESDUpac A9510 output file starts with the input data check to show the user if there are any warnings and errors. After that, a copy of the entire input data exists in the output. At the results section, aerodynamic loading due to incidence and aerodynamic loading at zero incidence due to camber are provided. At the end, the calculations at the specified overall lift coefficient are listed. This part is the main concern of the current sample problem. It consists of the incidence angle at specified lift coefficient, local overall lift coefficients, and local overall pitching moment coefficients at each spanwise station. These coefficients are used to determine the internal loads.

Table 2-7 shows the final part of the output file that contains the lift and the moment coefficients. Additionally, complete output file is given in Appendix A.

Table 2-7 Final Part of A9510 Output File

```
                  CALCULATIONS AT SPECIFIED OVERALL CL
                  ====================================


               TOTAL LOADING AT CLsp            =    .4355
               ------------------------------------------

                     Mach number, M     =   .7200
                     ----------------------------

Incidence (degrees) at specified CL                                =   2.6454

Lift coefficient of wing at specified incidence                    =    .4355

Dimensionless spanwise position of half-wing
centre of pressure from centre line: tip-up moment                 =    .4274

Dimensionless distance of wing centre of pressure behind
```

```
apex based on cbar                                                =    .6645

-------------------------------------------------------------------------
  Spanwise position       Local overall lift      Local overall pitching
         Eta                 coefficient            moment CmL.c/cbar
                             CLL.c/cbar         about local quarter chord
-------------------------------------------------------------------------
        .0000                    .5539                   -.0933
        .0500                    .5528                   -.0917
        .1000                    .5498                   -.0888
        .1500                    .5452                   -.0856
        .2000                    .5392                   -.0824
        .2500                    .5318                   -.0796
        .3000                    .5231                   -.0767
        .3500                    .5131                   -.0740
        .4000                    .5017                   -.0712
        .4500                    .4888                   -.0684
        .5000                    .4745                   -.0656
        .5500                    .4585                   -.0627
        .6000                    .4408                   -.0597
        .6500                    .4208                   -.0565
        .7000                    .3982                   -.0531
        .7500                    .3723                   -.0494
        .8000                    .3420                   -.0453
        .8500                    .3052                   -.0404
        .9000                    .2579                   -.0343
        .9500                    .1905                   -.0257
        .9800                    .1248                   -.0173
        .9999                    .0116                   -.0016
-------------------------------------------------------------------------

***  RUN COMPLETED

END OF OUTPUT  ------------------------------------------------------------
```

At this point, A9510 program has finished its job and provided the necessary information about the external loading of PC-21 wing. After this step, an additional procedure is needed to get the internal loading. Calculation of the internal loads using the output coefficients are explained in the following section.

2.1.4.4 Calculation of Internal Loads from External Loads

A9510 program provides the lift and the pitching moment coefficients as a multiplication by the *c/cbar* value. The *cbar* parameter stands for the mean chord length of the wing. Spanwise local lift coefficients and local pitching moment coefficients can be found by dividing the output lists with *c/cbar* for every station. Table 2-8 shows the chord lengths and the *c/cbar* parameter at each station. Table 2-9 shows the CLL and CMC values after A9510 outputs are divided by *c/cbar*.

Table 2-8 Coefficients, Chord Lengths and *c/cbar* Fractions at Each Station

Spanwise position η	Local lift coefficient CLL.c/cbar	Local pitching moment CmL.c/cbar	cbar	chord [mm]	c/cbar
0	0.5539	-0.0933	1671.5	2258.00	1.3509
0.05	0.5528	-0.0917		2199.35	1.3158
0.1	0.5498	-0.0888		2140.70	1.2807
0.15	0.5452	-0.0856		2082.05	1.2456
0.2	0.5392	-0.0824		2023.40	1.2105
0.25	0.5318	-0.0796		1964.75	1.1754
0.3	0.5231	-0.0767		1906.10	1.1404
0.35	0.5131	-0.074		1847.45	1.1053
0.4	0.5017	-0.0712		1788.80	1.0702
0.45	0.4888	-0.0684		1730.15	1.0351
0.5	0.4745	-0.0656		1671.50	1.0000
0.55	0.4585	-0.0627		1612.85	0.9649
0.6	0.4408	-0.0597		1554.20	0.9298
0.65	0.4208	-0.0565		1495.55	0.8947
0.7	0.3982	-0.0531		1436.90	0.8596
0.75	0.3723	-0.0494		1378.25	0.8246
0.8	0.342	-0.0453		1319.60	0.7895
0.85	0.3052	-0.0404		1260.95	0.7544
0.9	0.2579	-0.0343		1202.30	0.7193
0.95	0.1905	-0.0257		1143.65	0.6842
0.98	0.1248	-0.0173		1108.46	0.6632
0.9999	0.0116	-0.0016		1085.12	0.6492
1				1085.00	0.6491

input
linked cell
calculation

Table 2-9 Spanwise Local Lift and Pitching Moment Coefficients

η	CLL	CMC
0	0.4100	-0.0691
0.05	0.4201	-0.0697
0.1	0.4293	-0.0693
0.15	0.4377	-0.0687
0.2	0.4454	-0.0681
0.25	0.4524	-0.0677
0.3	0.4587	-0.0673
0.35	0.4642	-0.0670
0.4	0.4688	-0.0665
0.45	0.4722	-0.0661
0.5	0.4745	-0.0656
0.55	0.4752	-0.0650
0.6	0.4741	-0.0642
0.65	0.4703	-0.0631
0.7	0.4632	-0.0618
0.75	0.4515	-0.0599

0.8	0.4332	-0.0574
0.85	0.4046	-0.0536
0.9	0.3585	-0.0477
0.95	0.2784	-0.0376
0.98	0.1882	-0.0261
0.9999	0.0179	-0.0025

After this point, it is better to have a notation for the wing stations and sections because repetitive calculations are carried out for each section along the span. Figure 2-2 is useful for the load calculation process.

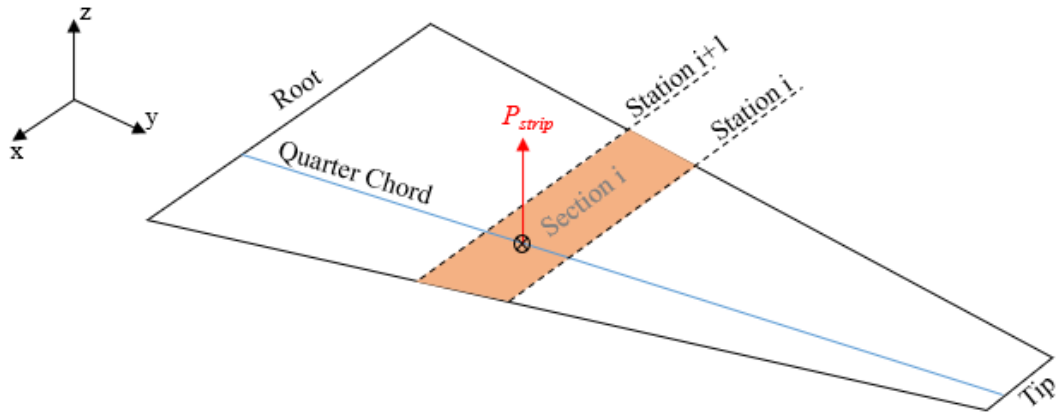

Figure 2-2 Coordinate System and Notation for the Internal Load Calculation

Lift and pitching moment per unit span can be found easily using the coefficients in Table 2-9. General formulas of the lift and the moment can be used for this purpose:

$$L_i^{'} = 0.5 \cdot \rho_\infty \cdot V_\infty^{\,2} \cdot CLL_i \cdot c_i \tag{2.20}$$

$$M_{MAC,i}^{'} = 0.5 \cdot \rho_\infty \cdot V_\infty^{\,2} \cdot CMC_i \cdot c_i^{\,2} \tag{2.21}$$

Average running load in a section is derived by averaging the lift per unit span ($L^{'}$) values at the adjacent stations:

$$L'_{run,i} = \frac{L'_i + L'_{i+1}}{2} \tag{2.22}$$

By multiplying the average running load with the distance between stations, average strip load acting on the section can be found:

$$P_{strip,i} = L'_{run,i} \cdot (y_i - y_{i+1}) \tag{2.23}$$

Then, the shear force at a station can be calculated by summing all strip loads from the tip to that station:

$$V_{i+1} = V_i + P_{strip,i} \tag{2.24}$$

Consequently, shear forces at all stations along the span are obtained. Table 2-10 gives the shear forces at stations together with the steps explained in above equations.

Table 2-10 Shear Force at the Stations

η	Lift/Unit Span [N/m]	Pitching Moment/Unit Span [N.mm/m] (positive: LE up)	Average Running Load [N/m]	Distance between stations [m]	Average Strip load in each section [N]	Shear Force at the Stations [N]
0	33983.4	-12925307	33950	0.2278	7732	**121701**
0.05	33915.9	-12373683	33824	0.2278	7703	**113969**
0.1	33731.8	-11662834	33591	0.2278	7650	**106265**
0.15	33449.6	-10934533	33266	0.2278	7576	**98615**
0.2	33081.5	-10229261	32854	0.2278	7483	**91039**
0.25	32627.5	-9595236	32361	0.2278	7370	**83556**
0.3	32093.7	-8969668	31787	0.2278	7239	**76186**
0.35	31480.2	-8387639	31130	0.2278	7090	**68947**
0.4	30780.8	-7814066	30385	0.2278	6920	**61857**
0.45	29989.3	-7260644	29551	0.2278	6730	**54937**
0.5	29112.0	-6727373	28621	0.2278	6518	**48206**
0.55	28130.3	-6204358	27587	0.2278	6283	**41688**
0.6	27044.4	-5692677	26431	0.2278	6020	**35405**
0.65	25817.3	-5184235	25124	0.2278	5722	**29385**
0.7	24430.7	-4681191	23636	0.2278	5383	**23663**
0.75	22841.7	-4177248	21912	0.2278	4991	**18280**
0.8	20982.7	-3667548	19854	0.2278	4522	**13290**
0.85	18724.9	-3125464	17274	0.2278	3934	**8768**
0.9	15822.9	-2530127	13755	0.2278	3133	**4834**
0.95	11687.7	-1803273	9672	0.1367	1322	**1701**
0.98	7656.8	-1176526	4184	0.0906	379	**379**
0.9999	711.7	-106520				**0**

Graphical representation of the shear force along the span is shown in Figure 2-3.

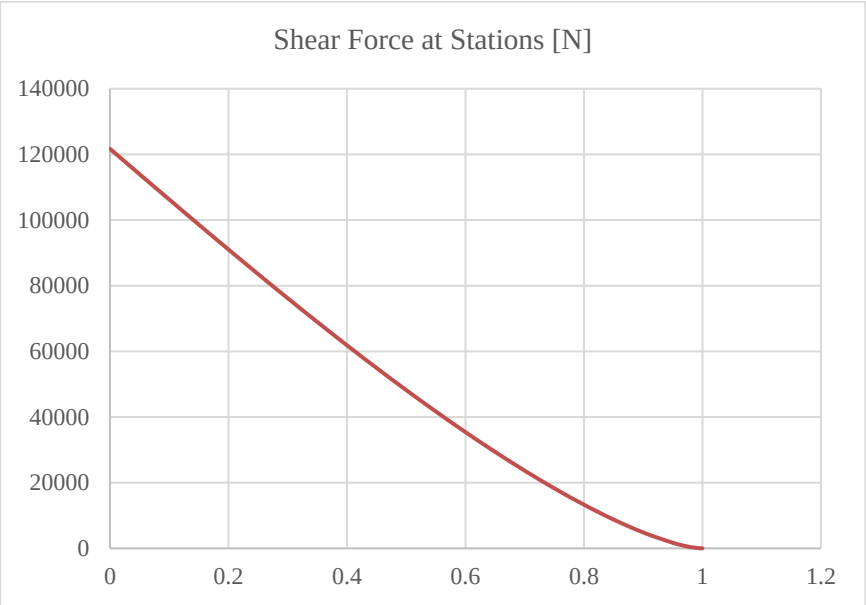

Figure 2-3 Variation of the Shear Force along the Wing Span

This is a typical shear force distribution along the wing span. It should be noted that the shear force at wing root is nearly equal to the half aircraft weight with +8g acceleration. Half aircraft weight is calculated as:

$$\frac{nW}{2} = 121644N$$

The shear force at the root is $121701N$ as shown at the upper right of Table 2-10. This is a good match and gives confidence about the reliability of the calculated loads.

Bending moments at each station can be found at this stage. Firstly, moments at the stations, caused by the shear forces acting on the next outer station, are found using the following expression:

$$M_{i+1} = V_i \cdot (y_i - y_{i+1}) \tag{2.25}$$

In addition to this, moments of the average strip force are to be calculated. Strip force is multiplied by the distance between the centroid of the trapezoidal load distribution and the station. This distance is found by:

$$d_i = \frac{L'_{i+1} \cdot (y_i - y_{i+1})}{L'_i + L'_{i+1}} \tag{2.26}$$

Then, for every section, bending moment caused by the average strip force is given by:

$$M_{s,i+1} = P_{strip,i} \cdot d_i \tag{2.27}$$

Total bending moment at a station can be calculated by summing all moments from the tip to that station. Sum of the moments caused by the shear and strip forces are also added to the total at each station. The total bending moments at each station are shown in Table 2-11.

Table 2-11 Bending Moments at Stations

Centroid of the trapezoid load [m]	Shear Force at Stations [N]	Bending Moment of the Shear Force [Nm]	Bending Moment of the Av Strip Force [Nm]	Total Bending Moment at Each Station [Nm]
0.1138	**121701**	25956	880	**236832**
0.1136	**113969**	24202	875	**209996**
0.1134	**106265**	22460	868	**184919**
0.1132	**98615**	20734	858	**161592**
0.1131	**91039**	19030	846	**140000**
0.1129	**83556**	17351	832	**120124**
0.1128	**76186**	15703	816	**101940**
0.1126	**68947**	14088	798	**85421**
0.1124	**61857**	12512	778	**70535**
0.1122	**54937**	10979	755	**57245**
0.1119	**48206**	9494	730	**45511**
0.1116	**41688**	8063	701	**35287**
0.1112	**35405**	6692	670	**26522**
0.1107	**29385**	5389	634	**19160**
0.1100	**23663**	4163	592	**13137**
0.1090	**18280**	3027	544	**8381**
0.1074	**13290**	1997	486	**4811**
0.1043	**8768**	1101	410	**2328**
0.0968	**4834**	387	303	**817**
0.0541	**1701**	52	71	**126**
0.0077	**379**	0	3	**3**
	0			**0**

Graphical representation of the bending moment along the span is shown in Figure 2-4.

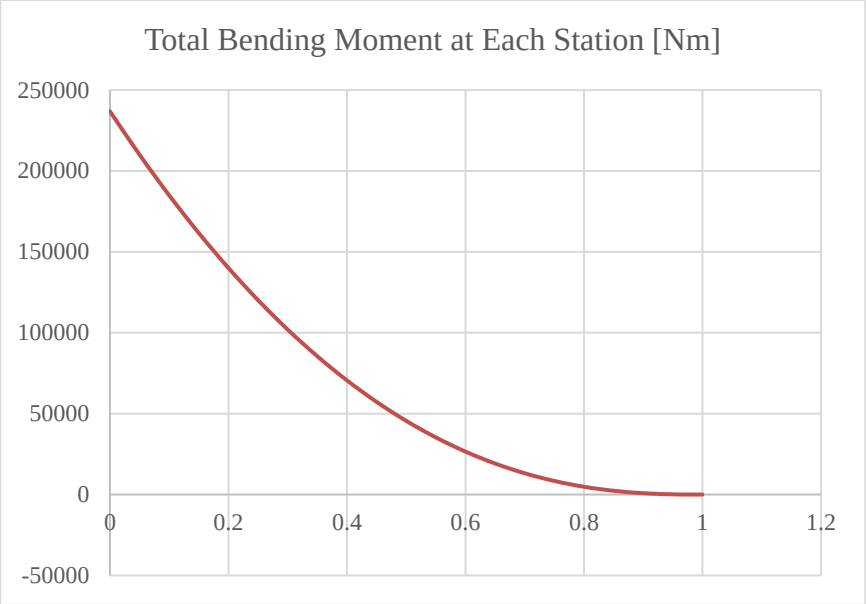

Figure 2-4 Bending Moment Distribution along the Wing Span

And finally, the pitching moment at each station are calculated by adding up the average running pitching moments at each section. Average running pitching moment load is given by:

$$M'_{MAC,run,i} = \frac{M'_{MAC,i} + M'_{MAC,i+1}}{2} \tag{2.28}$$

And average pitching moment in each section can be found by:

$$M_{p,strip,i} = M'_{MAC,run,i} \cdot (y_i - y_{i+1}) \tag{2.29}$$

Adding up the calculated values:

$$M_{p,i+1} = M_{p,i} + M_{p,strip,i} \tag{2.30}$$

Total pitching moments at each station are listed in Table 2-12.

Table 2-12 Pitching Moments at Each Section

Average Running Pitching Moment Load [N.mm/m]	Average Pitching Moment in each section [Nm]	Total Pitching Moment at Each Station [Nm]
-12649495	-2881	**-31368**
-12018258	-2737	**-28487**
-11298683	-2573	**-25750**
-10581897	-2410	**-23177**
-9912249	-2258	**-20767**
-9282452	-2114	**-18509**
-8678653	-1977	**-16395**
-8100852	-1845	**-14419**
-7537355	-1717	**-12574**
-6994009	-1593	**-10857**
-6465865	-1473	**-9264**
-5948517	-1355	**-7792**
-5438456	-1239	**-6437**
-4932713	-1123	**-5198**
-4429219	-1009	**-4075**
-3922398	-893	**-3066**
-3396506	-774	**-2173**
-2827795	-644	**-1399**
-2166700	-493	**-755**
-1489900	-204	**-262**
-641523	-58	**-58**
		0

Graphical representation of the pitching moment along the span is shown in Figure 2-5.

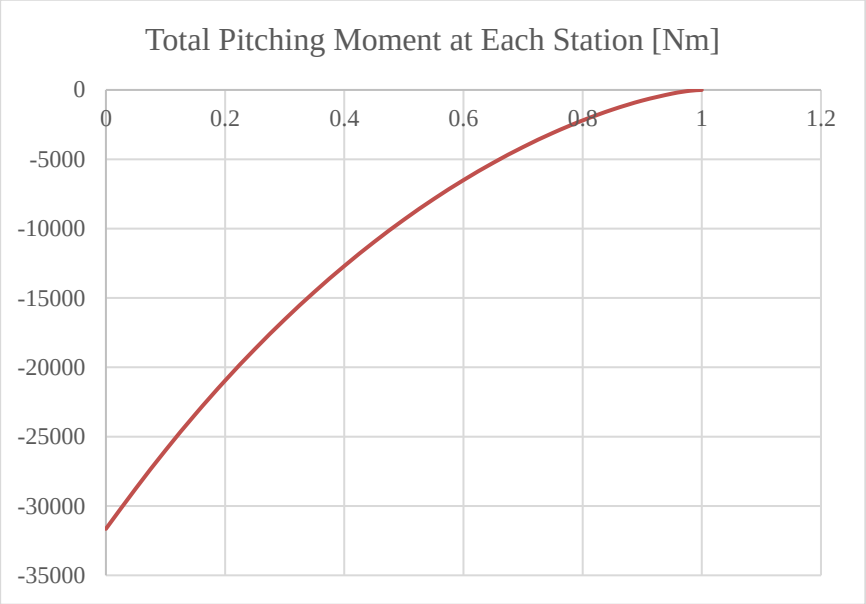

Figure 2-5 Pitching Moment Distribution along the Wing Span

In conclusion, three major internal load components at all wing stations are obtained using the external loads found by the ESDU code A9510. These internal loads are used for the sizing of the subsonic wing structures.

It should be recalled that the tool developed for this thesis automatically creates the A9510 input file. After running the A9510 program, it makes the above calculations and obtains the shears and moments along the wing. Subsequently, it stores the calculated loads and uses them for the sizing of the corresponding structure. The portion of the MATLAB code that creates the A9510 input, executes the program, and stores the output is provided in Appendix B. The sizing procedure is going to be explained in the following chapters.

2.2 Supersonic Wing Loads

For supersonic wings, ESDU A9510 program is not used because it is limited to the subsonic attached flows. Therefore, a simpler approximation method is utilized for supersonic vehicles. Schrenk's approximation is an unsophisticated and easy kind of approach that provides a very meaningful spanwise lift distribution. The method is

based on the idea that spanwise distribution is an average of the actual wing chord distribution and the ideal elliptical distribution that has the same area and same span.

Therefore, the arithmetic mean of the following is calculated:

(1) A load distribution representing the actual planform shape (rectangle, trapezoid, or triangle)

(2) Elliptic distribution of the same span and area.

To be more precise, the formula for the load per unit span over a trapezoid wing is given by:

$$w_{tr}(y) = \frac{4nW(\lambda - 1)y}{(1+\lambda)b^2} + \frac{2nW}{(1+\lambda)b} \tag{2.31}$$

It should be noted that with a taper ratio of one, above formulation results in a rectangular wing. Similarly, with a taper ratio of zero, one gets a triangle.

The elliptical load distribution is calculated by:

$$w_{el}(y) = \frac{4nW}{\pi b}\sqrt{1-\left(\frac{2y}{b}\right)^2} \tag{2.32}$$

where n is the maneuvering load factor, W is the weight of the aircraft, b is the wing span, and λ is the taper ratio of the wing.

Consequently, overall loads are given by;

$$w(y) = \frac{w_{el}(y) + w_{tr}(y)}{2} \tag{2.33}$$

where $\frac{dV}{dy} = w$

$\frac{dM}{dy} = V$.

For illustration purposes, a hypothetical supersonic aircraft with the following characteristics are used:

W = 15000 kg,

n = 9 g,

λ = 0.25,

b = 11 m.

Calculated loads using the formulas (2.31), (2.32), and (2.33) are listed in Table 2-13.

Table 2-13 Calculated Loads with Schrenk Approximation

η	y [m]	Trapezoidal Distr. [N/m]	Elliptical Distr. [N/m]	Average [N/m]
0	0	192633	153292	172962
0.05	0.55	178185	152524	165355
0.1	1.1	163738	150195	156966
0.15	1.65	149290	146231	147761
0.25	2.75	120395	132755	126575
0.3	3.3	105948	122634	114291
0.35	3.85	91501	109473	100487
0.4	4.4	77053	91975	84514
0.45	4.95	62606	66819	64712
0.46	5.06	59716	60078	59897
0.47	5.17	56827	52299	54563
0.48	5.28	53937	42922	48429
0.49	5.39	51048	30505	40776
0.492	5.412	50470	27312	38891
0.494	5.434	49892	23677	36784
0.496	5.456	49314	19351	34333
0.498	5.478	48736	13697	31217
0.5	5.5	48158	0	24079

Graphical representation of the load distribution along the wing span is shown in Figure 2-6.

It should be noted that the Schrenk loads are typically applied at the center of pressure, which is located at the back of the aerodynamic center and generally lies at around 50% chord for supersonic wings. As a result, no pitching moments are calculated by the Schrenk method because the main assumption is that the obtained loads are acting at the center of pressure. This can be regarded as a disadvantage of the method.

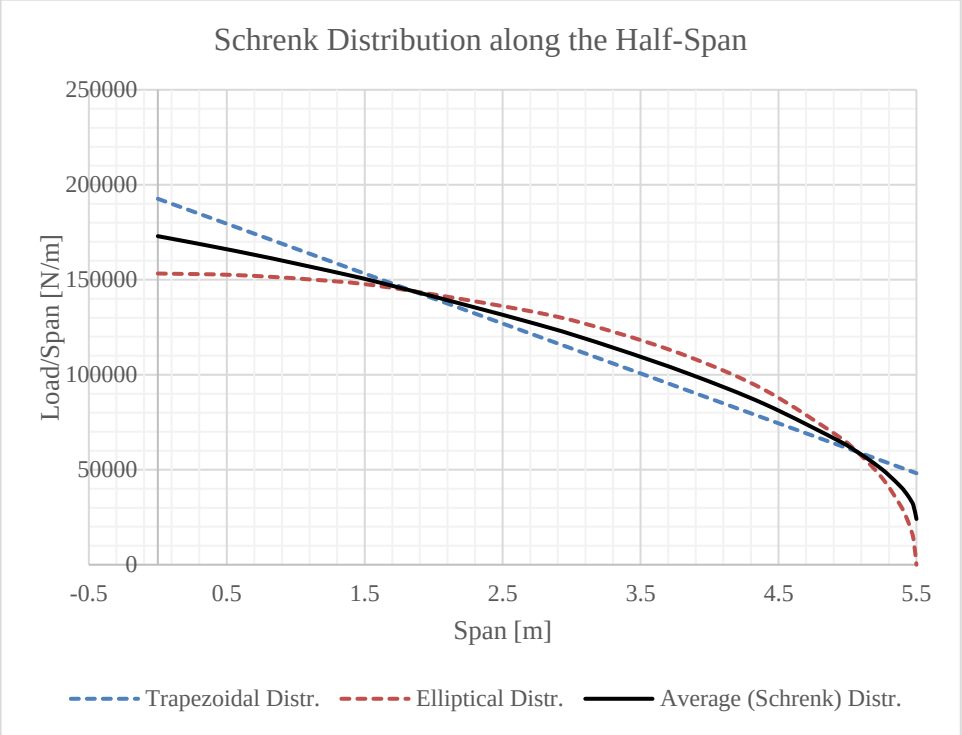

Figure 2-6 Lift Distribution along the Half-Span

Generation of the internal loads is simpler than the one at subsonic (ESDU) case. For example, integrating from zero to half span returns the shear force at the root section. Double integration returns the root moment. MATLAB symbolic toolbox makes it possible to evaluate the integrals at any required location (y) along the wing span. Therefore, the tool developed for this thesis can calculate the shears and moments in a single step at any spanwise station where the internal loads are needed.

CHAPTER 3

SIZING OF STRUCTURAL ELEMENTS

3.1 General Wing Structure Layout and Wingbox Design

Basic structural members of an aircraft wing are;

- The stringers running along the wing span,
- Ribs located at stations along the spanwise direction,
- Spars that act as main structural members along the wing,
- Skins covering all these components.

The wing is generally a cantilever structure where the root is clamped to the fuselage and the tip is free. A distributed aerodynamic pressure on the skin and concentrated loads from landing gear, power plants, passenger seats etc. are distributed as external loads to the structure. Consequently, the wing box structure is subjected to shear force, bending moment and torsion as the internal loads. Mainly, the spar caps and stringers are usually located at maximum possible distance from the neutral axis to provide bending capability and the skin encloses a large area to increase torque capability. Figure 3-1 shows all the important elements of a typical subsonic wing.

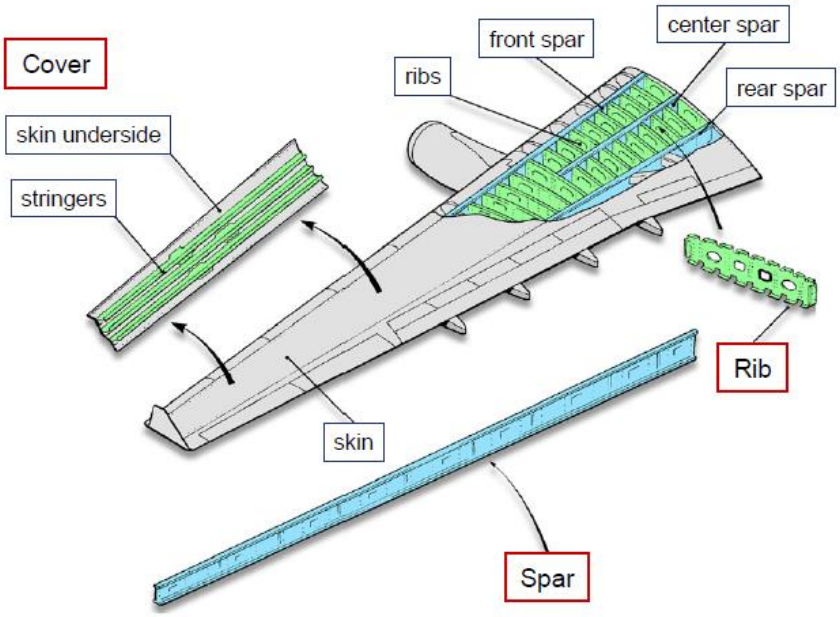

Figure 3-1 General Layout of a Wing Structure

The spar is composed of a web and the caps, which are located at the top and bottom of the web. The web essentially resists transverse shear due to the wing vertical shear force and the torque. On the other hand, the cap resists axial load caused by the wing bending moment.

The skin encloses the spar, stringers and the ribs. Main roles of the skin are to transfer the air pressure loads by transverse shear forces to the stringers, resist the wing torque by the skin shear and resist the bending moment by its axial load (tension and compression) capacity.

The stringers are slender axial members and their main function is to resist the wing bending by their axial load capacity. In addition, stringers are used as stiffening members to increase the compressive load capability of skins. Stringers also function as local load distributors as they transfer the transverse shear forces from the skin to the adjacent ribs.

The ribs are placed at certain stations along the wing span and are composed of a web, caps and vertical stiffeners. Ribs provide the aerodynamic shape of the wing by resisting the crushing load between the upper and lower skin. By doing so, they protect the airfoil shape of the wing. Ribs also redistribute the torque to spar webs and wing skins through their webs. They transfer the point loads coming from the stringers to the spars by the vertical shear through their webs. Moreover, ribs are used as panel breakers for skins to increase the compressive load capability by delaying the initial buckling.

Wing structures of subsonic and supersonic aircrafts generally differ from each other by the maximum thickness of their airfoils. Supersonic wings are generally much thinner than subsonic wings. Weissberg et al. [17] made another classification according to the bending load path provided by the skins as shown in Figure 3-2.

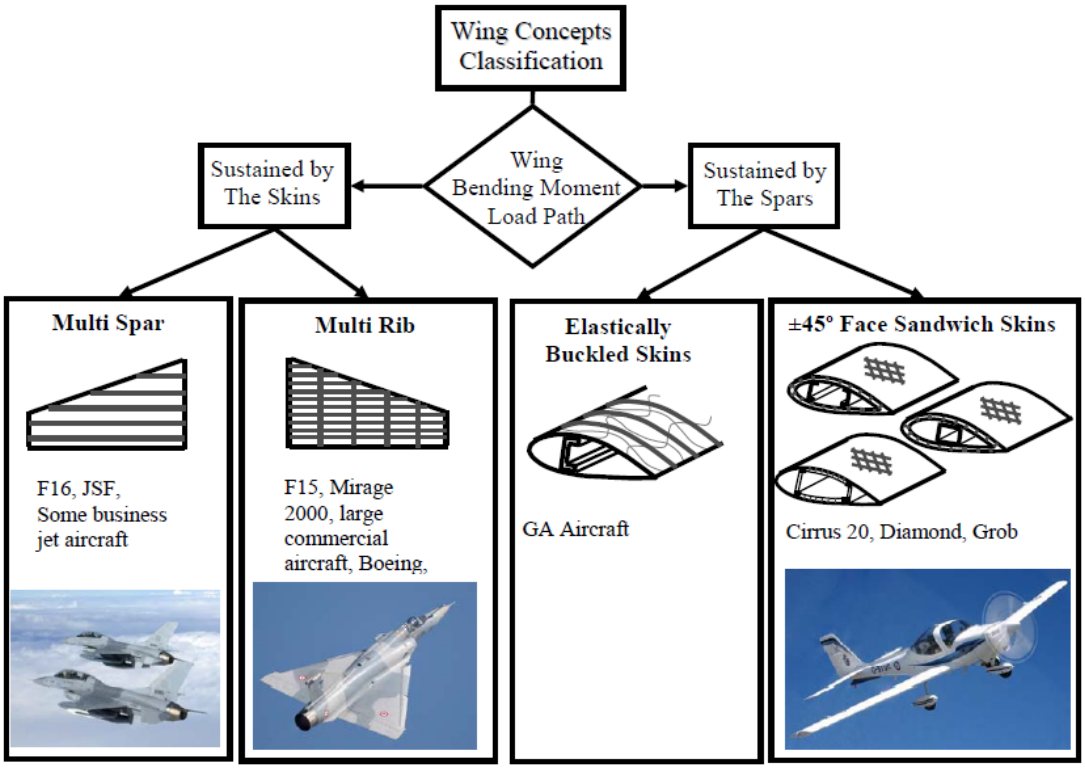

Figure 3-2 Wing Structure Classification [17]

This classification mainly states that, if the skins sustain the load, then elastic buckling of the skins is not allowed. On the other hand, when spars sustain the load, elastically buckled skins may be incorporated. Skin buckling is the main concern while deciding on the skin thickness. This is important because skins form the largest portion of the entire wing, so they have an essential contribution to the overall weight.

3.2 Wingbox Structural Idealization

Simplifying assumptions are needed to decrease the complexity of the preliminary analysis of aerospace structures. The idea behind the wingbox structural idealization is to have a mechanical model that behaves nearly the same way as the actual structure [18]. A typical wing section and the idealized version of it are shown in Figure 3-3 and Figure 3-4.

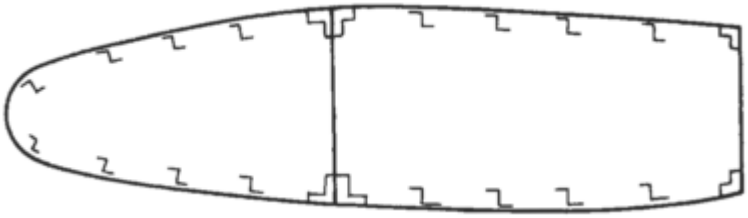

Figure 3-3 Typical Wing Section [18]

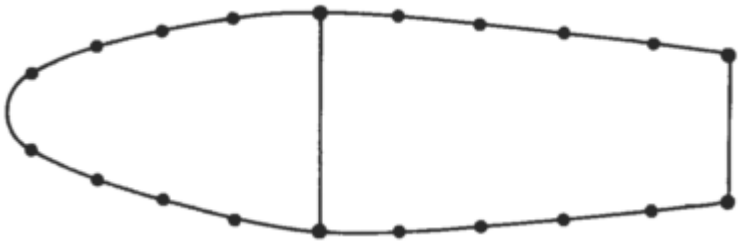

Figure 3-4 Idealized Wing Section [18]

There are some basic ideas behind the idealization process. For instance, the stringers and spar flanges have small areas when compared to entire wing section. Thus, the variation in stress over the stringer and the spar flanges are expected to be small. In other words, it can be assumed that the stress over the stringer and spar flange cross sections is constant. Therefore, spar flanges and stringers can be regarded as concentrated areas, which are generally called as *booms*. The booms are located at the mid-line of the skin because the distance of the centroids of the spar flange and the stringers to the wing section axis are nearly the same as the distance of the adjacent skin to the wing section axis.

Sometimes, the skins and webs are assumed to carry only shear stress whereas all axial stress is assumed to be carried by the flanges and stringers. In this thesis, this assumption is not used. Skins and webs are effective in both shear and axial load in the approach taken in this thesis.

The wingbox is regarded as a multicell box beam in this thesis. It is necessary to have a closer look at the behavior of the multicell box under certain loading conditions. More specifically, the wingbox is effective in shear, bending, and torsion and the idealization approach taken is very important to determine the stress states of structural elements.

In this thesis, all panels (skins and webs) are assumed to have a constant shear flow. The classical approach to obtain the shear flows is outlined in the following section.

3.2.1 Shear Flow and Shear Stress Calculations

Cross section of a sample multicell box beam can be used for demonstration in this section. Figure 3-5 shows a vertical shear load acting on a closed section with two cells.

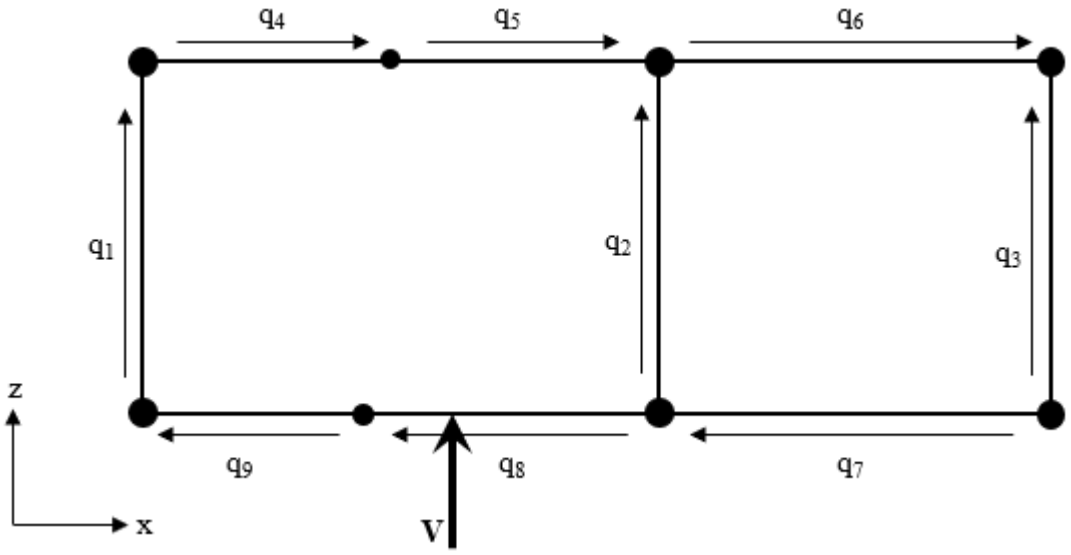

Figure 3-5 Example Multicell Closed Section

Considering the upper left joint, the representation shown in Figure 3-6 is obtained.

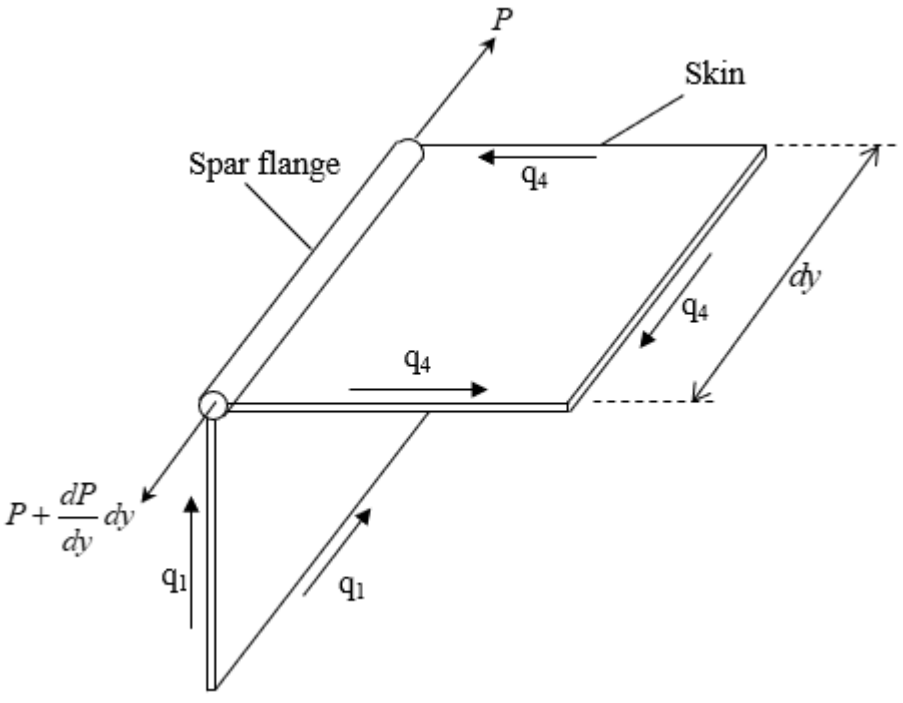

Figure 3-6 Upper Left Joint Equilibrium

Force equilibrium along the y direction:

$$-P + P + \frac{dP}{dy}dy + q_1 dy - q_4 dy = 0$$

Therefore,

$$q_1 = q_4 - \frac{dP}{dy}$$

Spars and the upper skin seem to be perpendicular to each other in Figure 3-5 but the angle between the panels actually does not matter because the shear flows in the above equations would always be in the y direction. For this reason, the shear flows can be renamed as flows *into* the joint and flows *out of* the joint to have a more general expression. Therefore,

$$q_{out} = q_{in} - \frac{dP}{dy} \tag{3.1}$$

It is known that,

$$P = A \cdot \sigma_y$$

Therefore, rewriting Equation (3.1),

$$q_{out} = q_{in} - \left(A\frac{d\sigma_y}{dy} + \sigma_y \frac{dA}{dy} \right)$$

where *A* stands for the spar flange or boom area at the joint. The area is constant within the section. Therefore, the second term in the differentiation drops. In a more general case, the joint equilibrium takes the form:

$$q_{out} = q_{in} - A\frac{d\sigma_y}{dy} \tag{3.2}$$

Further assumptions can be made to simplify Equation (3.2). For instance, normal stress can be assumed to be caused by the bending of the wing where only the M_x moment exist, i.e. $M_z = 0$. Moreover, symmetric section assumption can be made for the wing section. Although airfoil shapes and material distribution are not fully symmetric, this is not a cruel assumption. This assumption drops all the product moment of inertia (I_{xz}) terms in the general bending stress formula. Thus,

$$\sigma_y = \frac{M_x z}{I_x}$$

Inserting into the load expression,

$$\frac{dP}{dy} = A\frac{d}{dy}\left(\frac{M_x z}{I_x}\right)$$

Or,

$$\frac{dP}{dy} = \frac{Az}{I_x}\left(\frac{dM_x}{dy}\right)$$

It should be recalled that the shear force is the derivative of the bending moment:

$$\frac{dM_x}{dy} = V_z$$

Additionally, the first moment of area about x is given by:

$$Az = Q_x$$

Consequently, rewriting Equation (3.2), one obtains Equation (3.3):

$$q_{out} = q_{in} - \frac{V_z Q_x}{I_x} \tag{3.3}$$

Equation (3.3) is a simple and easy form of the joint equilibrium that can be repeated for every joint within the section. Including only the first moments of the spar

flanges and the stringers in Equation (3.3) accounts for constant shear flow panels, which is very advantageous to obtain all shear stresses within the section.

Considering the multicell box shown in Figure 3-5, nine shear flows are to be calculated. Equation (3.3) can be used for all eight joints. However, one of the eight equations is going to be redundant. Therefore, seven equations can be obtained to solve for the shear flows. More generally, if the total number of shear flows is *m*, and the total number of closed cells is *n*; then *m-n* equations can be obtained using the joint equilibriums.

The missing *n* equations can easily be obtained by twist equalities and the moment equilibrium within the section. For the multicell box shown in Figure 3-5, twist angles of the two cells have to be equal to each other, and this provides one extra equation for the system. More generally, twist equalities give *n-1* equations. The last equation comes from the moment equilibrium in the xy plane. Therefore, a total of *m* equations corresponding to *m* unknowns are obtained so that all the shear flows can be calculated.

Twist angle equality of the cells is derived from the general expression for the rate of twist of a loaded closed section;

$$\frac{d\theta}{dz} = \frac{1}{2A}\oint \frac{q_s}{Gt} ds \tag{3.4}$$

where G is the shear modulus, A is the area of the closed section, and t is the panel thickness.

Considering the illustrative multicell closed section shown in Figure 3-5, equality of the twists of the two cells takes the form:

$$\left(\frac{1}{2AG}\sum \frac{q\Delta s}{t}\right)_{cell-1} = \left(\frac{1}{2AG}\sum \frac{q\Delta s}{t}\right)_{cell-2} \tag{3.5}$$

where s term stands for the cross-section length of each panel.

Lastly, the moment equilibrium of the externally applied shear, pitching moment and the panel shears within a section is used to complete the system of equations:

$$\sum M_{external} = \sum M_{internal} \tag{3.6}$$

After having all the shear flows within the section, shear stresses in a panel *i* can be calculated by dividing the shear flow in a panel to the thickness of the panel.

$$\tau_i = \frac{q_i}{t_i} \tag{3.7}$$

3.2.2 Axial Stress Calculations

In this thesis, axial stress is assumed to be caused by the wing bending only. No additional longitudinal direct stress (tension or compression) comes from the external loading. Symmetric bending assumption was already explained and used for the derivation of Equation (3.3). Therefore, at any distance *z* from the neutral axis, the axial stress is given by;

$$\sigma_y = \frac{M_x z}{I_x} \tag{3.8}$$

For subsonic wings, an important treatment is to be added in order to calculate the axial stresses in the structural members after the local buckling of the skins. In this thesis, the user of the developed tool can allow compressive buckling of the upper skin panels before the limit load is reached. Chapter 5 explains post buckling load redistribution phenomenon in extensive detail. This section emphasizes on the calculation of the axial stresses in the section after buckling.

For the post buckling stress calculations, the stress distribution and the effective second moment of the cross-section must be calculated with an iterative approach. Following steps are followed:

1. Buckled panels are identified.

2. The *equivalent thickness* of the buckled panel, which is obtained using the *effective widths* in post buckling regime, is obtained using the stiffener stresses. The equivalent thickness is the portion of the original thickness that remains effective after the initial buckling. Detail for the definition and the calculation of the equivalent thickness is provided in Section 5.3.2.3. In the first step, equivalent thicknesses are calculated using the stiffener stresses in a fully effective (non-buckled) cross section.

3. Original thicknesses of upper panels are replaced with the equivalent thicknesses.

4. Centroid of the cross-section is updated due to the decrease in the upper panel thicknesses. Then the moment of inertia of the cross-section is recalculated.

5. All axial stresses are calculated with the updated moment of inertia.

6. Updated stresses are used to calculate the new equivalent thicknesses.

7. Steps 2 to 6 are repeated until the convergence. It should be noted that the convergence is reached for all parameters such as the effective widths, equivalent thicknesses, cross-section second moment, and the stiffener stresses.

Above steps are illustrated in the flowchart provided in Figure 3-7.

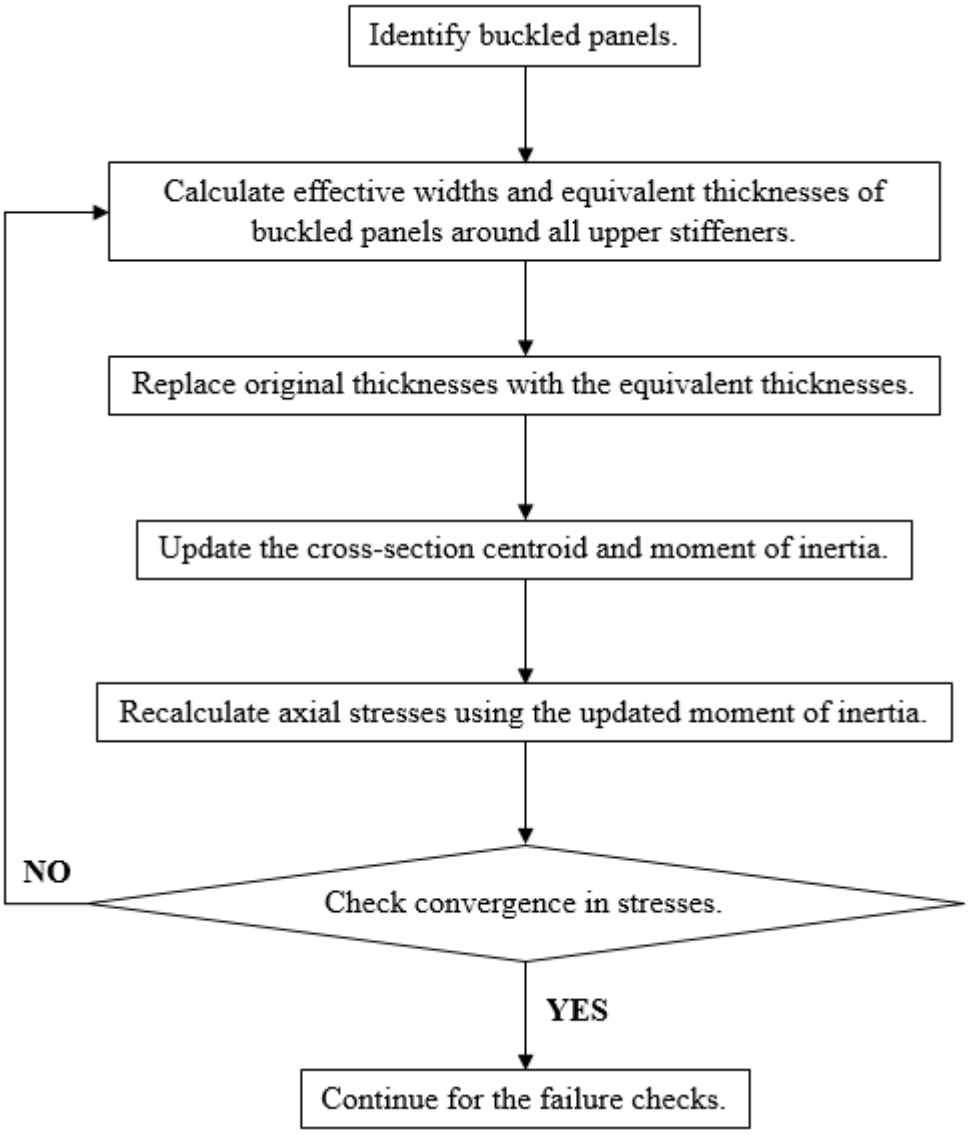

Figure 3-7 Flow Chart of the Post-Buckling Stress Calculation

It should be recalled that elastic buckling of skins before the limit load is not acceptable for supersonic wings. Therefore, the above steps are valid only for subsonic wings.

For supersonic wings, buckling resistant panels are fully effective for the second moment of the cross section. Thus, all axial stresses can be found in a single step.

3.3 Buckling Checks

3.3.1 Buckling Under Pure Compression

A rectangular plate with thickness *t* under applied compressive stress, σ_c is shown in Figure 3-8.

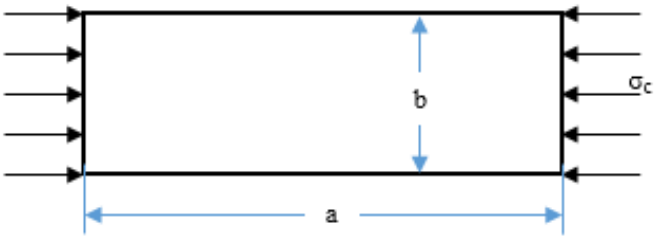

Figure 3-8 Rectangular Flat Plate under Pure Compression

Compressive buckling strength of the plate can be found using Equation (3.9) :

$$\sigma_{cr} = \frac{\pi^2 k_c E}{12(1-\nu^2)}\left(\frac{t}{b}\right)^2 \tag{3.9}$$

where k_c is the buckling coefficient. The buckling coefficient depends on the aspect ratio of the plate *a/b* and the edge boundary (fixity) conditions. In the case when the compressive stress σ_c is greater than the critical buckling stress σ_{cr}, the panel buckles.

Buckling coefficient k_c that depends on the edge fixity can be read from Figure 3-9.

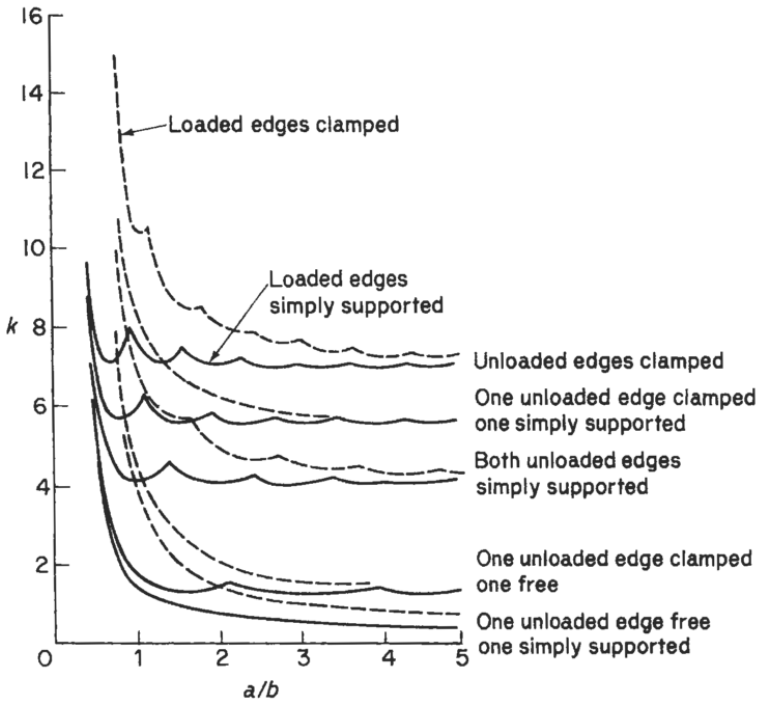

Figure 3-9 Buckling Coefficients for Flat Plates in Compression [18]

For simply supported loaded and unloaded edges and the aspect ratio *a/b* greater than 3, the buckling coefficient is approximately equal to 4. Thus, the critical buckling expression takes the form of Equation (3.10) for the aluminum material:

$$\sigma_{cr} = \frac{\pi^2 \cdot 4 \cdot E}{12(1-0.3^2)}\left(\frac{t}{b}\right)^2 = 3.62E\left(\frac{t}{b}\right)^2 \tag{3.10}$$

where Poisson ratio of aluminum is taken as 0.3. It should be noted that Equation (3.10) calculates the critical buckling stress under pure compression. In the case of combined loading, buckling criterion would change. Buckling under combined loading conditions is examined in the following sections.

3.3.2 Buckling under Pure Shear

Critical shear stress for the buckling of a flat plate is defined by Equation (3.11).

$$\tau_{cr} = \frac{\pi^2 k_s E}{12(1-\nu^2)}\left(\frac{t}{b}\right)^2 \tag{3.11}$$

where k_s is the shear buckling coefficient, that depends on edge boundary (fixity) conditions and aspect ratio of the plate *a/b*. Shear buckling coefficient can be extracted from Figure 3-10.

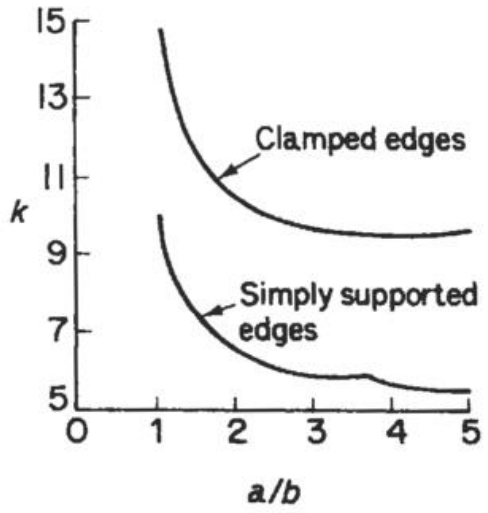

Figure 3-10 Shear Buckling Coefficients for Flat Plates [18]

It is important that *b* stands for the shorter dimension of the rectangular plate in Equation (3.11). By definition, if the shear stress τ exceeds the critical stress τ_{cr}, shear buckling occurs.

3.3.3 Buckling under In-Plane Bending

For in-plane bending, elastic buckling equation is given by:

$$\sigma_{b,cr} = \frac{\pi^2 \cdot k_b \cdot E}{12(1-\nu^2)}\left(\frac{t}{b}\right)^2 \tag{3.12}$$

It should be noted that the equation is the same as for compression except for the coefficient. Buckling coefficient is provided in Figure 3-11.

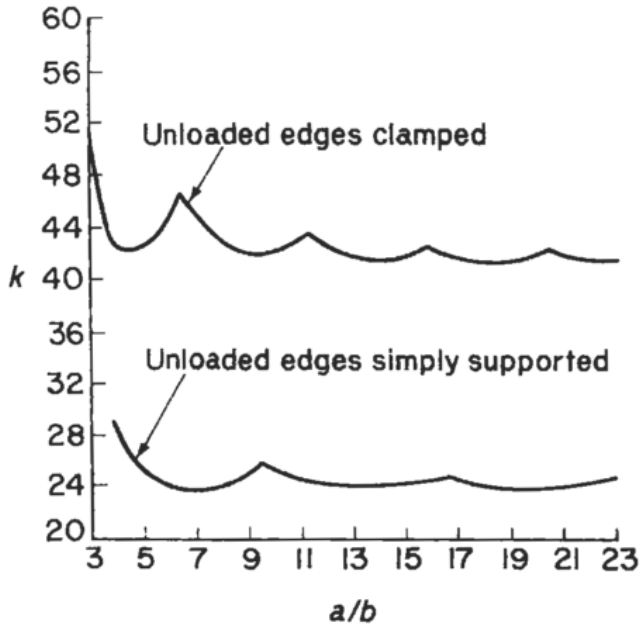

Figure 3-11 Buckling Coefficients for Flat Plates Subject to In-Plane Bending [18]

It is obvious that the buckling coefficient k_b is much larger than compression coefficients k_c. This is because the plate has shorter wavelength when it buckles under in-plane bending. Figure 3-12 [19] illustrates this fact as the waves are of length 2/3 *b* in the example plate. Smaller buckle patterns result in high buckling coefficients.

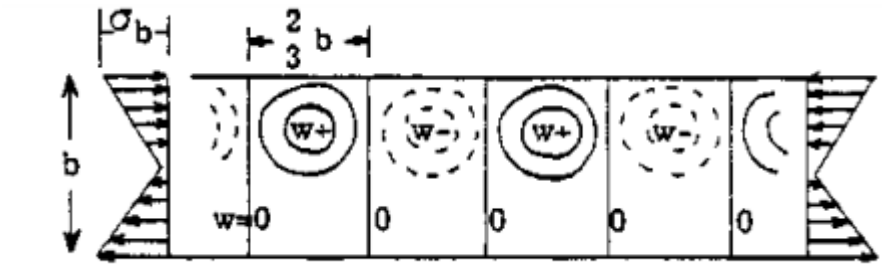

Figure 3-12 In-Plane Bending Buckle Patterns [19]

3.3.4 Buckling under Combined Compression and Shear

A rectangular flat plate under compression and shear loading is shown in Figure 3-13.

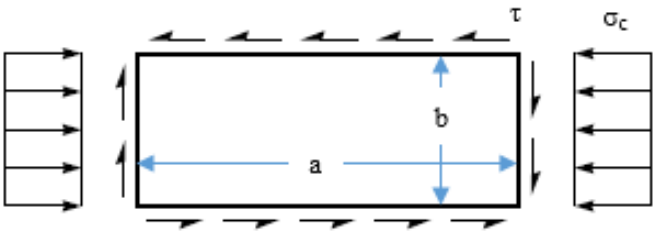

Figure 3-13 Flat Rectangular Plate under Combined Compression and Shear

Bruhn [19] defines the Interaction Equation (3.13) to determine the safety margin of a flat rectangular plate under combined compression and shear.

$$\frac{\sigma_c}{\sigma_{cr}} + \left(\frac{\tau_c}{\tau_{cr}}\right)^2 = 1 \tag{3.13}$$

3.3.5 Buckling under Combined Compression and Bending

For this case, Bruhn [19] gives a similar interaction equation;

$$\frac{\sigma_c}{\sigma_{cr}} + \left(\frac{\sigma_b}{\sigma_{b,cr}}\right)^{1.75} = 1 \tag{3.14}$$

3.3.6 Buckling under Combined Bending and Shear

The interaction equation for this combined load is [19]:

$$\left(\frac{\sigma_b}{\sigma_{b,cr}}\right)^2 + \left(\frac{\tau_c}{\tau_{cr}}\right)^2 = 1 \tag{3.15}$$

3.4 Strength Checks

Reduced form of the von Mises equation is used to make the strength checks for structures under combined axial and shear stresses:

$$\sigma_{vM} = \sqrt{\sigma^2 + 3 \cdot \tau^2} \tag{3.16}$$

Von Mises stress is compared with the material allowable stress values in order to check for the failure.

3.5 Failure Conditions for Structural Elements

Buckling and strength checks are introduced in the previous sections. In this section, the application of those checks to individual structural elements is outlined.

3.5.1 Spar Flanges and Stringers

It is a common design practice that the spar caps and stringers must return a positive margin under *ultimate* loads. Ultimate loads are obtained by applying the *ultimate factor* to the limit (calculated) loads. An ultimate factor (*UF*) of 1.5 is commonly used in aircraft industry.

The general criteria of material failure states that the permanent, detrimental deformation (yielding) shall not occur before the limit load. In addition, the structure shall not collapse under the ultimate loading. Therefore, limit check is to be made using the material yield allowable whereas the ultimate check is made using the ultimate allowable.

Since the ultimate material allowable (F_{tu}) of common aerospace metals is generally less than the 1.5 times of their yield allowable (F_{ty}), the ultimate check covers the limit check. For instance, Aluminum 7050 T7451, which is a very common aerospace material, has an F_{tu} of 510 MPa. Its F_{ty} value is around 420 MPa, which is greater than the two thirds of the F_{tu}. Consequently, the following checks in Equations (3.17) and (3.18) also cover the limit checks.

For upper stringers and spar flanges (stiffeners in compression), following condition should be satisfied:

$$\frac{F_{cy}}{\sigma_{stf} \cdot UF} > 1.00 \tag{3.17}$$

Similarly, for lower stringers and spar flanges (stiffeners in tension):

$$\frac{F_{tu}}{\sigma_{stf} \cdot UF} > 1.00 \tag{3.18}$$

It is important to note that the σ_{stf} in Equations (3.17) and (3.18) are the stiffener stresses at the limit load. Although the ultimate tensile strength is used for the lower side, upper stiffeners are checked with compression yield strength (F_{cy}). This is mainly due to the behavior of ductile metals under compression. Under compression, the material yields and swells out but no fracture is observed. The material continues to support the load. Therefore, it is not possible to set an ultimate strength for compression [20].

3.5.2 Upper Skins

Buckling of upper skins is checked using the combined compression and shear formulation in Section 3.3.4.

Determination of the shear and buckling coefficients k_s and k_c is very important for the buckling checks. As already stated in Section 3.3, the buckling coefficients depend on the edge support (fixity). Therefore, the selection between simply supported and clamped boundaries is very essential.

3.5.2.1 Determination of k_c

In this thesis, spar flanges are assumed to provide clamped boundaries, whereas the ribs and stringers are assumed to provide simply supported boundaries. Therefore, the solid lines in Figure 3-9 are valid because the loaded edges of upper skins (rib attachments) are simply supported. Support condition of the unloaded edges are determined according to the type of the stiffeners they are attached. For example, if two spar flanges enclose an upper skin panel, then the unloaded edges are clamped. On the contrary, if two stringers enclose the panel, then the unloaded edges are simply supported. Lastly, if a stringer at one end and a spar flange at the other end enclose the panel, then the curve named “one unloaded edge clamped one simply supported” in Figure 3-9 is used.

The tool developed for this thesis automatically gets the compressive buckling coefficient of upper skins. All curves in Figure 3-9 are digitized using more than 500 data points. As an illustration, the first few entries of the text file containing the data points of simply supported loaded and unloaded edges are provided in Appendix C. The tool calculates the aspect ratio *a*/*b* of each upper panel, and then finds the closest aspect ratio value (in column 1) in the text file, and gets the corresponding buckling coefficient (from column 2 of the text file).

3.5.2.2 Determination of k_s

The shear buckling coefficient is determined by a similar approach. It should be recalled that Figure 3-10 is used to get k_s. The figure has two curves corresponding to simply supported and clamped edges. The level of edge support is approximated using a fixity value in order to obtain correct shear buckling coefficients. As already stated, spar flanges are assumed to provide clamped boundaries, whereas the ribs and stringers are assumed to provide simply supported boundaries. Thus:

- *Fixity* = 0.5 if two spar flanges enclose the upper panel,
- *Fixity* = 0.0 if two stringers enclose the upper panel,
- *Fixity* = 0.25 if a stringer at one end and a spar flange at the other enclose the panel

Then the shear buckling coefficient can be calculated by:

$$k_s = \left(k_s\right)_{cl} \cdot Fixity + \left(k_s\right)_{ss} \cdot (1 - Fixity) \tag{3.19}$$

where subscript *cl* stands for the shear buckling coefficient for clamped boundaries and *ss* stands for the shear buckling coefficient for simply supported boundaries.

It should be recalled that k_c curves are available for various edge conditions. However, for k_s, there are only two curves available (one for clamped edges and one for simply supported edges). Hence, Equation (3.19), which is derived from common

design practices, is necessary for the shear buckling to account for the intermediate edge conditions.

The tool automatically gets the shear buckling coefficients of each upper skin. It calculates the aspect ratios, read the valid text file, and then utilize Equation (3.19) to solve for the k_s value.

3.5.2.3 Safety Margin Calculation

Firstly, the upper skins must have a positive margin with respect to the percentage of the limit load specified for elastic buckling. For instance, if the user sets an initial buckling of 50% limit load, then the interaction equation (3.13) should return a safety margin greater than -0.5 as shown below.

$$\frac{2}{\left[\frac{\sigma_c}{\sigma_{cr}}+\sqrt{\left(\frac{\sigma_c}{\sigma_{cr}}\right)^2+4\left(\frac{\tau_c}{\tau_{cr}}\right)^2}\right]}-1>-0.5 \tag{3.20}$$

Re-arranging:

$$\frac{2}{0.5\cdot\left[\frac{\sigma_c}{\sigma_{cr}}+\sqrt{\left(\frac{\sigma_c}{\sigma_{cr}}\right)^2+4\left(\frac{\tau_c}{\tau_{cr}}\right)^2}\right]}>1.00 \tag{3.21}$$

If the initial buckling of the skins is not allowed before limit load, then the initial buckling coefficient of 0.5 in Equation (3.21) would drop.

Secondly, the upper skins must have a positive margin under ultimate load against the von Mises failure criterion.

$$\frac{F_{tu}}{\sigma_{vM}\cdot UF}>1.00 \tag{3.22}$$

In the end, the tool selects the minimum of two margins coming from Equations (3.21) and (3.22) for the following steps.

3.5.3 Lower Skins

Common design practices imply that the lower skins must have a positive shear buckling margin under the limit load according to Section 3.3.2. Determination of k_s is the same as the one outlined in Section 3.5.2.2.

It is known that tension has a relief effect on panel buckling. Therefore, no combined tension and shear buckling check exists in the literature. However, in order to have a reasonable sizing for the lower skins, a combined compressive and shear buckling check is carried out. Since the wing load cases used in this thesis are based on the most critical positive limit load factors, lower sides are always in tension. However, aircrafts also have negative load factors, which is generally smaller than the half of the positive load factors. Considering this fact, the lower skins are checked under an artificial load case in which half of the applied tensile stresses is assumed compressive. Applied shear stress is also halved. Thus, the following interaction equation is utilized for the lower skins as a second check.

$$\frac{2}{\left[\frac{0.5\cdot\sigma_c}{\sigma_{cr}}+\sqrt{\left(\frac{0.5\cdot\sigma_c}{\sigma_{cr}}\right)^2+4\left(\frac{0.5\cdot\tau_c}{\tau_{cr}}\right)^2}\right]}>1.00 \tag{3.23}$$

It should be noted that k_c for lower skins is also determined using the approach outlined in Section 3.5.2.1.

Lastly, the lower skins must have a positive margin under ultimate load against the von Mises failure criterion. Thus, Equation (3.22) is also valid for the lower skins.

Consequently, the tool selects the minimum of the three margins of safety coming from the shear buckling check at the limit load, combined shear and compression buckling check at the half of the limit load, and Von Mises check at the ultimate load.

3.5.4 Spar Webs

Spar webs must have a positive buckling margin for combined bending and shear under ultimate load. Section 3.3.6 is used for the combination checks. It should be recalled that the buckling checks for the skin panels are not performed at the ultimate load. Considering the entire wing cross-section, the buckling of spar webs is more complicated than the buckling of skins. This is the reason why spar webs are designed buckling resistant at the ultimate load. Thus, the following check must be satisfied for the webs.

$$\frac{1}{UF \cdot \sqrt{\left(\frac{\sigma_b}{\sigma_{b,cr}}\right)^2 + \left(\frac{\tau_c}{\tau_{cr}}\right)^2}} > 1.00 \tag{3.24}$$

Secondly, the webs must have a positive margin under ultimate load against the von Mises failure criterion. Thus, Equation (3.22) is also valid for the webs.

The tool selects the minimum of two margins to use for the following steps.

3.5.5 Rib Webs

In this thesis, ribs are assumed as simply supported rectangular plates. Length of the plate (side *a*) is taken as the distance between the front spar and the rear spar. Height of the plate (side *b*) is equal to the height of the longest spar web. It should be noted that all spars divide the ribs into smaller subpanels. However, this is ignored in rib sizing as the rib web is assumed as a single panel.

The rib webs are sized according to the shear stress acting on them. The largest shear flow in each design station is assumed to act on the entire rib web. Then, the rib thickness is calculated such that the shear buckling according to Equation (3.11) would not occur until the ultimate load.

The sizing results are going to show that the ribs are going to be the smallest contributor to overall wing weight. This is because they are sized according to the shear buckling only in this thesis. In a real-life situation, however, ribs may be

subject to loads coming from underwing carriages, fuel pressure or landing gear loads, which are not covered by the preliminary design load cases.

3.6 Design Simplifications and Assumptions

Some important assumptions have to be made to decrease the complexity of the preliminary design problem. Very important assumptions are already outlined in Section 3.2 for the idealization of the wingbox. Some additional remarks are provided in this section.

- Firstly, the portion of the wing between the front and the rear spars is the main concern of this study. In other words, the contributions of the leading and trailing edges are ignored. This assumption is generally valid for all wings except for certain light aircraft wings having only two spars. Leading edge portion may be important in that case. Since the tool developed for this thesis is expected to be used for more advanced aircrafts, ignorance of the leading edge would not be a problem.

- All panels in the longitudinal cross section are assumed flat. In other words, curvature due to the airfoil shape is ignored. Figure 3-14 shows a real airfoil shape (red, dotted lines) and the region of concern (black solid lines) formed by three spars, two stringers, and nine flat panels. It should be noted that the buckling checks stay on the conservative side due to this assumption because the curvature actually improves the buckling strength.

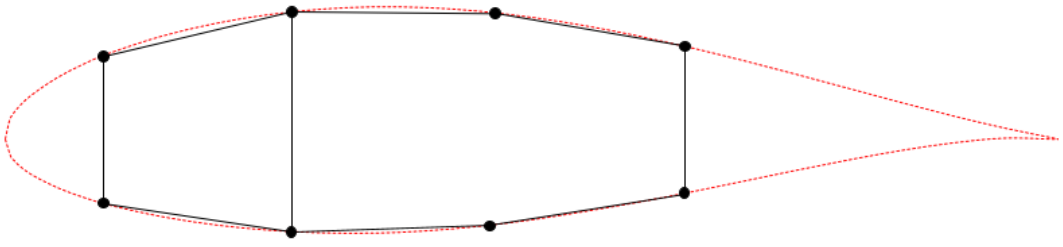

Figure 3-14 Representative Airfoil and Design Region

- The thin plate assumption, which is a very basic assumption in structural idealizations, is made and the stress variations within the thickness of the panels are ignored.

- Taper effects inside a section (i.e. between two stations) are ignored. Taper is considered while calculating the loads as already stated in Chapter 2. On the contrary, the dimensions and loads of a section are taken constant at the station closer to the root side. This is also a conservative approach since buckling characteristics also improve towards the tip because the panel width *b* gets smaller.

- Individual skin thicknesses and flange areas are constant within a section and changed discretely within sections.

- Skin Thickness Configuration: Skin thicknesses within a section are directly proportional to the vertical distance between the mid panel and the location of the *initial* centroid of the cross-section. The initial centroid is calculated by assuming that all panel thicknesses are the same. Since panels and flanges do not have any sizes at the beginning of the process, a constant thickness is assumed for all panels (upper skins, lower skins, and webs) to calculate the initial centroid. It should be noted that the location of the initial centroid is not the actual location of the centroid of the section. It is just an approximate location used to obtain the thickness coefficients of the skins. For instance, considering the cross-section shown in Figure 3-15, the distances of the upper skins to the initial centroid are denoted as d_i. Assuming that d_1 is the shortest distance in this configuration;

    - Thickness of the upper left panel is assigned as t_{us1}

    - Thickness of upper right panel (t_{us3}) is assigned as $t_{us1} \cdot \frac{d_3}{d_1}$

- Thickness of upper middle panel (t_{us2}) is assigned as $t_{us1} \cdot \frac{d_2}{d_1}$

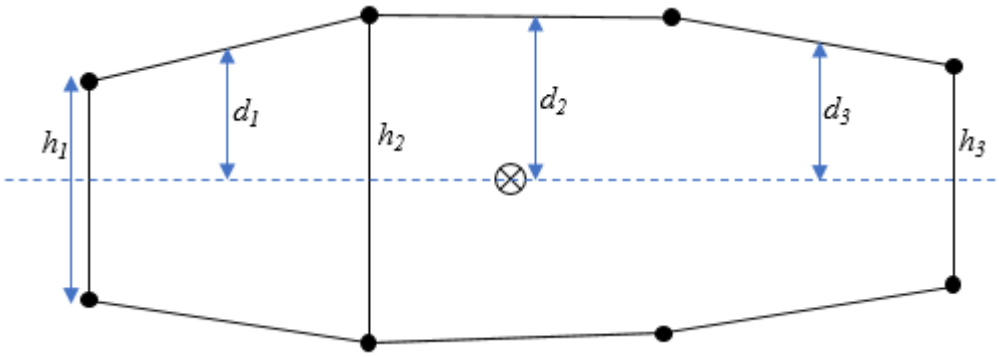

Figure 3-15 Distances of the Upper Panels to the *Initial* Centroid

Same thickness assignment approach is also valid for the lower skins.

It should be noted that the above thickness distribution has three advantages. First advantage is about the moment of inertia. Bending moment is very dominant for the wingbox sizing, hence the second moment of the area is very important. Above distribution favors the most effective panels so that the second moment of inertia gets sufficiently large. In addition, the above distribution would result in a smooth thickness transition between the neighboring panels. This is because the neighbor panel thicknesses are related to each other with a linear relation. If all the panels were sized independently from each other, then unrealistic thickness jumps within the section would be encountered. Lastly, since all panel thicknesses are dependent on a single thickness, the number of independent design variables is decreased.

- Spar Web Thickness Configuration: An approach similar to skin thickness distribution is taken for the spar web thicknesses. If the height of the shortest web is denoted h_3 as shown in Figure 3-15, then;

- Thickness of the rear spar (the spar at the right of the figure) web is assigned as t_w,
- Thickness of the front spar (the spar at the left of the figure) web is assigned as $t_w \cdot \frac{h_1}{h_3}$
- Thickness of the main spar (the spar in the middle) web is assigned as $t_w \cdot \frac{h_2}{h_3}$

Spar webs are generally sized according to buckling under combined bending and shear. For the buckling checks, the axial stress at the junction of spar web and spar flange is used. It is obvious that the axial stress linearly increases with the height of the web. For this reason, the above configuration is reasonable.

- Spar Flange Configuration: Spar flange areas must have a reasonable minimum area in order to satisfy the assembly requirements and clamped edge conditions. Therefore, an approximate minimum cap area is obtained using a common T-shape. Figure 3-16 shows a T-section spar flange with double row attachments to the skin and the web.

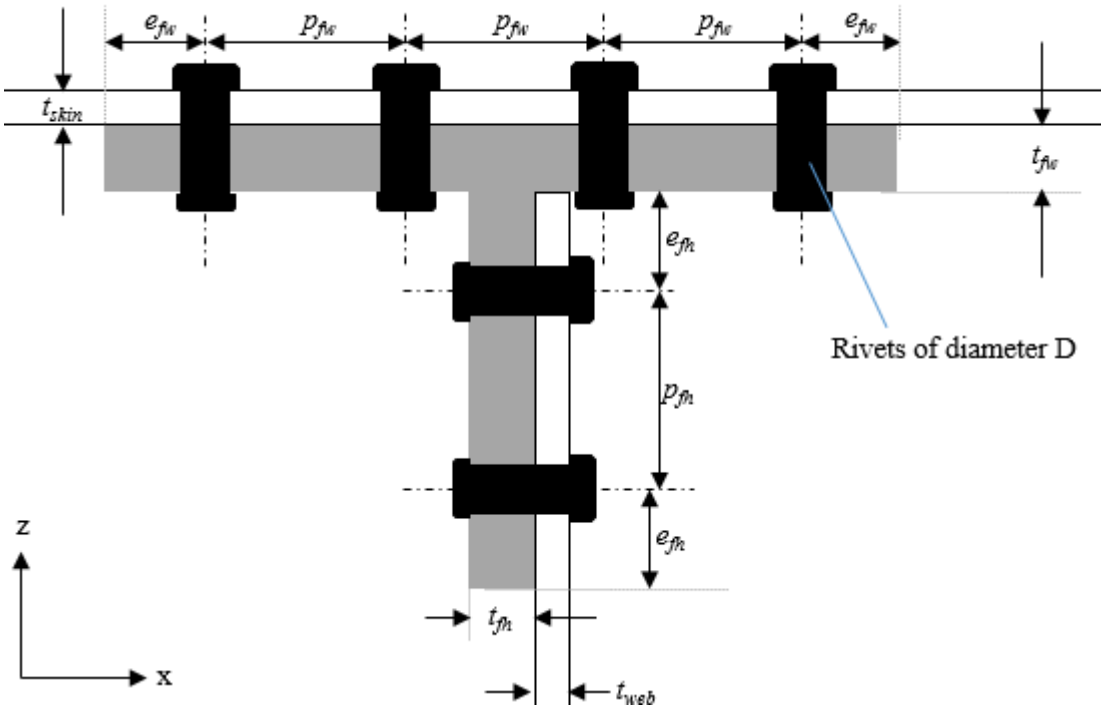

Figure 3-16 T-shape Spar Cap with Double Row Fasteners on Each Adjacent Panel

It should be noted that using the double row fasteners for skin and web attachments are among the rules of thumb for spar design [21]. Thus, single row fasteners are avoided. Double row fasteners can be assumed to secure the clamped edge condition.

The spacing of the rivets can be approximated with the general fastener spacing rules. It is known that the edge distance (e) is not less than two diameter ($2D$) and the pitch distance (p) is approximately four diameter ($4D$) [21].

Another approximation can be made for the relation between the rivet diameter and the total thickness of the stack height it is attached to. For example, the skin attachments in Figure 3-16 are fastening a total thickness of the skin (t_{skin}) and spar flange width (t_{fw}). Aircraft design guidelines state that

the rivet diameter shall not be less than the half of the total thickness they are used to attach, i.e. $D_{min} = 0.5\ t_{total}$.

Last assumption can be made for the relation between the flange thicknesses and the adjacent panel thickness. It can be assumed that the flange thickness should be at least two times thicker than the adjacent skin panel, i.e. $t_{fh,min} = 2\ t_{web}$ and $t_{fw,min} = 2\ t_{skin}$. It should be noted that this assumption is based on a rough approximation. It is not easy to have this kind of general expressions for real life applications but this assumption is logical and useful for the purposes of this thesis.

Going back to Figure 3-16,

$$Flange\ width = 3p_{fw} + 2e_{fw}$$

Using the relation of the rivet diameter to the fastener spacing:

$$Flange\ width = 3(4D) + 2(2D) = 16D$$

It is already stated that $D_{min} = 0.5\ t_{total}$.

Thus,

$$D_{min} = 0.5\ (t_{skin} + t_{fw}) = 0.5\ (t_{skin} + 2t_{skin})$$

Hence, the expression for the minimum area of the flange with is:

$$A_{fw,min} = 48\ t_{skin}^2$$

With a similar approach, minimum flange height area is approximated as:

$$A_{fh,min} = 24\ t_{web}^2$$

Consequently, minimum spar flange area can be related to the panel thicknesses by the following expression:

$$A_{f,min} = 48t_{skin}^2 + 24t_{web}^2 \qquad (3.25)$$

The above expression is very useful for two reasons. Firstly, it secures that the spar flange can satisfy enough space for double row attachments and clamped edge conditions. Thus, the possible problems for the manufacturability are avoided. Secondly, the flange areas are approximated using the panel thicknesses. Therefore, no additional unconstrained design variables (flange areas) are added to the problem.

- Stringer Configuration: A method similar to the one for the spars can be followed for stringer areas. There are various shapes for stringer cross sections, but two most common ones are used in this thesis. The user of the tool developed for this thesis selects between the two. Z type and L type stringers attached to skin with a single row of fasteners are shown in Figure 3-17 and Figure 3-18.

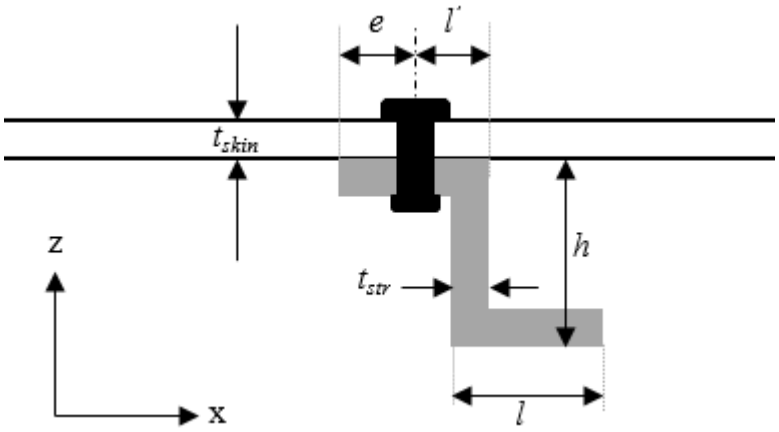

Figure 3-17 Z Type Stringer

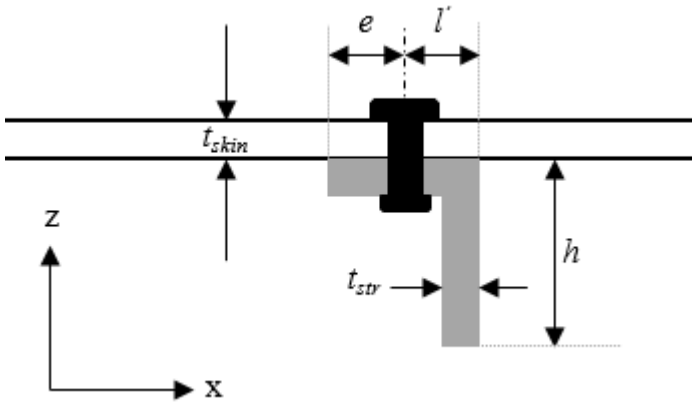

Figure 3-18 L Type Stringer

Approximate minimum stringer area for the Z type stringer can be found by making some reasonable assumptions about the geometry. Firstly, the stringer thickness is not expected to be smaller than the skin thickness, i.e. $t_{str,min} = t_{skin}$

Edge distance requirement was already shown in the spar arrangement. Assuming that the l' length is equal to e; and $D_{min} = 0.5\ t_{total}$; then the minimum stringer width equals to $4\ t_{skin}$. Stringer height can be approximated as $5\ t_{skin}$. Lastly, upper and lower flanges of the stringer can be assumed to be of the same length. Therefore;

$$A_{str,min,Z} = 11\ t_{skin}^2$$

Similarly, minimum area of the L type stringer should be:

$$A_{str,min,L} = 8\ t_{skin}^2$$

- Rib Flanges: After the rib web thicknesses are determined, rib flange areas are calculated assuming that L-shape angles attach the ribs to all spar webs and skins. Therefore, using the formula of L type stringers, rib flange areas at all connections are approximated as:

$$A_{ribfl} = 8\ t_{ribweb}^2$$

Finally, to sum up the approaches for the panel, spar, and stringer cross-section configurations:

1. Skin thickness distribution is made according to the distance of the mid panel to the cross-section centroid. By this way, the relationship of all upper panel thicknesses to each other is determined. Similarly, thickness distribution of the lower panels is also specified.
2. Spar web thickness distribution is made according to the web heights.
3. Minimum spar flange area is a function of the adjacent panel (skin and web) thicknesses.
4. Minimum stringer area is a function of the attached skin thickness.

3.7 Design Strategy

3.7.1 Sizing Procedure

The tool developed for this thesis,

- Reads all data that comes in the input file (airfoil data, planform geometry, numbers and locations of ribs, spars, stringers, aircraft weight, maximum speed, load factor, materials of members, allowable values, specified initial buckling level, etc.)
- Calculates the external loads by the automated use of;
    - ESDUpac A9510 computer program for subsonic vehicles,
    - Schrenk approximation for supersonic vehicles.
- For each design station from the root to the tip:
    - Calculates the internal loads.
    - Locates the structural members on the airfoil and creates the cross section.

- Makes the initial panel thickness distribution according to the *Skin Thickness Configuration* and *Spar Web Thickness Configuration* explained in Section 3.6. Initial thickness of the thinnest panel is the thinnest available metal thickness used in aircraft industry, which is generally 0.016” (0.4064mm). The tool assigns all other panel thicknesses using the coefficients described in Section 3.6.

- Assigns initial spar flange areas according to *Spar Configuration* explained in Section 3.6. Thicknesses of the neighbor skins and web are taken into account for the area approximation. The skins at the two sides of the flange width may have different thicknesses. In that case, the larger thickness is taken.

- Assigns initial stringer areas (if there are any stringers defined by the user) according to *Stringer Configuration* explained in Section 3.6. Thickness of the neighboring skins is considered for the area approximation.

- Calculates the shear flows and the shear stresses in panels using the approach in Section 3.2.1. The function that calculates the shear flows obtains the centroid, first moment, and the second moment of the cross-section in order to set up the necessary system of equations. It is important to note that the contribution of skins and webs are not included in the centroid, first moment, and second moment calculations.

- Calculates the axial stresses for all panels, spar flanges, and stringers according to Section 3.2.2. This time, contribution of skins is included in the inertia calculations. If the initial buckling of the compression panels is allowed before the limit load, the remaining effective amount of the panels are calculated and used while deriving the

centroid and the second moment of inertia as explained in Section 3.2.2.

- Calculates the margins of safety and increase the thickness of all panels by a certain increment (i.e. 0.1%) if any of the following checks fails:
  - Margin of safety check for the spar caps and stringers: They must return a positive margin under ultimate loads. In other words, material tensile / compressive allowable stresses must not be exceeded according to Section 3.5.1.
  - Margin of safety check for upper skins: Upper skins are checked according to the procedure outlined in Section 3.5.2.
  - Margin of safety check for lower skins: Lower skins are checked according to the procedure outlined in Section 3.5.3.
  - Margin of safety check for spar webs: Spar webs are checked according to Section 3.5.4.
- Repeats increasing the panel thicknesses by a certain increment (like 0.1%) and update spar flange areas, and stringer areas accordingly until all failure modes return positive margins of safety. When all margins are positive, a *feasible solution* is achieved.
- Calculates the rib web thicknesses and rib flange areas using the approach outlined in Section 3.5.5.
- Sums the weight of all components (spars, stringers, upper skins, lower skins, and the rib) within the section.

- Sums the weight of all sections to calculate the overall weight of the half wing.

At this point, the tool has obtained an overall sizing with positive margins of safety. This can be called as a feasible solution. Next section outlines the exploration study that creates more feasible solutions in order to achieve the minimum wingbox weight.

3.7.2 Design Exploration

Section 3.7.1 defined how the tool finds the minimum sizes that make all safety margins positive. In the end, one feasible solution was obtained. However, there are actually many feasible solutions for the problem of wingbox sizing. Wingbox sizing is actually a big optimization problem with a single objective function (weight) and numerous design variables. In this thesis, the optimization problem is being downsized under the light of certain considerations explained throughout this chapter. Nonetheless, there is still a small domain to be searched for achieving minimum weight. Design exploration study aims to perform this research.

It should be recalled that the thickness distribution within the upper skins, lower skins, and spar webs were already made at the beginning of the sizing such that:

$$\{UpperSkinTh\}_{NUS} = \{Multipliers_{US}\}_{NUS} \cdot t_{US,\min} \tag{3.26}$$

where the number of upper skin panels denoted as *NUS* is the size of the vector. For example, for the sample cross section shown in Figure 3-15, Equation (3.26) gets into the form:

$$\{t_{us1}, t_{us2}, t_{us3}\} = \left\{1, \frac{d_2}{d_1}, \frac{d_3}{d_1}\right\} \cdot t_{us1} \tag{3.27}$$

Similarly, for the lower skins and spar webs:

$$\{LowerSkinTh\}_{NLS} = \{Multipliers_{LS}\}_{NLS} \cdot t_{LS,\min} \tag{3.28}$$

$$\{SparWebTh\}_{NSW} = \{Multipliers_{SW}\}_{NSW} \cdot t_{SW,\min} \tag{3.29}$$

where the number of lower skin panels is denoted as *NLS*, and the number of spar webs is denoted as *NSW*. Equations (3.26) to (3.29) are sufficient to express the internal relation between all three panel groups.

Having recalled the internal relation between the thicknesses, the idea behind the design exploration can be introduced. In this section, the relation *between* the thickness groups (upper skins, lower skins, and spar webs) are examined. For this purpose, the following coefficients are added as multiplications to the thickness vectors.

Upper skins: $\{UpperSkinTh\}_{NUS} \cdot Coefficient\ A$

Lower skins: $\{LowerSkinTh\}_{NLS} \cdot Coefficient\ B$

Spar webs: $\{SparWebTh\}_{NSW} \cdot Coefficient\ C$

Above coefficients are to be used to adjust the thickness relation between the skins and webs. By changing the coefficients, various design conditions can be created. For instance, the effect of thicker upper skins can be checked by selecting *Coefficient A* larger than *Coefficients B* and *C*.

The multipliers can actually be decreased from three to two because the ratios of them to each other are actually examined. Thus, the final form of the thickness functions is:

Upper skins: $\{UpperSkinTh\}_{NUS} \cdot Coefficient\ 1$

Lower skins: $\{LowerSkinTh\}_{NLS} \cdot Coefficient\ 2$

Spar webs: $\{SparWebTh\}_{NSW}$

The weight is a function of the thickness distribution within a wingbox section and various thickness distributions can be examined by adjusting the above coefficients. In other words, the two design variables (*Coefficients 1* and *2*) are explored to

minimize the objective (weight) under the constraints that all safety margins must be positive.

The bounds for the coefficients are not very difficult to guess. Lower bound is obviously greater than zero to avoid zero or negative thicknesses. Very high coefficients would also be irrational. For instance, lower skins that are 10 times thicker than spar webs would not return a minimum overall weight. Therefore, exploring in the bounds of [0.2, 5.0] would be sufficient enough although it is never expected that a minimum weight would be achieved with one of the coefficients as low as 0.2 (or as high as 5.0).

In summary, design exploration study aims to solve the following problem:

Objective (Minimize): *Weight = f* (*Coefficient 1*, *Coefficient 2*)

2 variables within bounds: [0.01, 5.0]

Constraints: All safety margins > 0.001

In order to achieve the minimum weight, the tool developed for this thesis discretizes the design space and performs the sizing several times for each coefficient couple. The user can specify the bounds for the two coefficients. The user can also specify the number of internal grid points that would split the exploration region. For instance, if the number of grids is specified as 5, the sizing is performed in the 25 points shown in Figure 3-19.

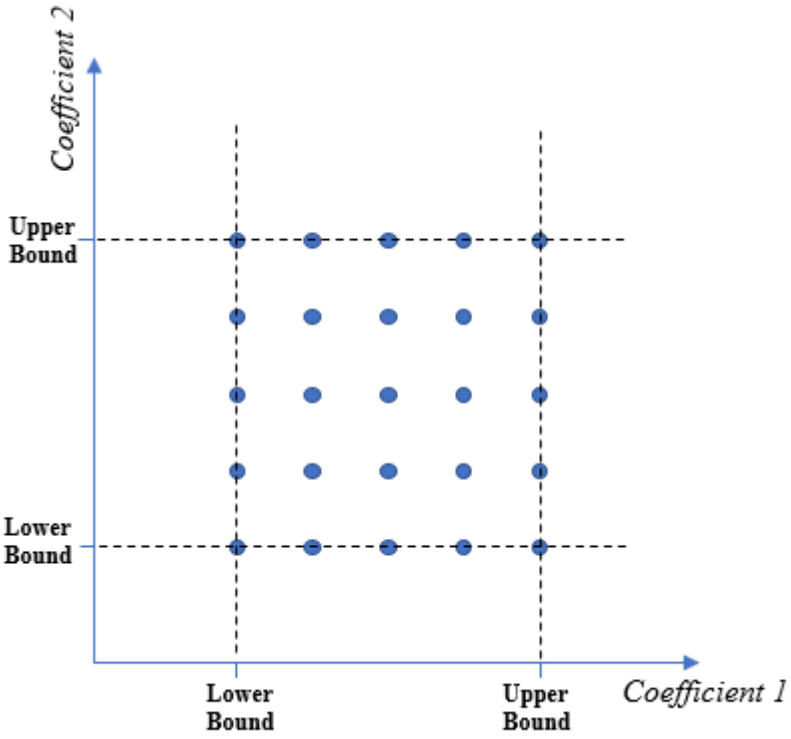

Figure 3-19 Representative Exploration Region with 25 Points

The user can also specify the number of *additional cycles* for the exploration. This is made in order to have a finer research around the point giving the minimum weight in the first cycle. Figure 3-20 shows the additional 25 grids for the second cycle of the exploration. In the second cycle, the black points in Figure 3-20 are examined, assuming that the red point was the point giving the minimum weight in the first cycle.

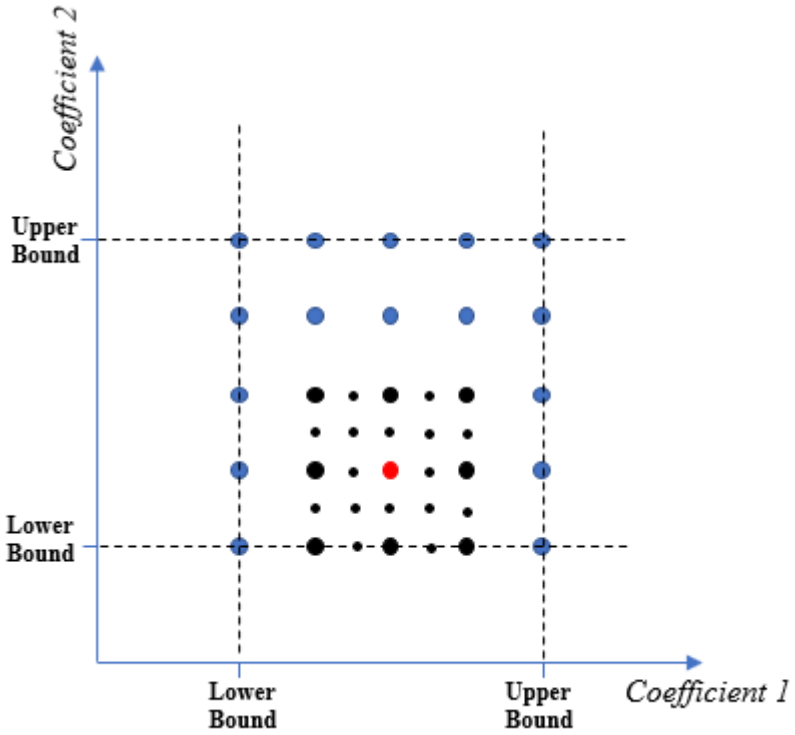

Figure 3-20 Additional 25 Grids for the Second Cycle of Exploration

It should be recalled that the number of internal grid points and the number of repetitive cycles can both be specified by the users of the tool.

Next chapter is going to show the results of some case studies in which the design exploration part is again emphasized. Additionally, the minimum weight result coming from the exploration is compared with the results coming from an advanced optimization routine of the MATLAB software.

Remark: It should be noted that the objective function has to be a smooth function with a single minimum in the specified domain. Chapter 4.5 shows the shape of the objective function in order to prove that it is suitable for this kind of exploration study.

CHAPTER 4

CASE STUDY RESULTS

Entire preliminary sizing procedure of two different wingboxes is explained in this chapter. The tool developed for this thesis is utilized three times for the following configurations:

- A subsonic turboprop trainer wing (3-spar and multi-stringer wing configuration) with buckling-resistant panels,
- Same subsonic turboprop trainer wing with 50% limit load set for compression buckling for the skin panels,
- A supersonic fighter wing (multi-spar configuration with no stringers).

This study makes it possible to examine all details of the sizing method outlined in Chapter 3. The first and second configurations are useful to understand the post-buckling effects on the overall wingbox weight. In addition, different load approximation methods used for subsonic and supersonic vehicles are utilized within the examples.

4.1 A Subsonic Turboprop Trainer Wing with Buckling Resistant Skins

4.1.1 Input File

A subsonic turboprop trainer wing is used for the first example. The wing of PC-21 aircraft, which was already used in Chapter 2, is selected for this study.

The main input file of the tool starts with a definition of study:

```
Definition of the study (Three Lines)
TEXT1 Wing Preliminary Design Study
TEXT2 PC-21 Aircraft Wing Planform
TEXT3 TUCANO Layout, NACA Airfoil
```

After the definition, the airfoil geometric data is entered as an input. Upper and lower curves are defined as two separate arrays. For this example, an assumption for the airfoil shape was already made in Chapter 2. Same assumption is also used for this study and NACA2412 airfoil is selected:

```
Upper Airfoil Data (UpAFData)
0      0
0.0125 0.0215
0.025  0.0299
0.05   0.0413
0.075  0.0496
0.1    0.0563
0.15   0.0661
0.2    0.0726
0.25   0.0767
0.3    0.0788
0.4    0.078
0.5    0.0724
0.6    0.0636
0.7    0.0518
0.8    0.0375
0.9    0.0208
0.95   0.0114
1      0.0013

Lower Airfoil Data (LoAFData)
0      0
0.0125 -0.0165
0.025  -0.0227
0.05   -0.0301
0.075  -0.0346
0.1    -0.0375
0.15   -0.041
0.2    -0.0423
0.25   -0.0422
0.3    -0.0412
0.4    -0.038
0.5    -0.0334
0.6    -0.0276
0.7    -0.0214
0.8    -0.015
0.9    -0.0082
0.95   -0.0048
1      -0.0013
```

Wing planform data (root and tip chord lengths, taper ratio, and half span) are the next inputs:

```
Root chord length (RootChord) [mm]
2258

Tip chord length (TipChord) [mm]
1085

Taper Ratio (Taper)
0.48

Wing Half Span (HalfSpan) [mm]
4555
```

Next input is the layout of structural members. The layout of the structural members within the cross-section is based on Figure 4-1, which is a cutaway drawing of Tucano Aircraft. Tucano is also a turboprop trainer similar and competitor to PC-21.

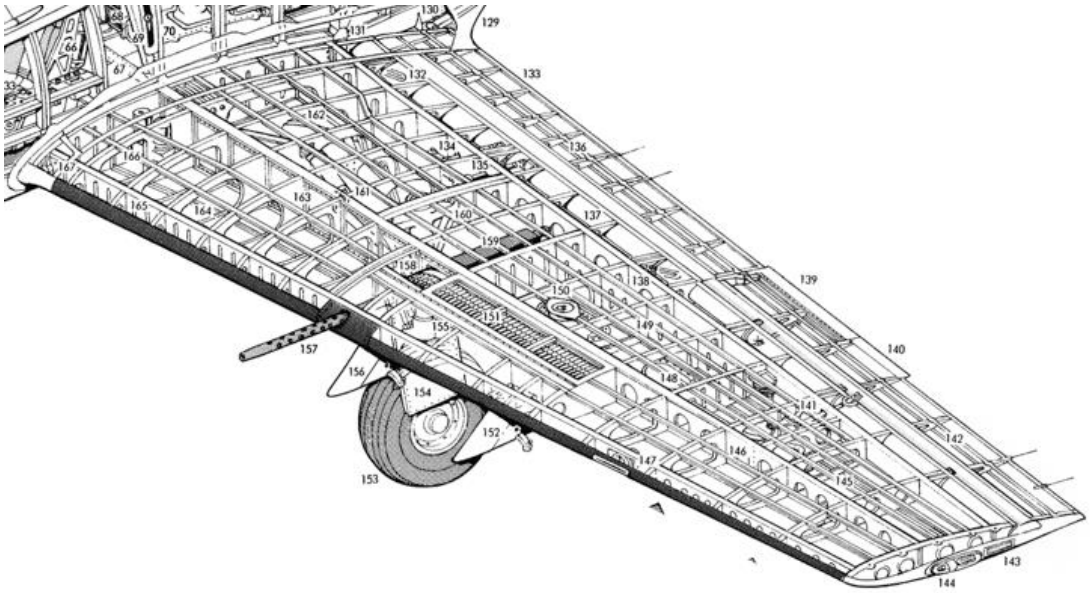

Figure 4-1 Embraer EMB-314 Super Tucano Wing Structural Layout

The tool developed for this thesis can make the sizing of any planform with any layout, but real aircraft data would be helpful for a logical comprehension. Therefore, a mixture of two turboprop trainers of the same family is used. Resulting overall

wingbox weight can be compared to that of the real trainers of this family. Structural layout data of Tucano wing is entered next:

```
Number of Spars (NumOfSpars)
3

Locations of Spars from L.E. (LocOfSpars) (% chord)
10
40
75

Number of Upper Stringers (NumOfUpStr)
6

Location of Upper Stringers from L.E. (LocOfUpStr) (% chord)
20
30
47
54
61
68

Number of Lower Stringers (NumOfLoStr)
5

Location of Lower Stringers from L.E. (LocOfLoStr) (% chord)
20
30
49
58
67

Number of Ribs (NumOfRibs)
17

Location of Ribs from Root (LocOfRibs) (% half span)
0
5
10
15
20
25
30
35
40
47
54
61
68
75
83
91
100
```

Cross-section of the wingbox with the above geometric input is shown in Figure 4-2. The numbers assigned for the panels are also provided.

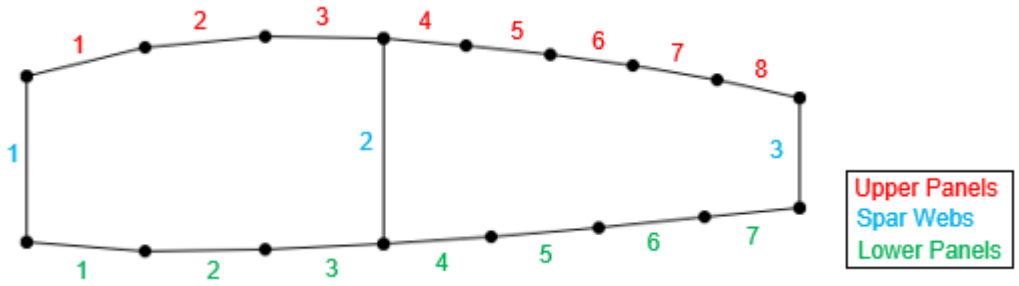

Figure 4-2 Panels and Booms at the Cross-Section of the Wingbox

Aircraft overall weight, positive limit load factor, and maximum speed of the PC-21 aircraft are also used by the tool as inputs. It should be recalled that the Mach number used in the input is the maximum operating Mach number already provided in Table 2-2.

```
Load Factor (LoadFactor) (g)
8.0

A/C Weight (ACweight) [kg]
3100.0

Value of Mach number
0.72
```

Finally, material properties of the spars, stringers, ribs, upper skins, and lower skins are entered to the input file. It should be noted that any isotropic material can be used by the tool. However, post-buckling studies are generally carried out on aluminum material. Only the upper skin part is shown here. Lower skin, spar, and rib materials, which are entered using the same scheme, can be seen in Appendix D.

```
Upper Skin Material
2024 T851

Upper Skin Ftu [MPa]
486.8

Upper Skin Fcy [MPa]
```

```
399.9

Upper Skin E [MPa]
72397

Upper Skin v
0.33

Upper Skin Density [kg/mm3]
2767.99e-9
```

Initial buckling stage is one the most important inputs for subsonic aircrafts. For the first example, all panels are buckling-resistant. Therefore, following entry is used:

```
Initial Buckling Stage (for Subsonic Wings) [%]
100
```

For supersonic wings, the input file is finished at this point. For subsonic wings, however, there are some additional inputs needed for the ESDU load calculations. Those parameters are provided below:

```
REST OF THE INPUT FILE IS FOR SUBSONIC VEHICLES ONLY (ESDU Inputs)

Wing Area (m2)
15.22

Aspect ratio of the wing
5.45

Sweep of 0th chord line
12

Sweep of the mid chord line
5

Max Camber, MC (%)
2

Max Camber Position, MCP (%)
40
```

These are all the inputs the tool needs. The overall input file sent to the tool can be seen in Appendix D.

4.1.2 Procedure

Some key points of the sizing procedure are highlighted in this section. Firstly, the load calculations are to be examined. The tool creates ESDUpac A9510 input for subsonic wings to obtain the loads. The following input file is the same as the one provided in Table 2-6 except for the spanwise load stations. The tool adds the rib locations to the input file in order to obtain the exact loads at rib stations. Consequently, the following A9510 input file is created by the tool.

Table 4-1 Automatically Generated ESDUpac A9510 Input File

```
TEXT1 Wing Preliminary Design Study
TEXT2 PC-21 Aircraft Wing Planform
TEXT3 TUCANO Layout, NACA Airfoil

33 5

2

1 3

1
0.72

28
0 0.05 0.1 0.15 0.2 0.25 0.3 0.35 0.4 0.45 0.47 0.5 0.54 0.55 0.6 0.61 0.65
0.68 0.7 0.75 0.8 0.83 0.85 0.9 0.91 0.95 0.98 0.9999

2
1
0.4355
0
5.45
0.48
12
0

2

0
18
0.000000 0.000000
0.012500 0.001230
0.025000 0.002422
0.050000 0.004687
0.075000 0.006797
0.100000 0.008750
0.150000 0.012187
0.200000 0.015000
0.250000 0.017187
0.300000 0.018750
0.400000 0.020000
0.500000 0.019444
0.600000 0.017778
0.700000 0.015000
```

```
0.800000 0.011111
0.900000 0.006111
0.950000 0.003194
1.000000 0.000000

1
18
0.000000 0.000000
0.012500 0.001230
0.025000 0.002422
0.050000 0.004687
0.075000 0.006797
0.100000 0.008750
0.150000 0.012187
0.200000 0.015000
0.250000 0.017187
0.300000 0.018750
0.400000 0.020000
0.500000 0.019444
0.600000 0.017778
0.700000 0.015000
0.800000 0.011111
0.900000 0.006111
0.950000 0.003194
1.000000 0.000000
```

After the execution of the A9510 program, internal loads (shear forces, bending moments, and the pitching moments) at the rib locations are calculated by the tool. All loads are listed in Table 4-2.

Table 4-2 Internal Loads at Rib Locations

Rib	**1 (root)**	**2**	**3**	**4**	**5**
V [N]	1.22E+05	1.14E+05	1.06E+05	9.86E+04	9.11E+04
M [Nmm]	2.37E+08	2.10E+08	1.85E+08	1.62E+08	1.40E+08
PM [Nmm]	-3.14E+07	-2.85E+07	-2.57E+07	-2.32E+07	-2.08E+07
Rib	**6**	**7**	**8**	**9**	**10**
V [N]	8.36E+04	7.62E+04	6.90E+04	6.19E+04	5.22E+04
M [Nmm]	1.20E+08	1.02E+08	8.55E+07	7.06E+07	5.25E+07
PM [Nmm]	-1.85E+07	-1.64E+07	-1.44E+07	-1.26E+07	-1.02E+07
Rib	**11**	**12**	**13**	**14**	**15**
V [N]	4.30E+04	3.42E+04	2.59E+04	1.83E+04	1.05E+04
M [Nmm]	3.73E+07	2.50E+07	1.54E+07	8.43E+06	3.23E+06
PM [Nmm]	-8.08E+06	-6.18E+06	-4.51E+06	-3.07E+06	-1.70E+06

Rib	16	17 (tip)			
V [N]	4.14E+03	0.00E+00			
M [Nmm]	6.30E+05	0.00E+00			
PM [Nmm]	-6.44E+05	0.00E+00			

For this problem, the bounds for the design variables are set as [0.5, 5.0]. It should be recalled that the design variables are the two coefficients explained in Section 3.7.2. Thus, the design exploration is made within this interval. The domain is divided into 4 regions because the number of internal grid points is set as 5. Therefore, for each cycle, the sizing is performed 25 times.

The initial thicknesses before the coefficients are applied are provided in Table 4-3. The initial thicknesses in Table 4-3 correspond to coefficients (1, 1). The initial thickness and area distribution are different for all 25 grids of the exploration. Initial thickness and area distribution for the best solution is provided in Section 4.1.3.

Table 4-3 Initial Thicknesses of Skins and Webs

	Upper Panels			Lower Panels			Spar Webs		
Minimum Sheet Th. [mm]	Panel	Multiplier	Initial Thickness [mm]	Panel	Multiplier	Initial Thickness [mm]	Panel	Multiplier	Initial Thickness [mm]
0.4064	1	1.4602	0.5934	1	1.7318	0.7038	1	1.4924	0.6065
	2	1.8043	0.7333	2	1.7884	0.7268	2	1.8457	0.7501
	3	1.8869	0.7669	3	1.7226	0.7001	3	1.0000	0.4064
	4	1.8147	0.7375	4	1.6103	0.6544			
	5	1.6753	0.6808	5	1.4690	0.5970			
	6	1.4969	0.6083	6	1.3069	0.5311			
	7	1.2718	0.5169	7	1.1454	0.4655			
	8	1.0000	0.4064						

The result of the first cycle of exploration can be visualized in Figure 4-3.

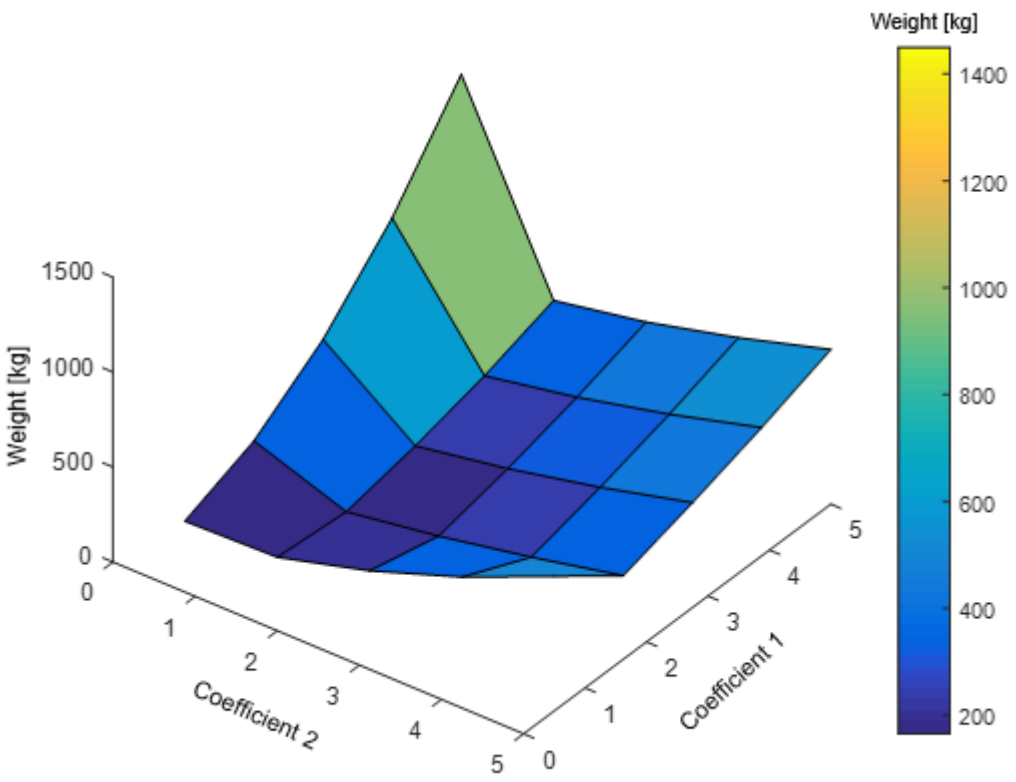

Figure 4-3 Result of the 1st Exploration Cycle

The sizing was carried out at 25 grids as shown in Figure 4-3. X and Y coordinates of the figure corresponds to the coefficients while the Z component is the weight. Side views of the same graph is useful in order to see the variation of weight with respect to each coefficient. Figure 4-4 and Figure 4-5 are helpful for this purpose.

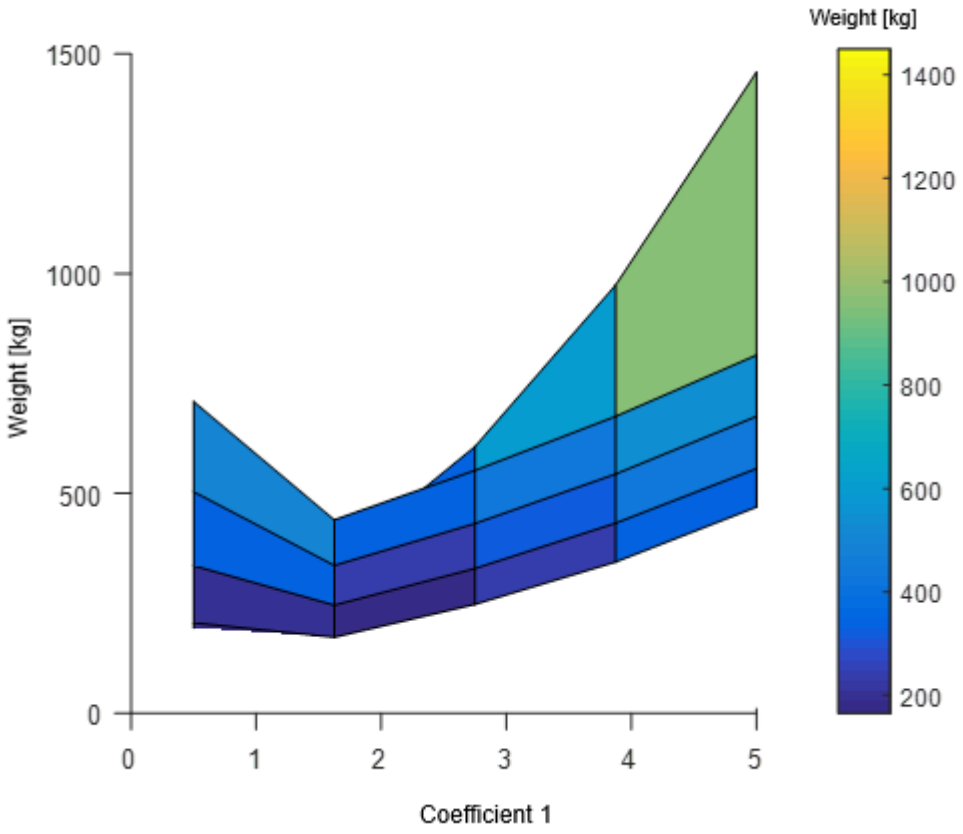

Figure 4-4 Variation of Weight vs. Coefficient 1 (Upper Skin Coefficient)

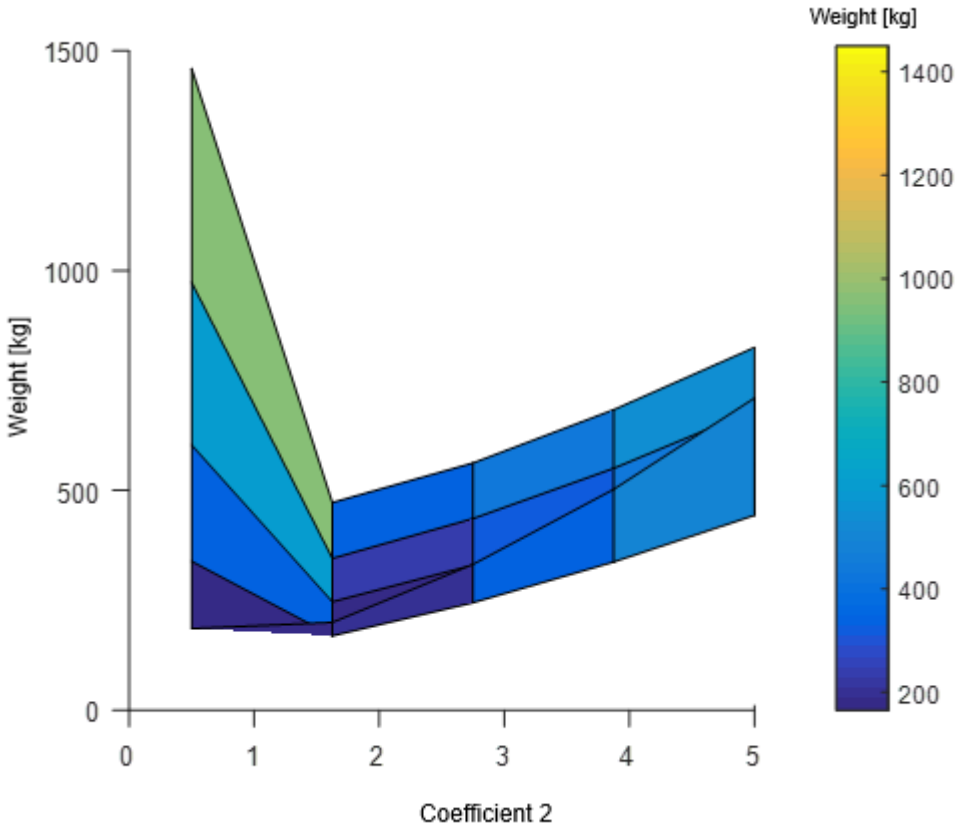

Figure 4-5 Variation of Weight vs. Coefficient 2 (Lower Skin Coefficient)

It is seen from Figure 4-4 that the weight is constantly increasing when the values of *Coefficient 1* are greater than 2. It is obvious that the values near zero are not reasonable either. Similar behavior is valid for the lower skin coefficient (*Coefficient 2*) as shown in Figure 4-5.

The location and the value of the minimum weight obtained in the first exploration cycle is shown in the figure below.

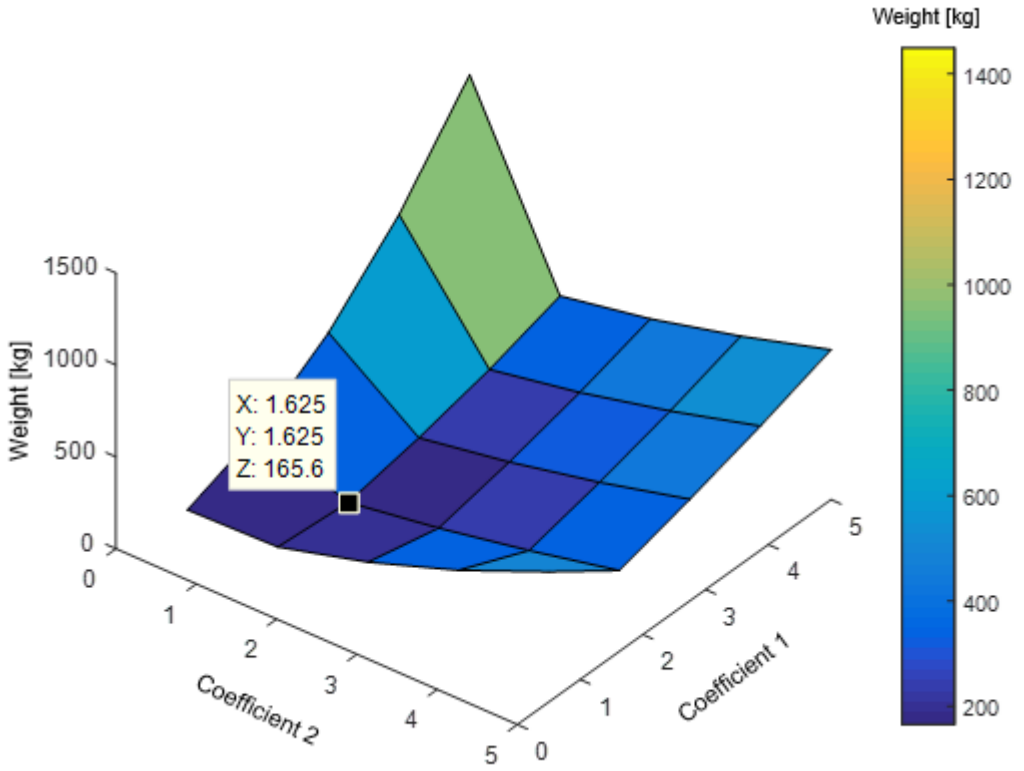

Figure 4-6 Location and the Value of the Minimum Weight (1st Exploration Cycle)

At this point, the second exploration cycle is performed in order to have a finer research around the point shown in Figure 4-6. The minimum weight for the half wing is 165.6 kg after the first cycle. The result coming from the second cycle is shown in Figure 4-7.

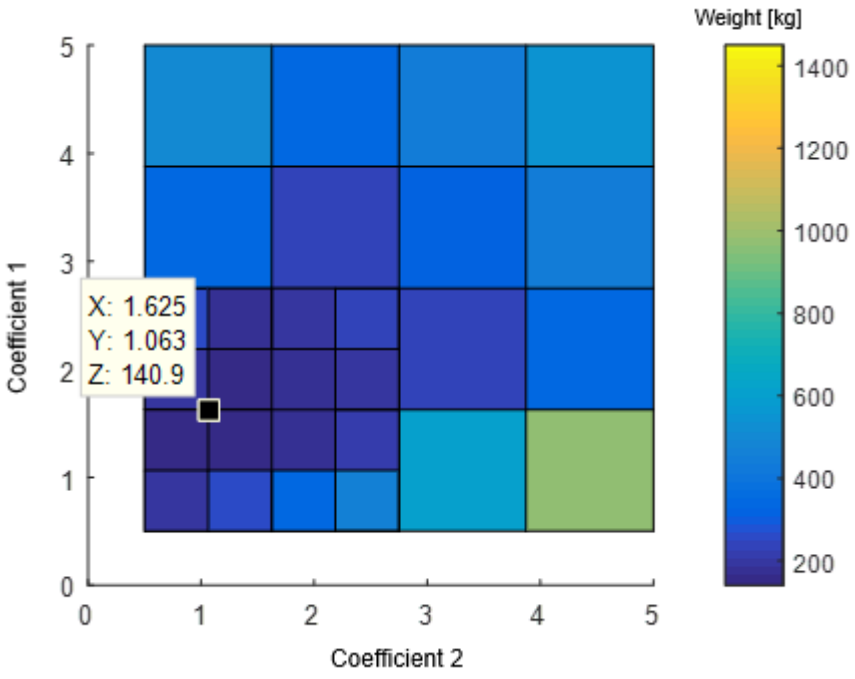

Figure 4-7 Location and the Value of the Minimum Weight (2nd Exploration Cycle)

In order for a better visualization, two-dimensional graph of the second cycle is shown in Figure 4-7. The weight is decreased to 140.9 kg after the second cycle. It is obvious that the second cycle significantly improved the weight result.

Further improvement is aimed after the third cycle, results of which are shown in Figure 4-8. This time, the weight is decreased to 132.5 kg at the point (1.344, 0.7813).

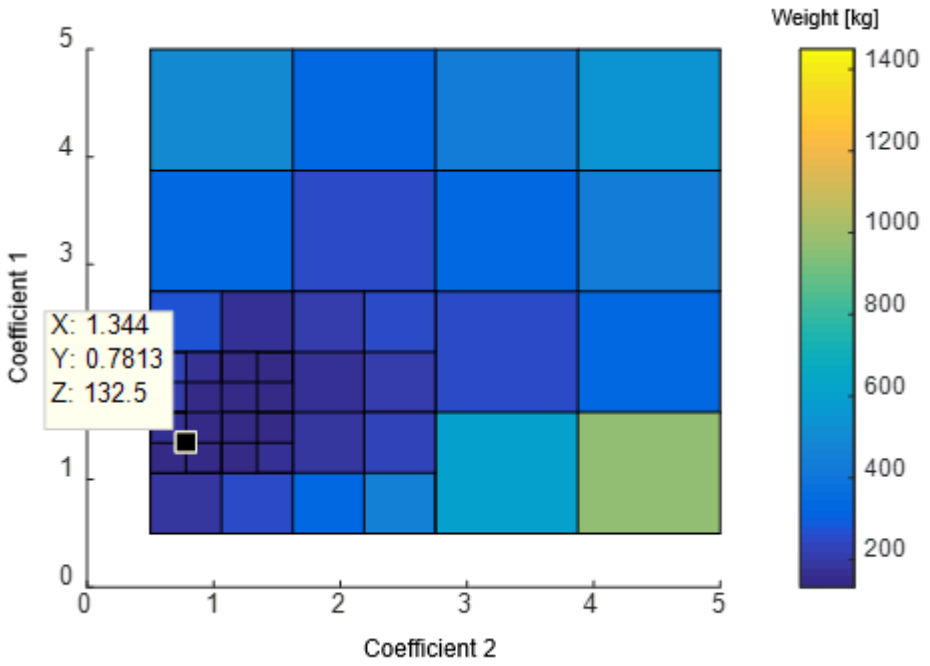

Figure 4-8 Location and the Value of the Minimum Weight (3rd Exploration Cycle)

Since the improvement after each cycle is still large, the fourth cycle is to be explored. It should be noted that the step sizes are getting smaller after each cycle. The results of the fourth cycle are shown in Figure 4-9. It is seen that the minimum weight did not improve at the 4th cycle. Therefore, the exploration can be finalized. The minimum weight found by the tool is 132.5 kg. A summary of the design exploration is provided in Table 4-4.

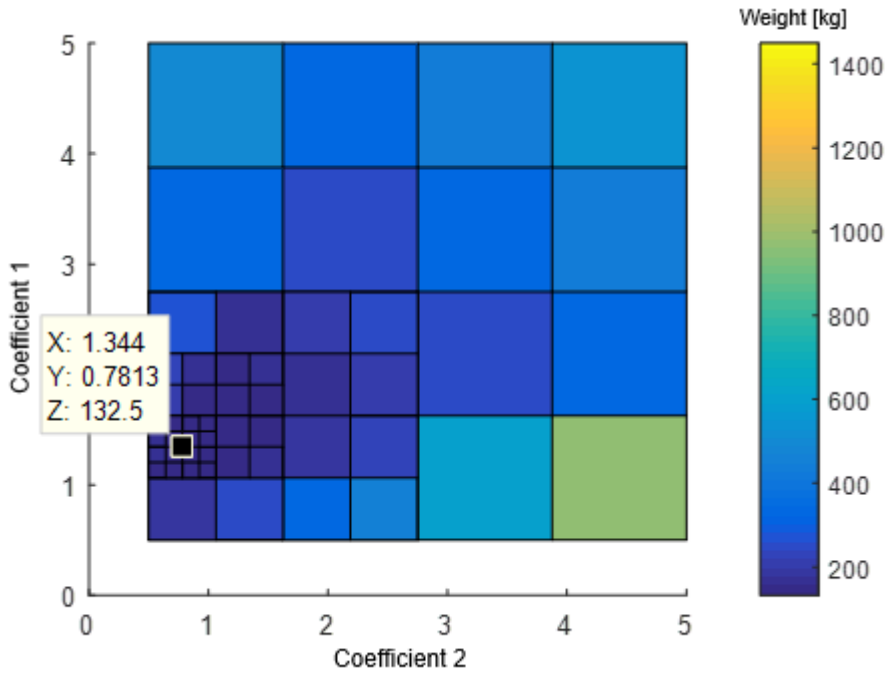

Figure 4-9 Location and the Value of the Minimum Weight (4th Exploration Cycle)

Table 4-4 Summary of the Exploration

Number of Internal Grids for Each Coefficient	5
Number of Repetitive Cycles	4
Lower Bound for the Variables	0.5
Upper Bound for the Variables	5.0
Minimum Wingbox Weight (Half Wing) [kg]	132.5
Coefficients @ the Minimum Weight	(1.344, 0.7813)

Next section provides the weight breakdown of the best solution. Thicknesses of the components at wing sections are listed.

Moreover, the same wingbox is examined by the tool for the second time in Section 4.2. In that case, initial buckling of the skins is allowed at 50% limit load. In addition, different bounds for the design variables are set and the result coming from

the exploration is compared to the results of an advanced optimizer routine of the MATLAB software.

4.1.3 Outputs

Weight breakdown of all structural members is provided in Table 4-5.

Table 4-5 Weight Breakdown of All Structural Members

Section	**1**	**2**	**3**	**4**	**5**
Weight of Upper Skins [kg]	4.46	4.18	3.91	3.63	3.38
Weight of Lower Skins [kg]	2.58	2.42	2.26	2.10	1.95
Weight of Spars (Webs+Flanges) [kg]	5.06	4.69	4.35	3.99	3.67
Weight of Stringers [kg]	1.01	0.93	0.86	0.79	0.72
Weight of Ribs (Webs+Flanges) [kg]	0.74	0.69	0.64	0.59	0.54
Total Section Weight [kg]	**13.86**	**12.91**	**12.02**	**11.11**	**10.26**
Section	**6**	**7**	**8**	**9**	**10**
Weight of Upper Skins [kg]	3.12	2.86	2.62	3.37	2.93
Weight of Lower Skins [kg]	1.80	1.66	1.51	1.95	1.69
Weight of Spars (Webs+Flanges) [kg]	3.34	3.01	2.70	3.43	2.88
Weight of Stringers [kg]	0.65	0.58	0.52	0.66	0.54
Weight of Ribs (Webs+Flanges) [kg]	0.50	0.45	0.41	0.37	0.32
Total Section Weight [kg]	**9.41**	**8.57**	**7.75**	**9.79**	**8.37**
Section	**11**	**12**	**13**	**14**	**15**
Weight of Upper Skins [kg]	2.51	2.12	1.81	1.72	1.32
Weight of Lower Skins [kg]	1.45	1.23	1.05	1.00	0.76
Weight of Spars (Webs+Flanges) [kg]	2.38	1.93	1.59	1.45	1.02
Weight of Stringers [kg]	0.44	0.35	0.28	0.25	0.17
Weight of Ribs (Webs+Flanges) [kg]	0.27	0.23	0.19	0.17	0.15
Total Section Weight [kg]	**7.05**	**5.86**	**4.93**	**4.60**	**3.42**
Section	**16**				
Weight of Upper Skins [kg]	0.99				
Weight of Lower Skins [kg]	0.57				
Weight of Spars (Webs+Flanges) [kg]	0.67				
Weight of Stringers [kg]	0.10				
Weight of Ribs (Webs+Flanges) [kg]	0.13				
Weight of the Tip Rib [kg]	0.13				
Total Section Weight [kg]	**2.60**				

It can be seen that the upper skins are heavier than the lower skins at each section. This is mainly because the failure condition for the upper skins is generally the most critical in the entire wingbox. The minimum weight was obtained at (1.344, 0.7813), meaning that the coefficient of the upper skins was about 1.34 times greater than the spar webs, and 1.7 times greater than the lower skins. Data in Table 4-5 shows correlation with this result as the upper skin weights are approximately 1.7 times greater than the lower skin weights in each section.

Weights of the sections decrease from the root to the tip as expected. However, the weight of section 9 is greater than the weight of section 8. This is because the length of the sections (i.e. the distances between the ribs) starts to increase after rib 9.

Thickness distribution is the most important point for the weight minimization problem. Therefore, a closer look at the thicknesses of skins and spar webs is essential. The initial thicknesses and flange areas corresponding to coefficients (1.344, 0.7813) are listed in Table 4-6 and Table 4-7.

Table 4-6 Initial Thicknesses

	Upper Panels				Lower Panels				Spar Webs		
Min. Sheet Th. [mm]	Panel	Multiplier	Coeff. 1	Initial Th. [mm]	Panel	Multiplier	Coeff. 2	Initial Th. [mm]	Panel	Multiplier	Initial Th. [mm]
0.4064	1	1.4602	1.344	0.7974	1	1.7318	0.7813	0.5498	1	1.4924	0.6065
	2	1.8043		0.9854	2	1.7884		0.5678	2	1.8457	0.7501
	3	1.8869		1.0305	3	1.7226		0.5469	3	1.0000	0.4064
	4	1.8147		0.9910	4	1.6103		0.5113			
	5	1.6753		0.9149	5	1.4690		0.4664			
	6	1.4969		0.8175	6	1.3069		0.4149			
	7	1.2718		0.6945	7	1.1454		0.3637			
	8	1.0000		0.5461							

Table 4-7 Initial Stiffener Areas

Upper Spar Flange Area [mm^2]		Lower Spar Flange Area [mm^2]		Upper Stringer Area [mm^2]		Lower Stringer Area [mm^2]	
1	39.4	**1**	23.3	**1**	7.8	**1**	2.6
2	64.5	**2**	27.9	**2**	8.5	**2**	2.6
3	18.3	**3**	10.3	**3**	7.9	**3**	2.1
				4	6.7	**4**	1.7
				5	5.3	**5**	1.4
				6	3.9		

All thicknesses at the root section (section 1) after the sizing is finished are listed in Table 4-8.

Table 4-8 Thicknesses of All Panels in Section 1 After Sizing

Section 1	Upper Skins [mm]	Lower Skins [mm]	Spar Webs [mm]	Rib Web [mm]
1	4.4564	3.0728	3.3896	0.6539
2	5.5066	3.1732	4.1918	
3	5.7587	3.0565	2.2711	
4	5.5383	2.8573		
5	5.1126	2.6065		
6	4.5684	2.3189		
7	3.8813	2.0323		
8	3.0519			

In a similar manner, all stiffener areas for the best solution after the sizing is finished are provided in Table 4-9.

Table 4-9 Stiffener Areas in Section 1 After Sizing

Upper Spar Flange Area [mm^2]		Lower Spar Flange Area [mm^2]		Upper Stringer Area [mm^2]		Lower Stringer Area [mm^2]	
1	1229.0	**1**	728.9	**1**	242.6	**1**	80.6
2	2013.5	**2**	870.1	**2**	265.3	**2**	80.6
3	570.9	**3**	322.0	**3**	245.4	**3**	65.3
				4	209.1	**4**	54.4
				5	167.0	**5**	43.0
				6	120.5		

The thickness distribution clearly shows the effect of the coefficients. It is also seen that the thickness of the rib web is much smaller than the other structural members as expected.

Table 4-10 clearly shows that the thicknesses are getting smaller towards the wing tip.

Table 4-10 Thickness Distribution in Various Sections

Section 2	Upper Skins [mm]	Lower Skins [mm]	Spar Webs [mm]	Rib Web [mm]
1	4.2821	2.9526	3.2570	0.6397
2	5.2912	3.0490	4.0278	
3	5.5334	2.9369	2.1823	
4	5.3217	2.7455		
5	4.9127	2.5046		
6	4.3897	2.2282		
7	3.7295	1.9528		
8	2.9325			

Section 9	Upper Skins [mm]	Lower Skins [mm]	Spar Webs [mm]	Rib Web [mm]
1	3.0352	2.0929	2.3086	0.5219
2	3.7506	2.1613	2.8550	
3	3.9222	2.0818	1.5469	
4	3.7722	1.9461		
5	3.4822	1.7753		
6	3.1115	1.5794		
7	2.6436	1.3842		
8	2.0786			

Section 16	Upper Skins [mm]	Lower Skins [mm]	Spar Webs [mm]	Rib Web [mm]
1	1.0439	0.7198	0.7940	0.4064
2	1.2899	0.7433	0.9819	
3	1.3490	0.7160	0.5320	
4	1.2973	0.6693		
5	1.1976	0.6106		
6	1.0701	0.5432		
7	0.9092	0.4761		
8	0.7149			

Thicknesses of all 16 sections would form a very long table. Therefore, thicknesses in Sections 2, 9, and 16 after the sizing are provided in order to understand the variation of the thicknesses from the root to the tip.

4.2 Subsonic Trainer Wing with an Initial Buckling Level of 50% Limit Load

Same trainer wing is sent to the tool with an initial buckling set of 50% limit load this time. Since all geometric data and the flight characteristics are the same as the previous section, loads calculated in Section 4.1 are also valid for this case. Design exploration is made in the interval of [0.2, 2.0] this time. This is because the first exploration showed that coefficients larger than 2.0 resulted in higher weights.

After all exploration cycles are finished, a minimum weight of 113.9 kg is achieved. The resulting design space is shown in Figure 4-10.

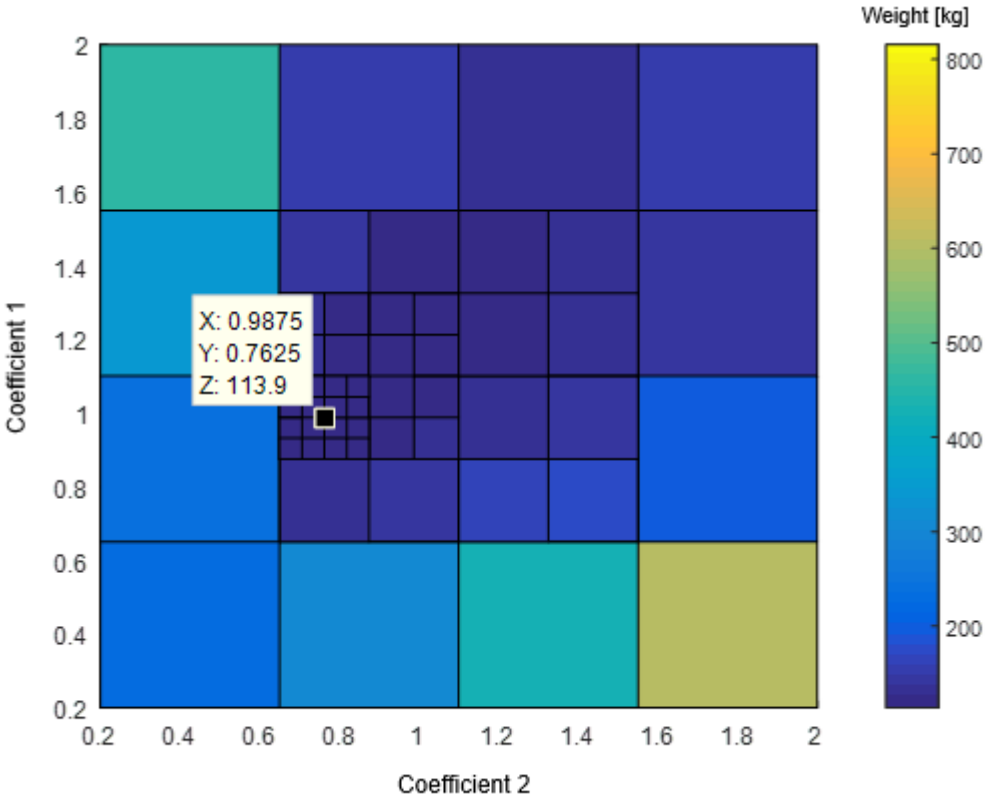

Figure 4-10 Design Space after the Exploration for the Buckling Level of 50% Limit Load

Summary of the exploration is provided in Table 4-11.

Table 4-11 Summary of the Exploration for the Buckling Level of 50% Limit Load

Number of Internal Grids for Each Coefficient	5
Number of Repetitive Cycles	4
Lower Bound for the Variables	0.2
Upper Bound for the Variables	2.0
Minimum Wingbox Weight (Half Wing) [kg]	113.9 kg
Coefficients @ the Minimum Weight	(0.9875, 0.7625)

The minimum weight found by the tool is compared with the one found by the optimization routine of the MATLAB software. The "*fminsearch*" function of

MATLAB is appropriate for this kind of problem. The function is used to find the minimum of the unconstrained multivariable functions using a derivative-free method.

In order to get reliable results from *fminsearch*, the entire sizing and weight calculation process is turned into a single function. This function increases the thicknesses until all margins of safety are positive. Once positive margins of safety are achieved, it returns to the main code. The function is a "black box" for the *fminsearch* optimizer such that the optimizer sends two variables (the coefficients) to the box and then gets the objective (weight) out of it but it has no interference with the content of the box. By this way, the primary constraint that "all margins of safety have to be positive" is automatically satisfied inside the box. This kind of optimizers has the ability to train themselves by examining the relation between the variables and the output. In the end, the optimizer finds the best set of variables that would return the optimum value for the objective. Figure 4-11 shows the "black box" and the optimization flow.

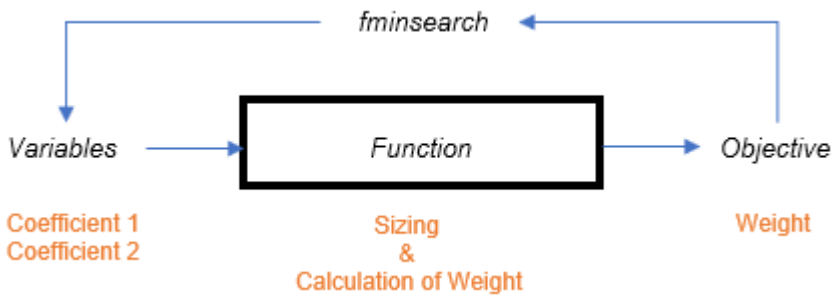

Figure 4-11 *fminsearch* Optimization Flow

The optimizer is executed for the wing configuration in this section with the initial guesses of (0.5, 0.5) for the coefficients. The minimum weight was obtained as 113.033 kg at (1.0469, 0.795). It is pretty obvious that the design exploration had obtained a very close value to the optimum found by the MATLAB optimizer routine. Optimization steps of the *fminsearch* function are provided in Appendix E.

The tool developed for this thesis offers the option to use both the exploration and the optimizer. Since one of the aims of this thesis is to minimize the usage of advanced commercial software, it was important to see that the exploration study can get sufficiently close to the advanced optimizer results.

Having correlated the results of the tool by the help of an optimizer, the analysis of the results can now take place. Most important outcome of this study is the weight reduction provided by the lower initial buckling load of upper skins. Same wingbox was 132.5 kg in the previous section. By the help of allowing the elastic buckling at 50% limit load, a weight reduction of 15% has been achieved. Weight breakdown of all structural members is provided in Table 4-12.

Table 4-12 Weight Breakdown of All Structural Members for the Buckling Level of 50% Limit Load

Section	**1**	**2**	**3**	**4**	**5**
Weight of Upper Skins [kg]	3.41	3.21	2.99	2.79	2.58
Weight of Lower Skins [kg]	2.62	2.47	2.29	2.14	1.98
Weight of Spars (Webs+Flanges) [kg]	4.43	4.14	3.81	3.53	3.22
Weight of Stringers [kg]	0.68	0.64	0.58	0.54	0.49
Weight of Ribs (Webs+Flanges) [kg]	0.75	0.70	0.64	0.59	0.55
Total Section Weight [kg]	**11.90**	**11.16**	**10.32**	**9.60**	**8.82**
Section	**6**	**7**	**8**	**9**	**10**
Weight of Upper Skins [kg]	2.40	2.20	2.01	2.58	2.25
Weight of Lower Skins [kg]	1.84	1.69	1.54	1.98	1.73
Weight of Spars (Webs+Flanges) [kg]	2.96	2.67	2.39	3.03	2.57
Weight of Stringers [kg]	0.45	0.40	0.35	0.44	0.37
Weight of Ribs (Webs+Flanges) [kg]	0.50	0.46	0.42	0.38	0.32
Total Section Weight [kg]	**8.14**	**7.42**	**6.72**	**8.41**	**7.24**
Section	**11**	**12**	**13**	**14**	**15**
Weight of Upper Skins [kg]	1.93	1.61	1.34	1.29	0.97
Weight of Lower Skins [kg]	1.48	1.23	1.03	0.99	0.75
Weight of Spars (Webs+Flanges) [kg]	2.13	1.69	1.36	1.25	0.88
Weight of Stringers [kg]	0.30	0.23	0.18	0.16	0.11
Weight of Ribs (Webs+Flanges) [kg]	0.27	0.23	0.19	0.17	0.15
Total Section Weight [kg]	**6.11**	**5.00**	**4.11**	**3.86**	**2.85**

Section	**16**				
Weight of Upper Skins [kg]	0.73				
Weight of Lower Skins [kg]	0.56				
Weight of Spars (Webs+Flanges) [kg]	0.58				
Weight of Stringers [kg]	0.06				
Weight of Ribs (Webs+Flanges) [kg]	0.13				
Weight of the Tip Rib [kg]	0.13				
Total Section Weight [kg]	**2.20**				

Finally, all thicknesses at the root section are listed in Table 4-13. It should be noted that the equivalent thicknesses of the upper skins after the buckling are also provided in Table 4-13. It should be noted that the equivalent thickness is the portion of the original thickness that remains effective after the initial buckling. Detail for the definition and the calculation of the equivalent thickness is provided in Section 5.3.2.3.

Table 4-13 Thicknesses of All Panels in Section 1 for the Buckling Level of 50% Limit Load

Section 1	Upper Skins [mm]	Eqv. Upper Skins [mm]	Lower Skins [mm]	Spar Webs [mm]	Rib Web [mm]
1	3.4082	2.4156	3.1211	3.5275	0.6590
2	4.2114	2.9214	3.2231	4.3624	
3	4.4042	3.6523	3.1046	2.3636	
4	4.2357	4.2357	2.9022		
5	3.9101	3.6987	2.6475		
6	3.4939	3.0782	2.3553		
7	2.9684	2.3540	2.0643		
8	2.3341	1.8472			

Additionally, the panel thicknesses in wing section 9 are listed in Table 4-14.

Table 4-14 Thicknesses of All Panels in Section 9 for the Buckling Level of 50% Limit Load

Section 9	Upper Skins [mm]	Eqv. Upper Skins [mm]	Lower Skins [mm]	Spar Webs [mm]	Rib Web [mm]
1	2.3214	1.6507	2.1258	2.4026	0.5259

2	2.8684	1.9963	2.1953	2.9713	
3	2.9997	2.4957	2.1145	1.6099	
4	2.8850	2.8850	1.9767		
5	2.6632	2.5275	1.8032		
6	2.3797	2.1034	1.6042		
7	2.0218	1.6086	1.4060		
8	1.5897	1.2623			

4.3 Supersonic Fighter Wing

A multi-spar fighter wing with no stringers is examined for the third example. In order to work on realistic aircraft data, the layout and the technical characteristics of Eurofighter Typhoon aircraft are used. Many details of the Typhoon Aircraft are provided in the official technical guide [23].

4.3.1 Input File

The first input to the tool developed for this thesis is the airfoil data. Since the airfoil shape is not provided in the Eurofighter technical guide, a typical thin airfoil (NACA 64-206) is used.

The part of the input that contains wing planform data (root and tip chord lengths, taper ratio, and half span) can be seen below:

```
Root chord length (RootChord) [mm]
7200

Tip chord length (TipChord) [mm]
1200

Taper Ratio (Taper)
0.1667

Wing Half Span (HalfSpan) [mm]
4385
```

It should be noted that the wing overall span is 10.95 m according to the technical guide [23]. This means that the half span is 5475mm. However, the fuselage width has to be subtracted from this value. Consequently, the wing half span (the distance from the wing-fuselage connection to the wing tip) is taken as 4385 mm in the input.

The layout of structural members is the next input. The technical guide [23] contains a cutaway drawing of Typhoon aircraft. The cutaway shown in Figure 4-12 can help to specify the numbers of spars and ribs.

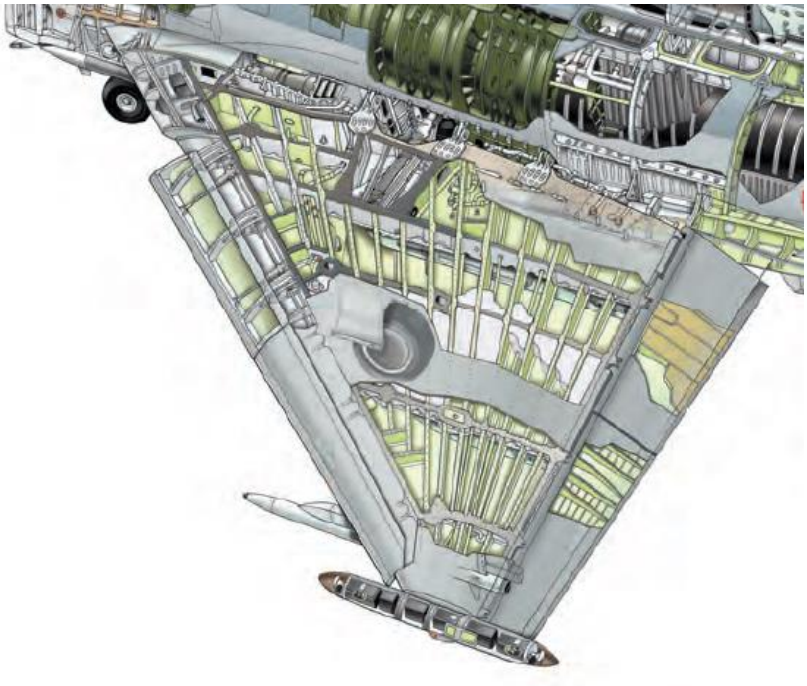

Figure 4-12 Eurofighter Typhoon Wing Cutaway Drawing [23]

It is seen that 15 spars and 7 ribs form the wingbox. The wingbox has many discontinuities as can be seen from the cutaway drawing. For the preliminary design, all structural members can be assumed continuous along the wing. Using this assumption, the numbers and the locations of the structural members are entered as input:

```
Number of Spars (NumOfSpars)
15

Locations of Spars from L.E. (LocOfSpars) (% chord)
12
17
22
27
32
37
42
```

```
47
52
57
62
67
72
77
82

Number of Upper Stringers (NumOfUpStr)
0

Location of Upper Stringers from L.E. (LocOfUpStr) (% chord)


Number of Lower Stringers (NumOfLoStr)
0

Location of Lower Stringers from L.E. (LocOfLoStr) (% chord)


Number of Ribs (NumOfRibs)
7

Location of Ribs from Root (LocOfRibs) (% half span)
0
10
20
35
60
80
100
```

Cross-section of the wingbox formed by the above geometric input is shown in Figure 4-13.

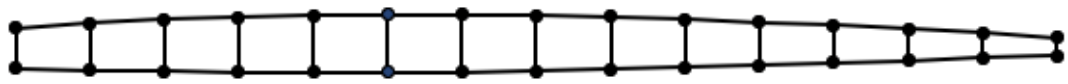

Figure 4-13 Panels and Booms at the Cross-Section of the Wingbox for the Supersonic Fighter Wing

Weight, positive limit load factor, and maximum speed of the Typhoon aircraft are listed below. It should be noted that the value of the Mach number is not used in any calculations but the tool checks whether it is greater than 1.0 in order to decide on the load calculation technique.

```
Load Factor (LoadFactor) (g)
9.0

A/C Weight (ACweight) [kg]
16000.0

Value of Mach number
2.0
```

Finally, material properties of the spars, ribs, upper skins, and lower skins are entered to the input file. It should be noted that Typhoon aircraft is generally made from carbon fiber composites. However, the tool developed for this thesis can only work with isotropic materials. Thus, some typical aircraft materials are used for the example:

```
Upper Skin Material
2024 T851

Upper Skin Ftu [MPa]
486.8

Upper Skin Fcy [MPa]
399.9

Upper Skin E [MPa]
72397

Upper Skin v
0.33

Upper Skin Density [kg/mm3]
2767.99e-9

Lower Skin Material
7475 T7651

Lower Skin Ftu [MPa]
482.6

Lower Skin Fcy [MPa]
413.7

Lower Skin E [MPa]
70329

Lower Skin v
0.33

Lower Skin Density [kg/mm3]
2795.67e-9

Spar Material
7050 T7451
```

```
Spar Ftu [MPa]
510.2

Spar Fcy [MPa]
434.3

Spar E [MPa]
71018

Spar v
0.33

Spar Density [kg/mm3]
2823.35e-9
```

For supersonic vehicles, ESDU inputs are not required. Therefore, all inputs that the tool needs are complete. The overall input file sent to the tool can be seen in Appendix D.

4.3.2 Procedure

The tool carries out the load calculations by Schrenk Approximation for supersonic vehicles. Resulting internal loads at the rib stations are listed in Table 4-15.

Table 4-15 Internal Loads at Rib Locations

Rib	1 (root)	2	3	4	5	6	7 (tip)
V [N]	7.06E+05	6.03E+05	5.06E+05	3.71E+05	1.81E+05	6.70E+04	-5.82E-11
M [Nmm]	1.25E+09	9.60E+08	7.17E+08	4.29E+08	1.31E+08	2.48E+07	2.38E-07

For this problem, the bounds for the design variables are set as [0.5, 5.0]. It should be recalled that the design variables are the two coefficients explained in Section 3.7.2. Thus, the design exploration is made within this interval. The domain is divided into 4 regions because the number of internal grid points is set as 5. Therefore, for each cycle, the sizing is performed 25 times.

After all exploration cycles are finished, a minimum half wing weight of 1008.0 kg is achieved. The resulting design space is shown in Figure 4-14.

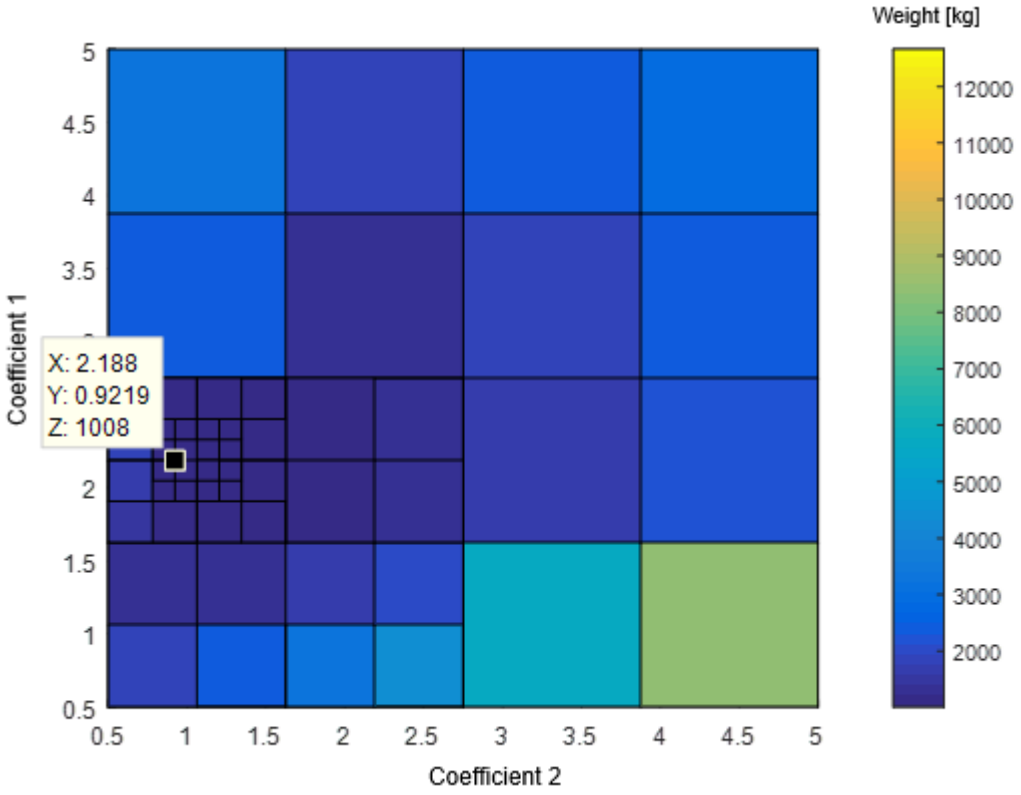

Figure 4-14 Design Space after the Exploration

Summary of the exploration is provided below.

Table 4-16 Summary of the Exploration

Number of Internal Grids for Each Coefficient	5
Number of Repetitive Cycles	4
Lower Bound for the Variables	0.5
Upper Bound for the Variables	5.0
Minimum Wingbox Weight (Half Wing) [kg]	1008.0 kg
Coefficients @ the Minimum Weight	(2.188, 0.9219)

Next section provides the weight breakdown of the best solution. Thicknesses of the components at wing sections are also listed.

4.3.3 Outputs

Weight breakdown of all structural members is provided in Table 4-17.

Table 4-17 Weight Breakdown of All Structural Members

Section	1	2	3	4	5	6
Weight of Upper Skins [kg]	52.99	44.63	55.91	67.52	26.36	10.94
Weight of Lower Skins [kg]	22.55	18.99	23.79	28.74	11.22	4.66
Weight of Spars (Webs+Flanges) [kg]	127.56	107.62	135.96	164.58	63.20	24.85
Weight of Stringers [kg]	-	-	-	-	-	-
Weight of Ribs (Webs+Flanges) [kg]	5.14	4.11	3.21	2.10	0.83	0.30
Total Section Weight [kg]	**208.25**	**175.35**	**218.87**	**262.93**	**101.61**	**41.04**

It is obvious that the upper skins are much heavier than the lower skins. This is because initial buckling of skins is not allowed for supersonic vehicles. Section 4 is heavier than Section 3 although it is closer to the tip. This is because the span of section 4 is much higher than the span of section 3.

The ratio of the total half wing weight to the overall aircraft weight is much higher than the one in turboprop trainer example. This is because Typhoon aircraft does not have horizontal tails so the wings have a very large area.

Finally, the thicknesses of all panels in the root section are provided in Table 4-18.

Table 4-18 Thicknesses of All Panels in Section 1

Section 1	Upper Skins [mm]	Lower Skins [mm]	Spar Webs [mm]	Rib Web [mm]
1	7.0384	3.9004	3.4923	0.8045
2	8.5441	4.1468	4.0489	
3	9.6704	4.3130	4.4598	
4	10.4742	4.4099	4.7527	
5	10.9820	4.4410	4.9382	
6	11.1861	4.3974	5.0219	
7	11.0520	4.2619	4.9847	
8	10.5977	4.0405	4.8111	
9	9.8782	3.7559	4.5313	
10	8.9325	3.4253	4.1655	
11	7.7900	3.0629	3.7305	
12	6.4779	2.6826	3.2387	
13	5.0233	2.3009	2.7056	
14	3.4520	1.9364	2.1463	
15			1.5781	

Table 4-18 show that there are thicknesses up to 11.2 mm at the root section. This value is reasonable when compared to the upper skin thicknesses of similar aircraft. For instance, the F/A-18A upper wing skin thickness goes up to 0.65” (16.5 mm) at the wing root [22]. Although the upper wing skin of F/A-18A aircraft is made of composite materials, the magnitude of the thickness provides a good idea for comparison. Another comparison can be made with the upper wing skin of General Dynamics F-16 aircraft. The wing of F-16 is made of aluminium and thicknesses are approximately 8 mm near the wing root. Since F-16 aircraft is smaller and lighter than Eurofighter, the sizing results of 11.2 mm seems appropriate.

4.4 Additional Treatment for the Exploration Study in Each Design Section

The case studies up to this point have been carried out using the same two coefficients, C1 and C2, throughout the entire wing. In other words, same C1 and C2 are used for all design stations.

In this section, an additional treatment, in which different C1 and C2 values are found for every rib station, is outlined. Design exploration is performed separately at

all stations and the obtained minimum weights are compared to the ones calculated in Sections 4.1 to 4.3.

4.4.1 Subsonic Trainer Wing

The turboprop wing (with an initial buckling level of 50% limit load) examined in Section 4.2 is used again in this study. For all 16 stations of the wing, different C1 and C2 coefficients are obtained. Weights of all 16 sections are minimized separately from each other. As a result, a small decrease in the total wing weight is achieved.

It should be recalled that the half wing weight was 113.9 kg at coefficients (0.9875, 0.7625) as can be seen in Table 4-11. The result of the current study is listed in Table 4-19.

Table 4-19 Summary of the Exploration with Different C1 and C2 at Each Station

Number of Internal Grids for Each Coefficient	5
Number of Repetitive Cycles	4
Lower Bound for the Variables	0.2
Upper Bound for the Variables	2.0
Minimum Wingbox Weight (Half Wing) [kg]	109.02 kg
Coefficients @ the Minimum Weight for Each Station (From 1 to 16)	1.3813, 1.0438 1.325, 1.0438 1.325, 1.0438 1.325, 0.9875 1.2688, 0.9875 1.2125, 0.93125 1.2125, 0.93125 1.2125, 0.93125 1.1, 0.875 1.1, 0.81875 1.0438, 0.81875 0.9875, 0.7625 0.93125, 0.70625 0.875, 0.70625 0.7625, 0.59375 0.65, 0.59375

Comparison of the weights of each section with constant and changing coefficients is provided in Table 4-20.

Table 4-20 Section Weight Comparison

Section	Weight (Constant C1&C2)	Weight (Changing C1&C2)
1	11.90	11.25
2	11.16	10.60
3	10.32	9.87
4	9.60	9.15
5	8.82	8.44
6	8.14	7.79
7	7.42	7.14
8	6.72	6.47
9	8.41	8.28
10	7.24	7.12
11	6.11	6.06
12	5.00	5.00
13	4.11	4.04
14	3.86	3.57
15	2.85	2.47
16	2.20	1.77
TOTAL	**113.87**	**109.02**

It is seen that the improvement in the total wing weight is less than 5%. Optimizing all sections separately resulted in a decrease in the weight but it is not very significant. This is because the structural elements are continuous along the wing and all section geometries are very similar to each other except they are scaled down towards the wing tip. It can be said that this study is an important improvement for the tool because many aircraft wings can have changing cross-section geometries at the rib stations. Number of spars and stringers can change between rib stations. If that was the case, then the optimization of each section would result in a bigger improvement.

The tool developed for this thesis reads a single structural layout from the input file and applies that layout to all stations considering the taper effect. However, it is not a

big challenge to define different stiffener layout for the stations. Once the layout is defined separately for the stations, the study in this chapter would be very useful to optimize each section.

4.4.2 Supersonic Fighter Wing

Similar study is carried out for the fighter wing examined in Section 4.3. It should be recalled that the half wing weight is 1008.0 kg at coefficients (2.188, 0.9219) as listed in Table 4-16.

The results with different C1 and C2 values for all 6 sections are listed in Table 4-21.

Table 4-21 Summary of the Exploration with Different C1 and C2 at Each Station

Number of Internal Grids for Each Coefficient	5
Number of Repetitive Cycles	4
Lower Bound for the Variables	0.5
Upper Bound for the Variables	5.0
Minimum Wingbox Weight (Half Wing) [kg]	995.59 kg
Coefficients @ the Minimum Weight	2.4688, 1.3438 2.4688, 1.2031 2.3281, 0.9219 2.1875, 0.9219 2.0469, 0.9219 1.9063, 0.9219

Comparison of the weights of each section with constant and changing coefficients is provided in Table 4-22.

Table 4-22 Section Weight Comparison

Section	Weight (Constant C1&C2)	Weight (Changing C1&C2)
1	208.25	203.75
2	175.35	171.97
3	218.87	217.96
4	262.93	262.93
5	101.61	100.37
6	41.04	38.62
TOTAL	**1008.05**	**995.59**

It is again seen that the improvement in the wing weight is small. Optimizing all sections separately resulted in a decrease in the weight but it is not very significant for this example due to the reasons explained in Section 4.4.1.

4.5 Remark on the Shape of the Objective Function

As already stated at the end of Section 3.7.2, the objective function has to be a smooth function with a single (global) minimum in the specified domain in order for the exploration study to be valid. Therefore, a detailed illustration for the first design station of the turboprop trainer example is provided in this section.

For this purpose, the tool was compiled with 50 internal grids for each coefficient. Thus, the sizing is performed 2500 times to have a finer discretization which clearly shows the shape of the function.

Side views of the three-dimensional graph are useful in order to better understand the shape of the objective function.

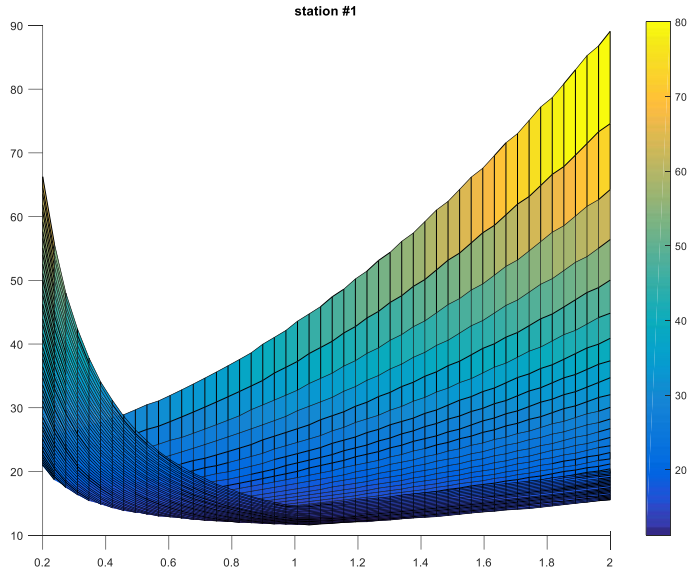

Figure 4-15 Side View 1 of the Objective Function

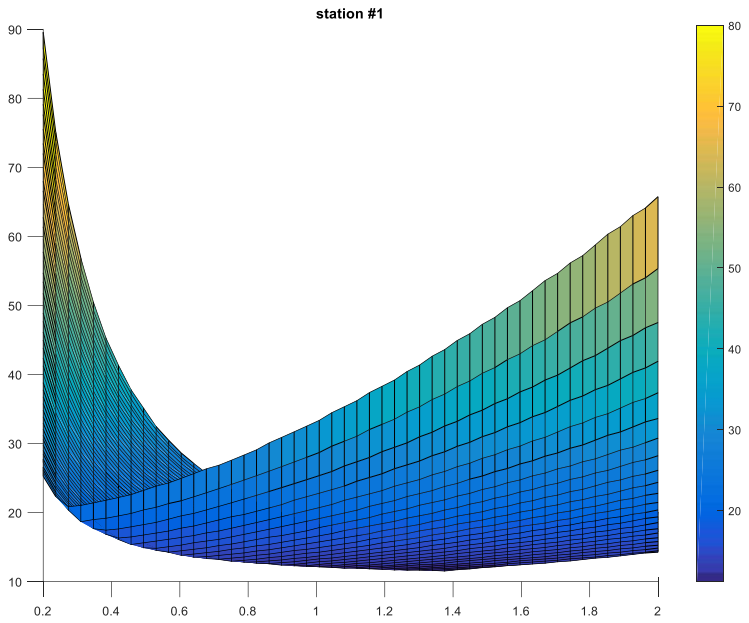

Figure 4-16 Side View 2 of the Objective Function

Another representation is made by adjusting the colors of the figure so that a clearer view of the region with the minimum weight is achieved. Dark blue stands for the minimum weight as can be seen from the color bar. Figure 4-17 is the top view of the objective and shows that the weight is a smooth function and has a single minimum in the specified domain.

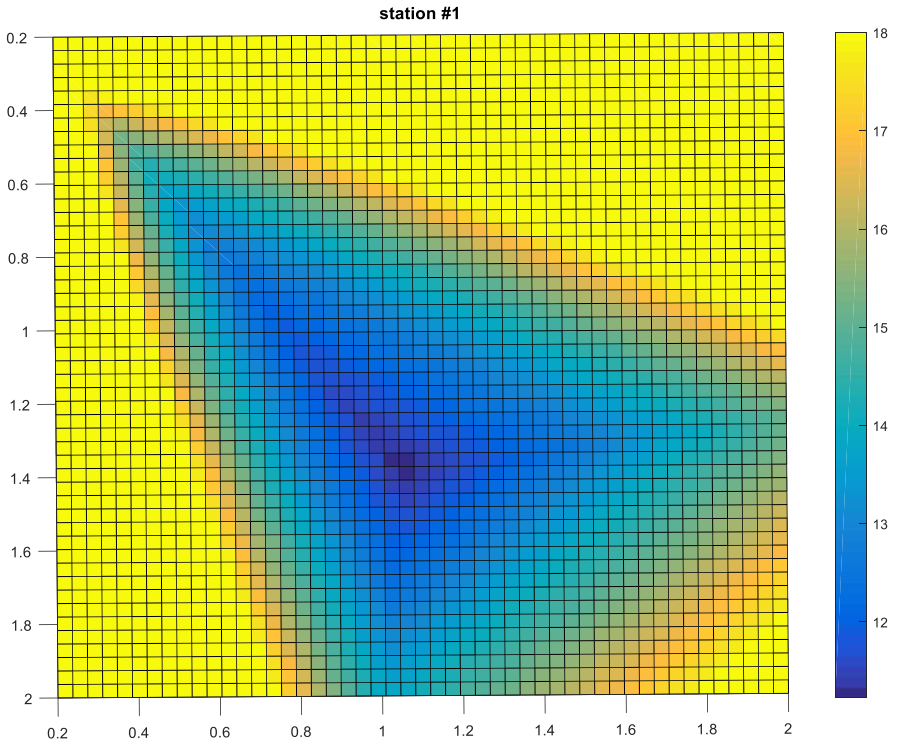

Figure 4-17 Top View of the Objective Function

CHAPTER 5

POST BUCKLING LOAD REDISTRIBUTION OF STIFFENED PANELS

5.1 Introduction

In this chapter, the local buckling of wing skins and the load redistribution after the buckling are examined in detail. The main goal of this chapter is to show:

- Post buckling load redistribution exist and it is important for wing structures,
- Post-buckling loads can be calculated with the methods in literature and can be verified using nonlinear finite element studies,
- A methodology containing iterative application of the linear static finite elements analysis can be used to calculate internal loads after the panel buckling.

As already stated in Chapter 1, compressive buckling of the wing skin panels are usually allowed before the limit load is reached. This saves a lot of weight since the skins are the largest structural elements of wing structures in terms of volume. Post buckling load redistribution is very important for this thesis because the developed tool allows the users to have the initial buckling in subsonic wings before the limit load is reached.

This chapter starts with the linear static finite element analysis approach taken for the internal load distribution. Then, the post buckling and the effective width concepts

are introduced. Significance of the panel edge support conditions are also examined in detail. Finally, the results obtained with the application of the linear and nonlinear finite element studies are compared.

5.2 Post-buckling Effects of Skin Local Buckling

In subsonic wings, elastic buckling of panels is usually allowed long before the limit loading of the wing. After the local buckling of skin panels, load distribution in wingbox is no longer linear. Buckled panel redistributes its load to adjacent stiffer structure, which can be a stringer or a spar cap. On the other side, buckled panel itself has a load carrying capacity that is dependent on the effective amount of the sheet that can still resist to compressive load. *Effective width* parameter represents the effective sheet. Determination of effective width is an iterative process. Realistic load distribution at the post-buckling stage can be obtained once the convergence in the effective width of skin panels is achieved. This thesis offers a methodology to calculate the effective width of skin panels and internal loads through the iterative application of the linear static finite element analysis. Finite element model uses a wingbox section with single two-dimensional shell elements that represent the skin panels between stiffeners and one-dimensional bar elements that represent the spar caps and stringers. Results of the developed methodology show a good agreement with the post-buckling results of nonlinear finite element analysis.

5.2.1 Local Buckling, Post-buckling and Global Buckling

In subsonic aircraft wings, skins in metallic stiffened panels are usually allowed to buckle at about 50% of the limit load. Local buckling of skin panels is therefore the lowest failure mode of a stiffened panel assembly. The first occurrence of panel buckling is referred to as the bifurcation point. The assembly is able to support additional load beyond bifurcation point until the global failure of the entire panel occurs due to material yielding or stiffener crippling.

5.2.2 Panel Buckling and Load Redistribution

At the onset of the local buckling of the skin, skin and stiffeners have the same stress levels. In the stage after the local buckling, which can be called as the post-buckling stage, the stiffened panel has a nonlinear stress distribution.

5.2.2.1 Compression Post-buckling

Skins, that are no longer effective to carry additional compressive load, redistribute the additional loading to the adjacent structural members. Stiffer neighboring structures are the spar caps (flanges) and the stringers. Compressive load and the stress distribution before buckling are shown in Figure 5-1 and Figure 5-2. The load distribution over the panel after buckling is represented in Figure 5-3. It is important to note that the region of skin panels at the stiffener attachment lines does not buckle. In other words, the stiffener and skin have the same strain at the attachment line. On the contrary, stresses stay at the bifurcation level at the mid-panel. Figure 5-3 shows the varying stress over the stiffened panel.

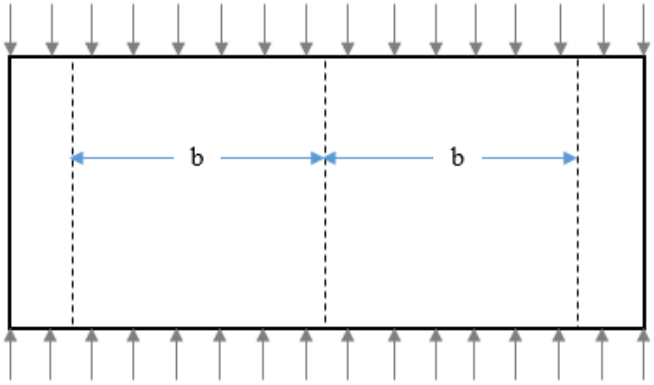

Figure 5-1 Representation of the Compressive Load on a Stiffened Panel

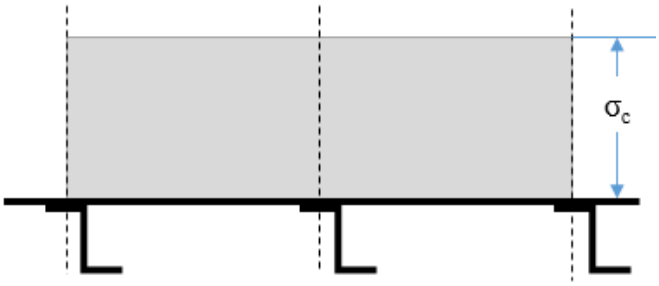

Figure 5-2 Stress Distribution before the Panel Buckling

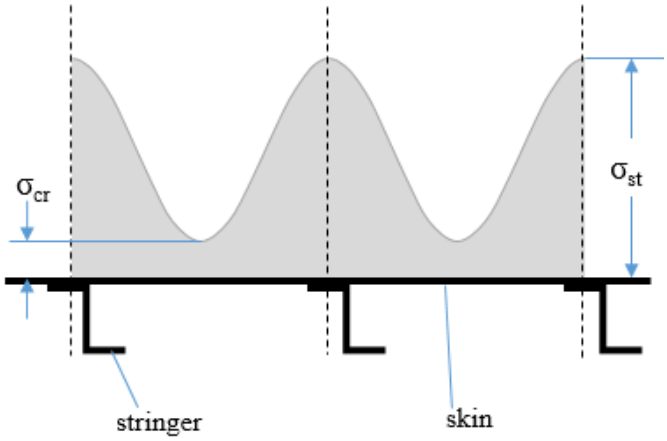

Figure 5-3 Stress Distribution after the Panel Buckling

Bruhn [19] makes use of an equivalent width that carries uniform stress instead of the actual panel width with continuous variable stress. This is useful to handle the variable post buckling stress over a panel. Hereby, effective portion of the panel that can still carry the compressive load is represented by an *effective width*. Figure 5-5 provides a representation of the effective width.

Effective width gets narrower with increasing applied load. Effective skin and the stiffener keep on carrying the stress until entire assembly (stiffener + effective skins) collapses. The collapse can also be called as the global failure of the stiffened panel. Figure 5-4 and Figure 5-5 show two adjacent panels of equal thickness and width attached to three stringers.

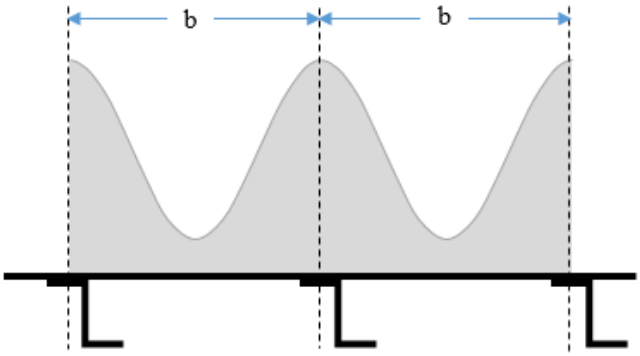

Figure 5-4 Actual Post Buckling Stress Distribution

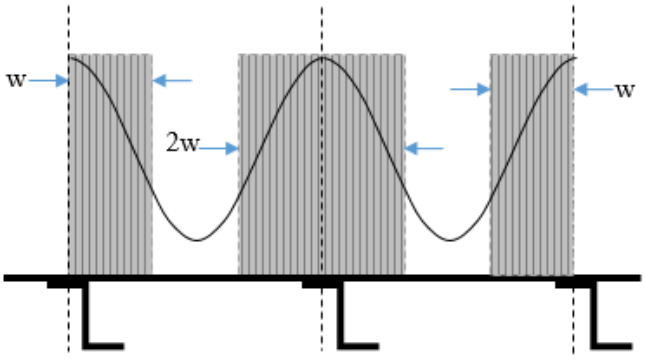

Figure 5-5 Equivalent Distribution with Effective Width Representation

Above figures are valid for uniform compression. Effective widths around stiffeners would be different from each other in the case of non-uniform loading and panel dimensions.

5.2.2.2 Shear Post-buckling

When local buckling occurs under shear, skin panel goes into a mode called as the diagonal tension mode. Figure 5-6 shows the internal diagonal compressive stresses produced by shear. Kuhn [24] uses a parallelogram frame of stiff bars to describe the diagonal tension as shown in Figure 5-6a. When the applied load P is small, diagonal bars have equal and opposite stresses. With the load P increasing, one diagonal (the one under compression) buckles (Figure 5-6b). In a similar manner, a thin sheet

inside a square frame (Figure 5-6c) experiences a pure shear up to a certain load level. After that level, tensile stress becomes rapidly predominant over the compressive stress (Figure 5-6d). This is because the sheet buckles due to diagonal compressive stress. Consequently, the diagonal tension, in a direction perpendicular to that of the buckle, starts being dominant.

This phenomenon is important in a wingbox structure because the presence of diagonal tension field results in an additional compressive load on the adjacent stiffeners. The procedure to calculate the additional loads is described by Kuhn [24].

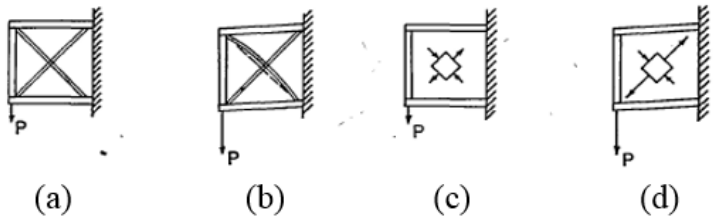

Figure 5-6 Diagonal Tension Represented on Diagonal Bars and a Flat Sheet

5.3 Post-buckling Load Redistribution Study

5.3.1 Model Approach

Linear static finite element solver may be used to tackle the load redistribution problem of buckled skin-stringer assemblies. Finite element model used for this study is a coarse model that is formed by a single shell element for each panel enclosed by stiffeners. One-dimensional bar elements are used to model the spar flanges and the stringers. These elements have axial and torsional stiffness about their longitudinal axis. Two-dimensional shell elements used to model the panels are general-purpose plate elements capable of carrying in plane force, bending, and transverse shear.

It should be noted that this is a very typical model approach in aircraft structures. This approach is preferred because it is simple and advantageous for error minimization. It also makes it straightforward to extract the skin-stringer and skin-

spar station loads/stresses at all design stations. On the other hand, this type of modelling is not helpful for the buckling of panels. A finer mesh is needed to have healthy buckling results. However, fine meshing is not generally desired for global finite element models because of the high computational cost. Global finite element models represent the entire vehicle and they are solved for hundreds of different load cases. This is why smaller element sizes and non-linear solutions would cause a great penalty in time and cost. A small portion of the finite element model of a wing panel is given in Figure 5-7. This representative figure does not include node and element numbers and is useful to visualize the modelling approach.

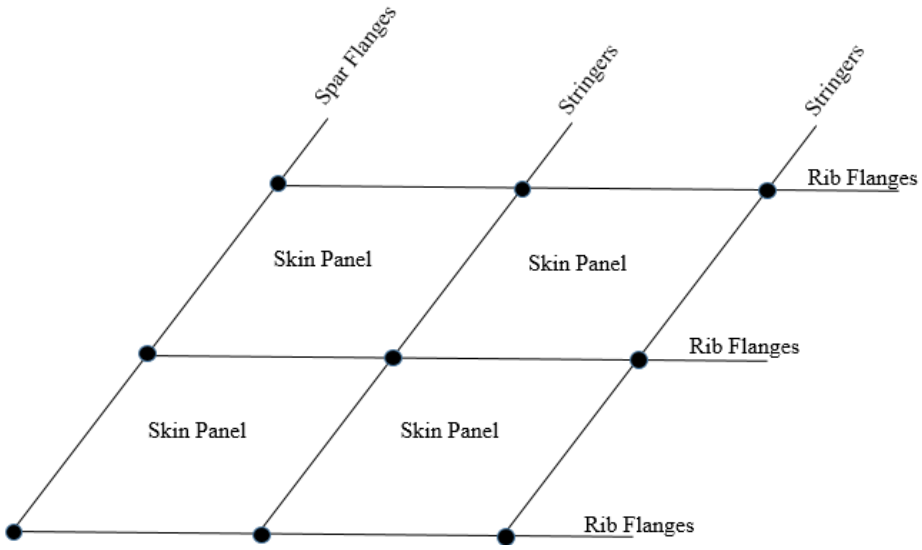

Figure 5-7 Representative Finite Element Model of a Stiffened Panel

5.3.2 Method

A methodology is developed to obtain the effective widths and internal loads through the iterative utilization of linear finite element analysis. Shell elements in the finite element model initially have the true design thicknesses. Stresses in skins, stringers, and spar caps are extracted after the first solution of the model based on initial element properties. Then, compressive buckling of skin panels is checked and buckled panels are identified. Since the buckled panels are no longer fully effective, the effective widths are to be determined. After the calculation of effective widths for

the particular stress state, finite element model is updated. The update is performed using the equivalent thicknesses of buckled panels. Subsequently, the finite element analysis is performed once again with the updated model. This iteration continues until the convergence in all effective widths and internal stresses. Figure 5-8 gives the flow chart of the iteration process used to determine the effective width through linear static finite element analysis.

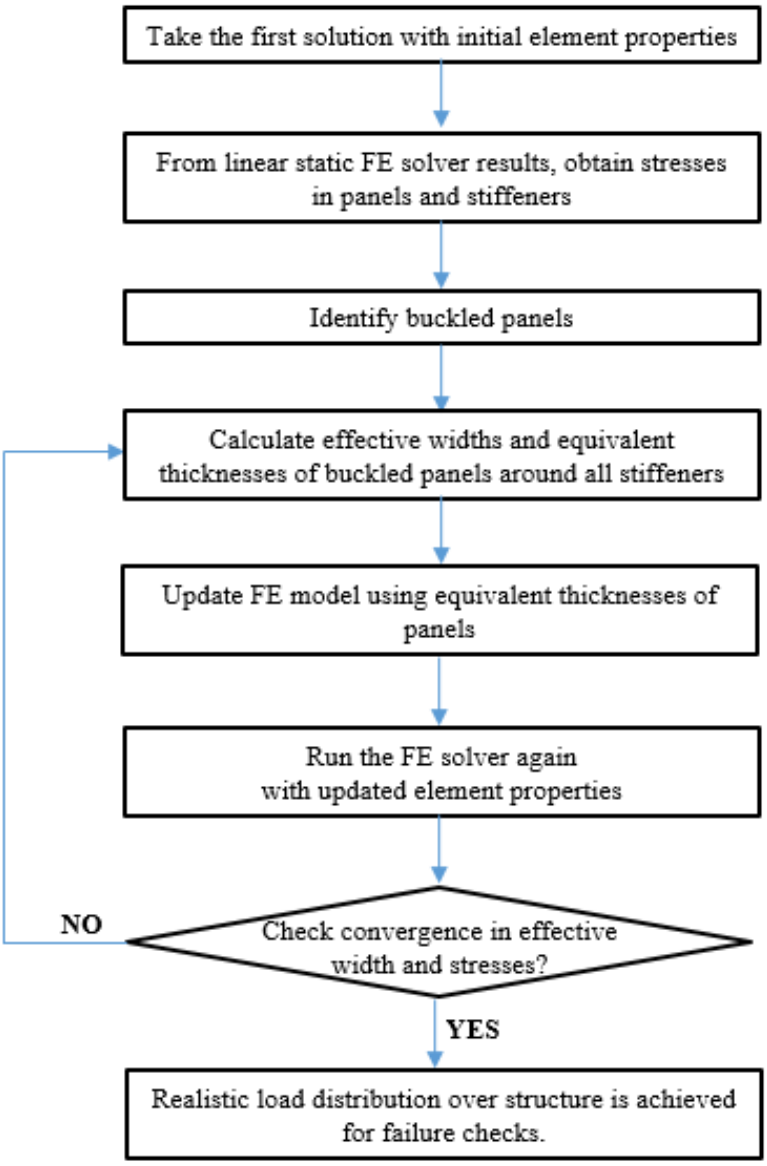

Figure 5-8 Flow Chart of the Iteration for the Determination of Effective Widths and Thicknesses

5.3.2.1 Buckling Check of Panels

Buckling of the panels is checked according to Section 3.3 of this thesis. Buckling allowable stresses are calculated using the panel geometries and material properties. Applied stresses are obtained from the linear static finite element results. Since all

panels are modelled using a single quadrilateral shell element, the average axial stress on the shell is directly available in the finite element solver output.

5.3.2.2 Calculation of the Effective Width

Effective width method handles the compressive post-buckling behavior after the elastic compressive buckling of skin panels. The concept is based on representing the effective compressive stiffness of skin panels using a semi-empirical method. Traditional effective width method is based on Von Karman's effective width formula and it works for compressive loads. However, effective width concept does not perfectly tackle the compression and shear cases. Heitmann and Horst [10] demonstrate the significant influence of shear to the effective compression stiffness of the skin. It is stated that the effective compressive stiffness decreases with increasing shear force. The reason for this decrease is the diagonal tension field.

Similarly, Heitmann and Horst [10] showed that the effective shear stiffness of the panel decreases with an increase in the compression force. Although this effect is not as significant as the influence of shear on the compression stiffness, it is still not negligible.

Practical effective width methodology for pure compression is used in successive iterations in this chapter. It is appropriate to neglect shear because compressive load on upper skin of the wing box structure is much more dominant when compared to shear, especially in the preliminary sizing loads. Nonetheless, buckling check for pure shear is made to verify that skins do not enter into diagonal tension mode because of shear buckling. Effective width method outlined below is reliable for the purpose of this study under this circumstance.

Equation (5.1) [19] defines the effective width:

$$2w = kt\sqrt{E / \sigma_{st}} \tag{5.1}$$

where t is the panel thickness, E is the panel elastic modulus, and σ_{st} is the axial stress on the stiffener around which the effective width is calculated. It should be

noted that *w* is the effective width on one side of the stringer and 2*w* stands for the both sides. Figure 5-9 shows the effective width representation of skin around a stringer.

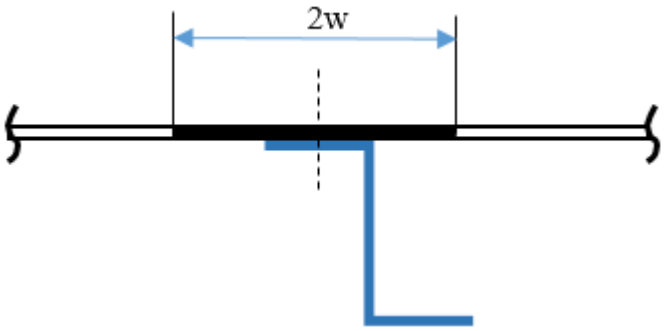

Figure 5-9 Effective Width Representation

Typical value for *k* in Equation (5.1) is 1.9 for simply supported boundaries [19]. Derivation of *k* depends on the assumption that the remaining effective strip must be at its buckling level under the assumed support conditions. In other words, the panel width is replaced with a new and narrower one and this new narrow panel has a buckling strength that is equal to the adjacent stiffener stress. If Equation (3.9) is rewritten by replacing the panel actual width *b* with the effective width *2w*, Equation (5.2) is obtained.

$$2w = t\sqrt{\frac{\pi^2 k_c E}{12(1-\nu^2)}\frac{1}{\sigma_{st}}} \tag{5.2}$$

In a similar manner, Equation (3.10) can be rewritten to have an expression for the effective width under simply support assumption:

$$2w = t\sqrt{\frac{(3.62)E}{\sigma_{st}}} \tag{5.3}$$

Above expression returns the *k* value in Equation (5.1) as 1.9. Thus, effective width formula used in the present study is given as:

$$w = 0.95t\sqrt{E/\sigma_{st}} \tag{5.4}$$

If fixed (clamped) boundaries can be assumed at the skin-stringer attachments, then the effective width increases. Equation (5.5) can be used for the calculation of the effective width [19] in that case.

$$w = 1.26t\sqrt{E/\sigma_{st}} \tag{5.5}$$

Equations (5.2) - (5.5) imply that the effective width method starts to work after the stress surpasses the buckling allowable stress under pure compression. If the panel buckles under combined loading according to Equation (3.13), the effective width formula is unable to calculate a realistic effective width value because axial stress of the stringer is less than the pure compression buckling strength of the panel. If, due to the contribution of shear, the panel buckles before reaching its pure compression buckling allowable stress, effective width formula returns an irrational value that is greater than original panel width. Therefore, in this study, load redistribution is not started until the stringer stress is greater than the compressive buckling strength of adjacent panels, i.e. until $\sigma_{st} > \sigma_{cr}$.

5.3.2.3 Calculation of the Equivalent Thickness

Equivalent thicknesses of panels can be calculated for the next iteration once the effective widths around all stiffeners are obtained. Figure 5-10 shows effective skin widths at the two sides of a panel around stiffeners.

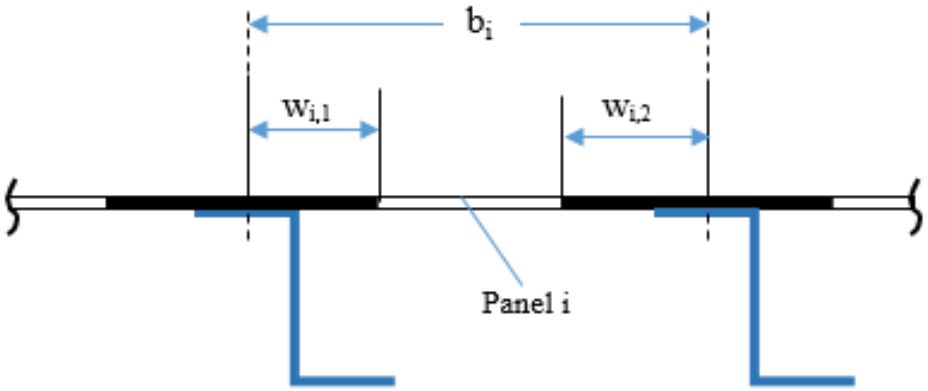

Figure 5-10 Effective Skin Width of a Panel around Stiffeners

Equation (5.6) can be used to relate the updated thickness of the panel to the effective width.

$$(w_{i,1} + w_{i,2}) \cdot t_i = b \cdot t_{eq,i} \tag{5.6}$$

Then, Equation (5.7) gives the equivalent thickness of the panel.

$$t_{eq,i} = \frac{(w_{i,1} + w_{i,2}) \cdot t_i}{b} \tag{5.7}$$

Equivalent thickness of the buckled panel is updated in the finite element model for each iteration and stiffener stresses are re-calculated. After that, using the updated stiffener stresses, effective widths and equivalent thicknesses of panels are calculated again. This iterative process continues until the convergence in all effective widths, equivalent thicknesses and stresses is achieved.

5.3.3 Results of a Sample Case

A typical wingbox is used to evaluate the results of the described post-buckling load redistribution technique. Figure 5-11a shows a sample wingbox provided by Bruhn [19] and Figure 5-11b is the finite element model of that wingbox. The model is generated using the finite element model approach described in the previous sections. Only the root portion of the wing is used for this study. Buckling of upper panels

adjacent to the root rib is examined and load redistribution study is carried out. Finite element model of the root portion is shown in Figure 5-12.

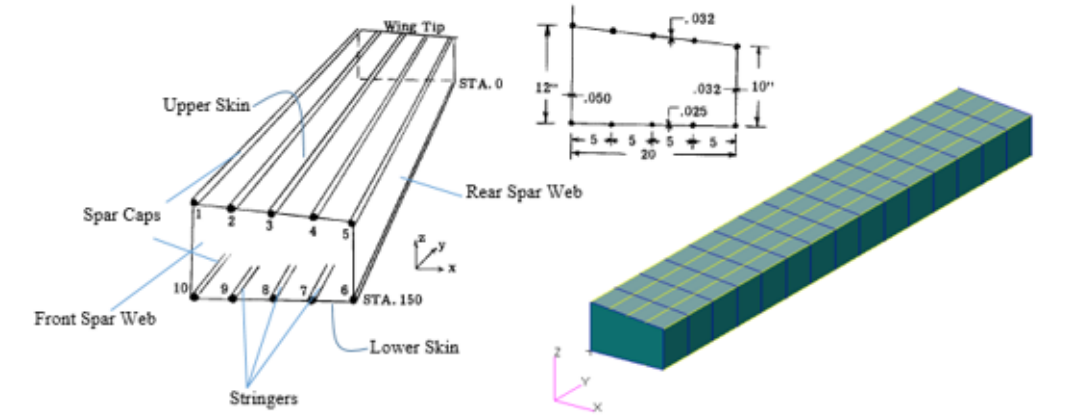

Figure 5-11 Example Wingbox [19] and the Finite Element Model

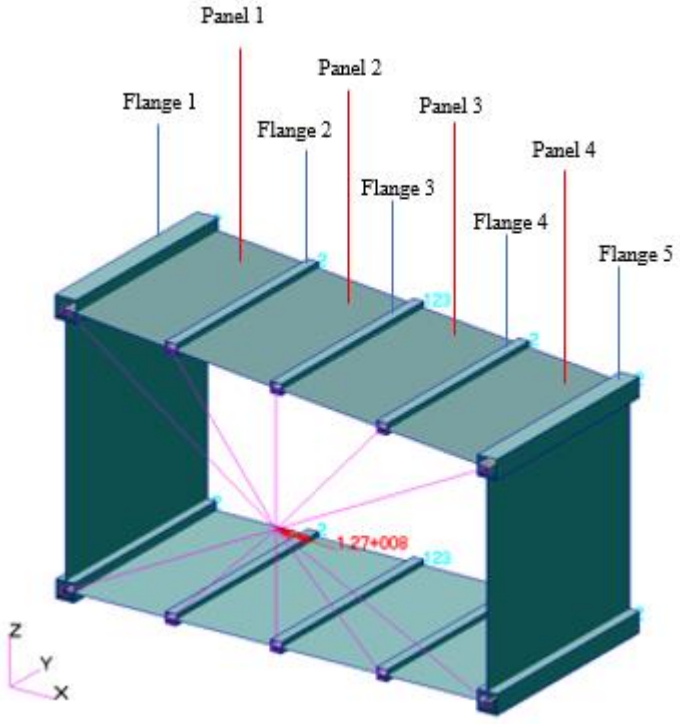

Figure 5-12 Root Section the Sample Wingbox

MSC NASTRAN SOL101 [25] linear static solution sequence is utilized for the linear static analysis of this problem. It is to be observed that root moments given in the problem is applied to the box using a RBE2 element [25]. RBE2 element is a multi-point constraint that is appropriate for this type of loading. RBE2 prevents the distortion of the cross section under applied moment. Unloaded side of the box is constrained in all translational degrees of freedom. The root portion of wingbox is loaded with a X moment of -127.1kNm and a Z moment of 7.6kNm. Upper flange areas and upper panel thicknesses of the box are listed in Table 5-1. Flange and panel numbers ascend along positive X direction according to the coordinate system seen on the lower left of the model.

Table 5-1 Wing Upper Panel Dimensions

a) Upper Flange Areas

Flange	1	2	3	4	5
	A_1	A_2	A_3	A_4	A_5
Area [mm^2]	645	161	161	161	516

b) Panel Thicknesses

Panel	1	2	3	4
	t_1	t_2	t_3	t_4
Thickness [mm]	0.8128	0.8128	0.8128	0.8128

It should be noted that the upper panels are all the same in terms of thickness, length, width, and material. Long dimension of skin panels is 254 mm and short (loaded) edges are 127.6 mm. This corresponds to an aspect ratio, *a/b* of 2. Compressive buckling coefficient corresponding to this aspect ratio is 4 for simply supported boundaries [19].

Skin and stiffener materials are all the same with an elastic modulus of 70000 MPa and Poisson's ratio of 0.3. Substituting these parameters into Equation (3.10) returns a buckling strength of 10.3 MPa for upper panels. Table 5-2 summarizes the geometric and material properties of the upper panels. It should be noted that

combined compression and shear buckling is not checked since the panels do not carry any shear stress due to the loading condition of the sample study.

Table 5-2 Upper Skins Properties

t [mm]	0.8128	ν	0.3
a [mm]	254	k_c	4
b [mm]	127.6	σ_{cr} [MPa]	10.3
E [MPa]	70000		

Results of the linear static finite element solution after the first iteration are listed in Table 5-3. The results of the initial solution, at which local buckling of the skin panels are disregarded, are listed in Table 5-3. Compressive stresses at upper panels are greater than 200 MPa as shown in Table 5-3c, which means that the panels would buckle at about 5% loading. This very small buckling level is not acceptable in real life but it is practical for this study to observe the post-buckling load redistribution.

Table 5-3 Results of the Initial Solution

a) Stresses at Upper Spar Caps and Stringers

Flange	1	2	3	4	5
	$\sigma_{st,1}$	$\sigma_{st,2}$	$\sigma_{st,3}$	$\sigma_{st,4}$	$\sigma_{st,5}$
Stress [MPa]	206.81	209.54	212.26	214.99	217.72

b) Loads at Upper Stations

Station	1	2	3	4	5
	P_1	P_2	P_3	P_4	P_5
Load [N]	152550	55474	56195	56917	131995

c) Average Stresses at Upper Panels

Upper Panel	1	2	3	4
	$\sigma_{up,1}$	$\sigma_{up,2}$	$\sigma_{up,3}$	$\sigma_{up,4}$
Stress [MPa]	-208.2	-210.9	-213.6	-216.4

The results obtained after convergence in effective widths and stiffener stresses are listed in Table 5-4. Realistic post-buckling load distribution is obtained after 4 iterations. This is a fast convergence but it is not surprising. Fast convergence was an expected result that is stated by Flabel [26]. The illustrative model used for this study is a simple and a small model, which is another contributor to the fast convergence.

Table 5-4 Results of the Final Solution

a) Stresses at Upper Spar Caps and Stringers

Flange	1	2	3	4	5
	$\sigma_{st,1}$	$\sigma_{st,2}$	$\sigma_{st,3}$	$\sigma_{st,4}$	$\sigma_{st,5}$
Stress [MPa]	242.11	245.42	248.73	252.03	255.34

b) Loads at Upper Stations

Station	1	2	3	4	5
	P_1	P_2	P_3	P_4	P_5
Load [N]	171281	44717	45285	45851	145508

c) Effective Widths of Panels

Panel	1	2	3	4
	w_1	w_2	w_3	w_4
Effective Width [mm]	26.17	25.99	25.82	25.65

Focusing on some specific parameters would be helpful at this stage. Change in the total effective width of ‘panel 2’ and change in the compressive stress in ‘stringer 2’ with respect to iterations can be seen in Figure 5-13.

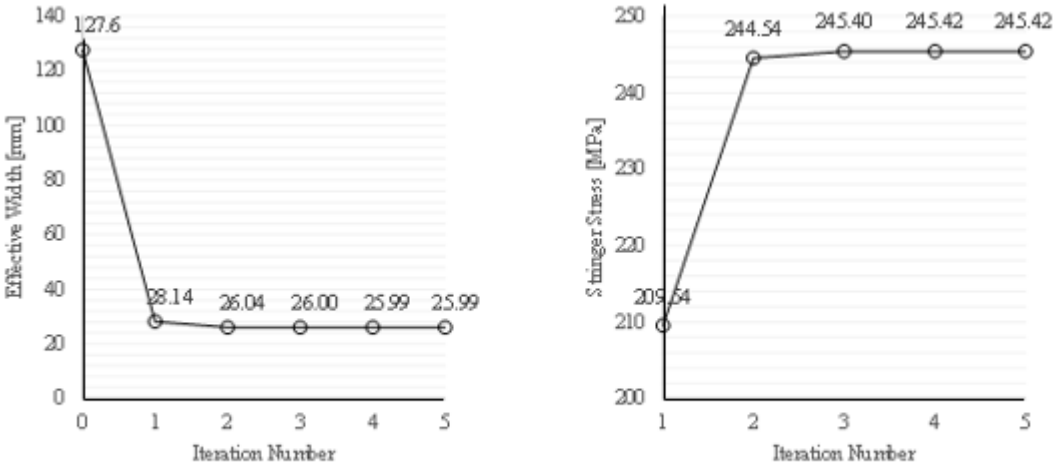

a) Change in Effective Width of Panel 2

b) Change in Stress at Stringer 2

Figure 5-13 Iteration History of Certain Parameters

It is obvious that very different stresses and loads are obtained when compared to the initial finite element solution. Results show that narrow effective widths resulted in small equivalent thicknesses, which caused a drastic decrease in the inertia of the section, and a drastic increase in spar cap and stringer stresses. Another significant point is that the forces at the spar caps (numbered as 1 and 5) are larger in the post-buckled state. This means that a marginal sizing (a sizing with very small margins of safety) based on the initial FE results would lead a failure in spar flanges. On the contrary, forces at stringer stations decrease after the buckling of panels. This is because of the narrow effective widths around the stringers. Loads at the stations are directly related to the total area at that station (the sum of the stiffener area and the effective skin width around that stiffener). Hence, the spar flanges become more dominant after the buckling and the loads the spar stations increase.

The clearest outcome of the study is that the initial finite element solution, that does not consider buckling effects, gives inaccurate results that should not be directly used in sizing. About 15% greater stress is obtained in the upper stringers and in the spar caps after the load redistribution. This shows correlation with expected post buckling

results. Overall, it is obvious that elastic buckling somehow has to be taken into account and the methodology offered in this study can be helpful for that purpose.

5.3.4 Comparison with Nonlinear Finite Element Solution

In order to check the validity of the obtained results, a sample study on a stiffened panel is carried out. Sample stiffened panel includes a thin panel and two half panels that are adjacent to stiffeners. The panel is first modeled with a fine mesh of 1600 quadrilateral shell elements for each half panel and 80 bar elements for each stringer. This model is used to obtain a geometric nonlinear finite element solution using MSC NASTRAN implicit nonlinear solver sequence SOL600 [27] which provides the capabilities required to simulate panel post-buckling behavior.

A second model of the same plate is generated using the modeling approach outlined in Section 5.3.1. The second model is much simpler than the first one. Load redistribution is performed on this model using the methodology offered in Figure 5-8. Fine and coarse models used for comparison study are shown in Figure 5-14.

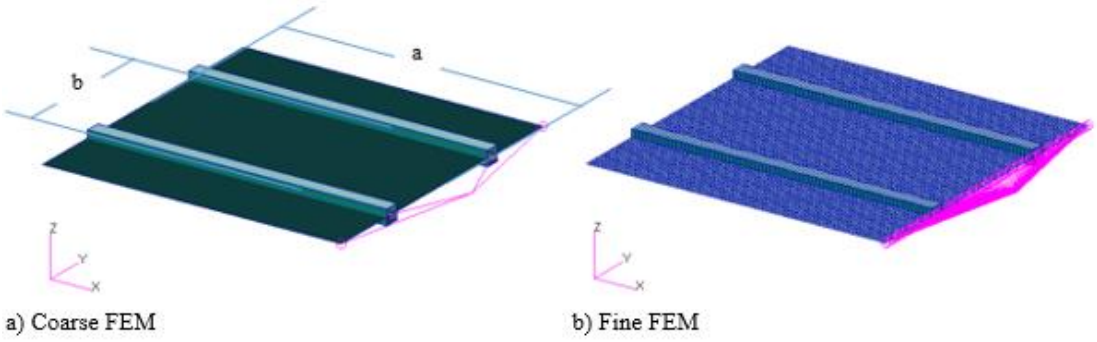

Figure 5-14 Finite Element Models for Comparison

Table 5-5 provides the geometric and material properties of the stiffened panel:

Table 5-5 Properties of the Sample Panel

Panel thickness	t [mm]	2.0
Long dimension of plate	a [mm]	200
Short dimension of panel (loaded edge)	b[mm]	100
Elasticity modulus of panel and stiffener	E [MPa]	70000
Poisson Ratio	ν	0.3
Compressive buckling factor	k_c	4
Panel Buckling Strength	σ_{cr} [MPa]	101.2
Stiffener Area	A [mm^2]	100

It is to be observed that RBE2 elements on right end of panels are used for load application. RBE2 element makes it possible to achieve a uniform end shortening. RBE2 connects all the edge nodes to a single node. An enforced displacement of 0.6mm in the longitudinal (negative X) direction is applied to that single node.

Simply supported boundaries are assumed for the comparison study. The support condition is first verified on the fine model. The verification is necessary because load redistribution calculations in the iterative linear finite element analysis are made using simply supported plate buckling coefficient. This is why a logical comparison is not possible unless the support condition of the nonlinear FEM is proven to fit the simply support assumption. It is known that 0.6 mm end shortening causes a compressive linear stress of 210.0 MPa in the panel assembly. Substituting the necessary parameters to Equation (3.10), it is calculated that local buckling occurs at 101.2 MPa (48% of the applied loading) if all edges are simply supported. Linear buckling analysis with MSC NASTRAN SOL105 is performed to compare the first buckling mode with the calculated bifurcation level of 48%. Loads, boundary conditions and the first buckling mode of the stiffened panel are shown in Figure 5-15.

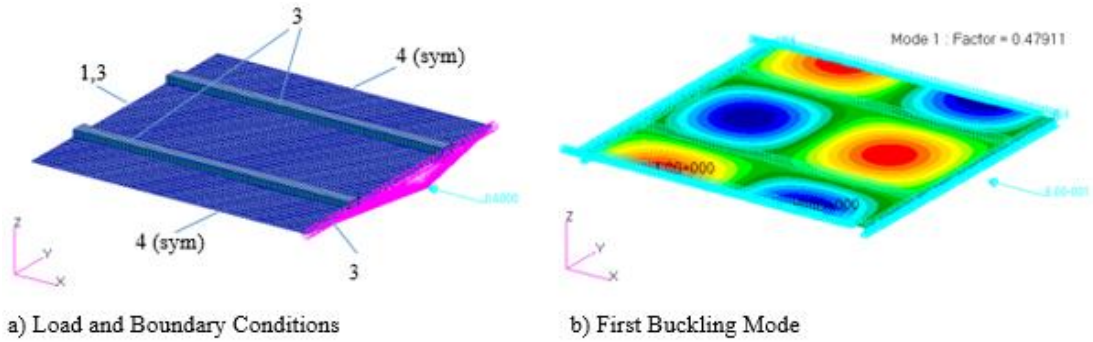

a) Load and Boundary Conditions b) First Buckling Mode

Figure 5-15 First Buckling Mode (SOL105 Result)

1, 2, and 3 in Figure 5-15a define translational restraints along the X, Y, and the Z directions, respectively. 4 stands for the rotational restraint along the X direction. Sides of stiffened panel is restrained in 4 to model the symmetry condition along Y direction. All edge nodes of the middle panel are fixed in Z direction. Stiffener nodes are also constrained in Z because they are modeled using bar elements with no bending stiffness. Thus, they cannot display an out-of-plane support for the panel without the help of the fixation in the Z direction. Load is applied to the right end of the panel through a RBE2 element. Left end is fixed in X direction to react loading. A small detail to notice is that a single node in left end is fixed along Y direction. Although there is no load acting along Y direction, this single point constraint is necessary to avoid rigid body motion.

Figure 5-15b shows the first buckling shape with a factor of 0.47911. This value exactly matches with the bifurcation level calculated using Equation (3.10). Therefore, the boundary conditions shown in Figure 5-15a can be used to obtain the post-buckling behavior of the simply supported stiffened panel in nonlinear finite element analysis. Although a successful verification is obtained for this sample problem, a detailed study is obligatory to better understand the effects of different boundary conditions. Following sections contain various trials and validations carried out on a flat rectangular plate. The following validation is the base to the edge conditions shown in Figure 5-15a.

5.3.4.1 Panel Compressive Buckling Factor Verification Study

Since the initial buckling stage (bifurcation) is the most important point on the study of post-buckling behavior, the verification on the edge conditions has to be made first. In this section, the first buckling mode of various support conditions are compared with the ones found from hand calculations using Equation (3.9) and Equation (3.10). This study is carried out on the panel, whose properties are shown in Table 5-5.

5.3.4.1.1 Loaded and Unloaded Edges Simply Supported

The panel is modeled using a mesh of 2D quadrilateral shell elements. The meshing is very fine in order not to miss any buckling modes that would come out of the finite element solver. No stiffener elements are modeled at the edges. Edge restraints are shown in Figure 5-16. All loaded and unloaded edges are fixed in 3, which is the out-of-plane or *Z* direction translation of the panel. It should be recalled that 1, 2, and 3 stand for translational restraints along X, Y, and Z directions, respectively. The panel is modeled in the XY plane, with respect to the coordinate frame at the lower left corner of the image. Enforced displacement of 0.6 mm is applied in the negative X direction. Geometric and material properties are the same as the ones provided in Table 5-5.

It should be noted that the fixed node in 2 direction has no effect on the solution or the buckling modes. A single arbitrary node has to be fixed in 2 just to avoid the rigid body motion and solver error.

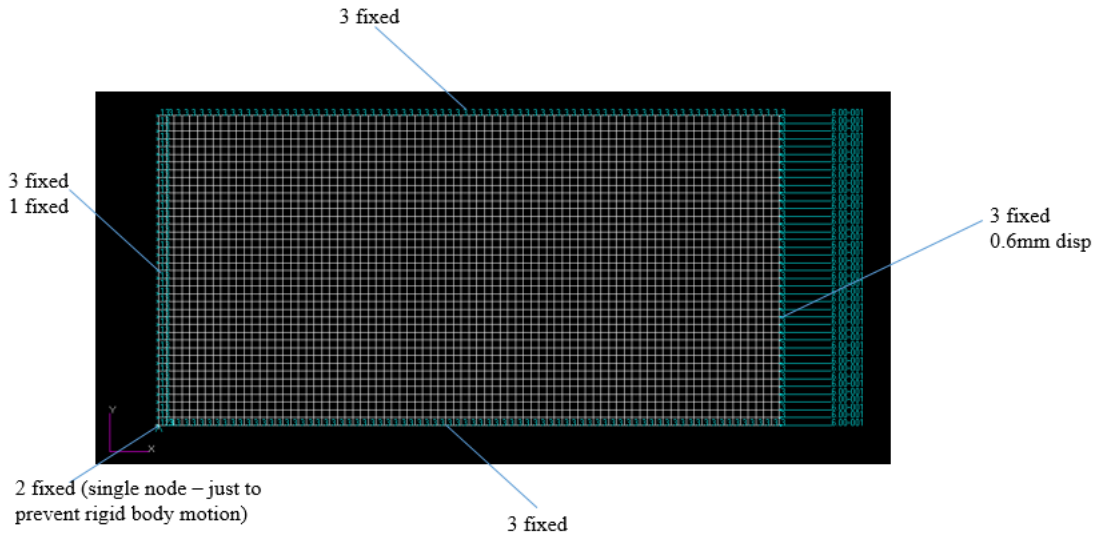

Figure 5-16 Load and Boundary Conditions (Loaded and Unloaded Edges *Simply Supported*)

Initial buckling mode is obtained using MSC NASTRAN's linear buckling solution sequence SOL105. The resulting first buckling mode is provided in Figure 5-17.

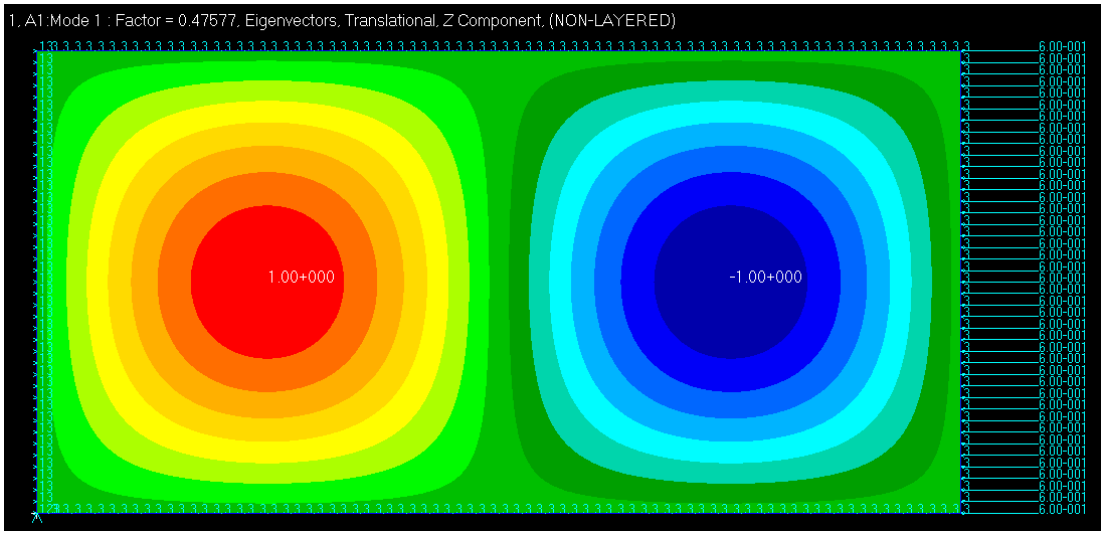

Figure 5-17 Finite Element Solution Results for Loaded and Unloaded Edges Simply Supported

The first mode has a buckling factor of 0.47577, as the factors of the first five modes are shown in Table 5-6.

Table 5-6 List of Factors (Loaded and Unloaded Edges Simply Supported)

Mode 1	Factor = 0.47577
Mode 2	Factor = 0.55843
Mode 3	Factor = 0.7441
Mode 4	Factor = 0.74741
Mode 5	Factor = 1.0014

The first mode of 0.47577 is to be compared to the one found with the hand calculation method. The graph shown in Figure 5-18 is used to determine the buckling coefficient.

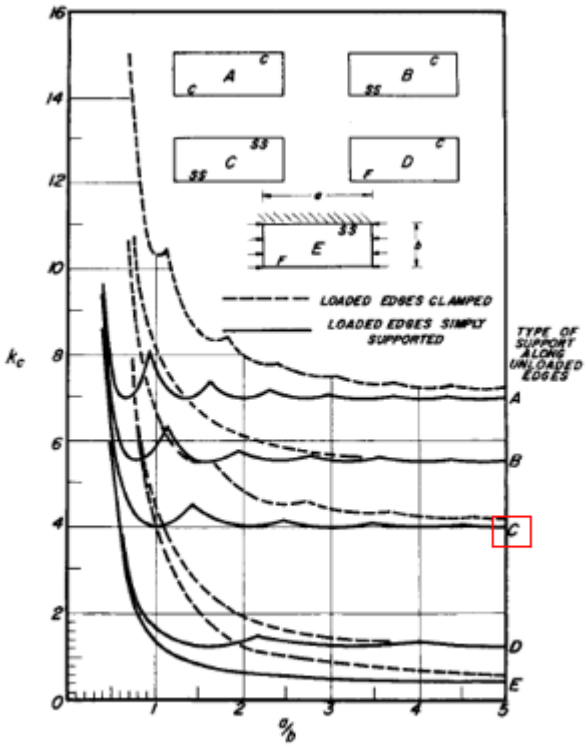

Fig. C5. 2 (Ref. 1) Compressive-buckling coefficients for flat rectangular plates.

Figure 5-18 Compressive Buckling Coefficients from Bruhn [19]

For this case, the compressive buckling coefficient, k_c is equal to 4.0 as can be seen on Figure 5-18. Condition "C" stands for the case for which all the loaded and the unloaded edges are *simply supported*.

Equation (3.10) returns a critical buckling strength of 101.2 MPa with the just determined buckling coefficient. It is known that the 0.6mm enforced displacement results in a compressive stress of 210.0 MPa in the linear range. Therefore, buckling initiation is calculated to be at the 48% (0.48) of the total load, which perfectly fits with the finite element result 0.47577.

Consequently, it is proven that the edge restraints used in this section can provide *simply supported* boundary conditions for the plate.

The main goal of this study is to achieve a configuration that provides simply supported boundaries. The configuration in this section has given successful results. Various edge configurations are examined in the following sections in order to examine different support conditions and stiffener model approaches.

5.3.4.1.2 Loaded Edges Simply Supported / Unloaded Edges Clamped

In this section, simply supported loaded edges are kept while the unloaded edges are clamped. Clamped edges are obtained by fixing all rotational (4, 5, and 6) degrees of freedom. Loading condition is the same as the previous section. Edge restraints and applied load for this case are shown in Figure 5-33.

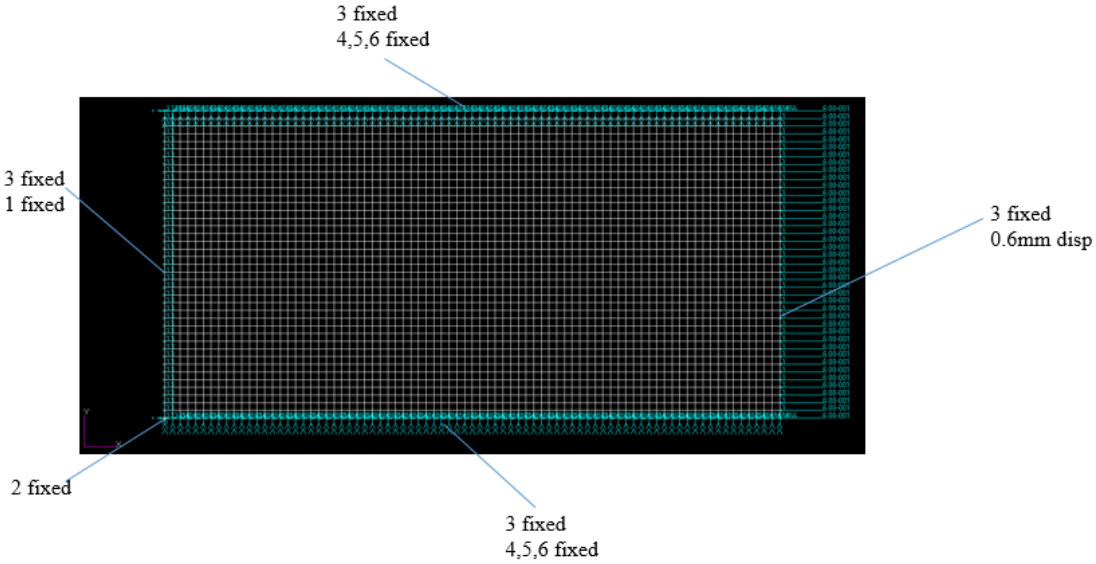

Figure 5-19 Load and Boundary Conditions (Loaded and Edges *Simply Supported* / Unloaded Edges *Clamped*)

Figure 5-18 is used once more to determine the buckling coefficient. For this configuration, the compressive buckling coefficient, k_c is equal to 6.97 as can be seen on Figure 5-18. Condition "A" stands for the case at which the loaded edges are *simply supported* and the unloaded edges are *clamped*.

Equation (3.10) returns a critical buckling strength of 176.4 MPa with this buckling coefficient. As already stated, 0.6mm enforced displacement results in a compressive stress of 210.0 MPa in the linear range. This means that the buckling initiation occurs at the 84% (0.84) of the total load. This is the value to be compared with the finite element results.

Initial buckling mode is obtained using MSC NASTRAN's linear buckling solution sequence SOL105 with the same way as in 5.3.4.1.1. The resulting first buckling mode is provided in Figure 5-20.

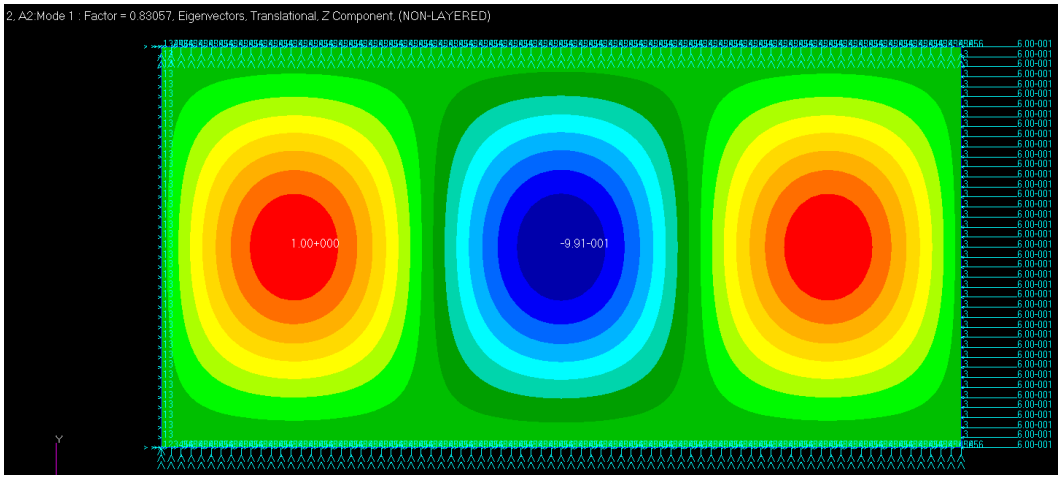

Figure 5-20 Finite Element Solution Results for Loaded Edges *Simply Supported* and Unloaded Edges *Clamped*

The first mode has a buckling factor of 0.83057, as the factors of the first five modes are shown in Table 5-7.

Table 5-7 List of Factors (Loaded Edges *Simply Supported* and Unloaded Edges *Clamped*)

Mode 1	Factor = 0.83057
Mode 2	Factor = 0.91569
Mode 3	Factor = 1.0271
Mode 4	Factor = 1.1243
Mode 5	Factor = 1.4171

The first mode with a factor of 0.83057 perfectly matches to 0.84, which is found by hand calculations. Therefore, it can be concluded that the edge restraints in this section can provide *clamped* boundary conditions for the plate.

5.3.4.1.3 Loaded Edges Simply Supported / Unloaded Edges Simply Supported and Free

The configuration in this section is the same as the one examined in Section 5.3.4.1.1 except one of the unloaded edges is *free*. Edge restraints for this case are shown in Figure 5-21.

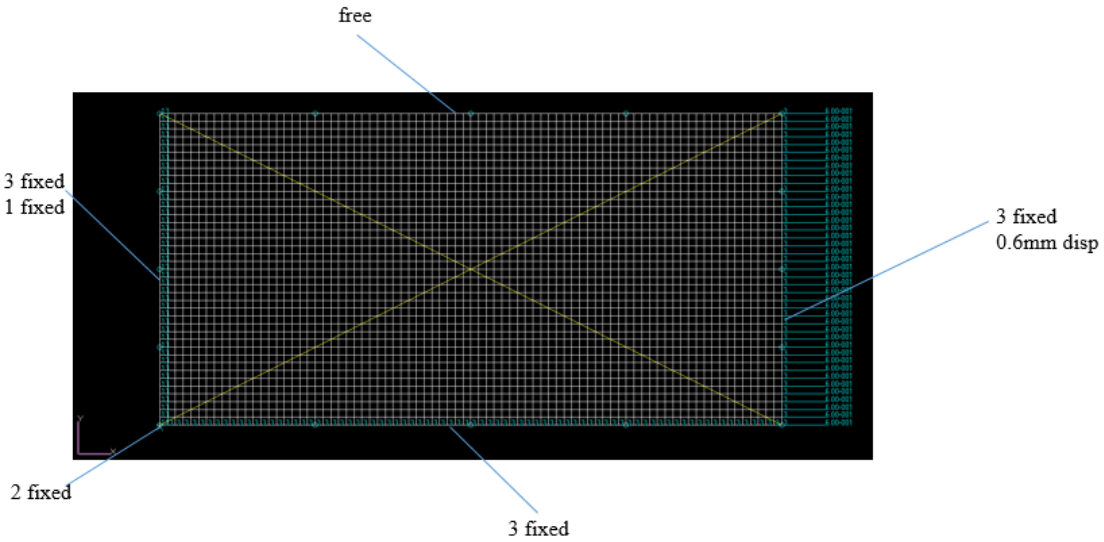

Figure 5-21 Load and Boundary Conditions (Loaded and Edges *Simply Supported* / Unloaded Edges *Simply Supported* and *Free*)

Figure 5-18 is used to determine the buckling coefficient. Condition "E" stands for the case at which the loaded edges are *simply supported* and unloaded edges are *simply supported* and *free*. Aspect ratio of the plate is 2.0 as already stated. Therefore, the compressive buckling coefficient, k_c is equal to 0.65.

Equation (3.10) returns a critical buckling strength of 16.4 MPa for this buckling coefficient. As already stated, 0.6mm enforced displacement results in a compressive stress of 210.0 MPa in linear range. Therefore, buckling initiation is calculated to be at the 7.8% (0.078) of the total load. Following finite element solution results are compared with this bifurcation level.

Initial buckling mode is again obtained using MSC NASTRAN's linear buckling solution sequence SOL105. The resulting buckling mode and the first factor are shown in Figure 5-22.

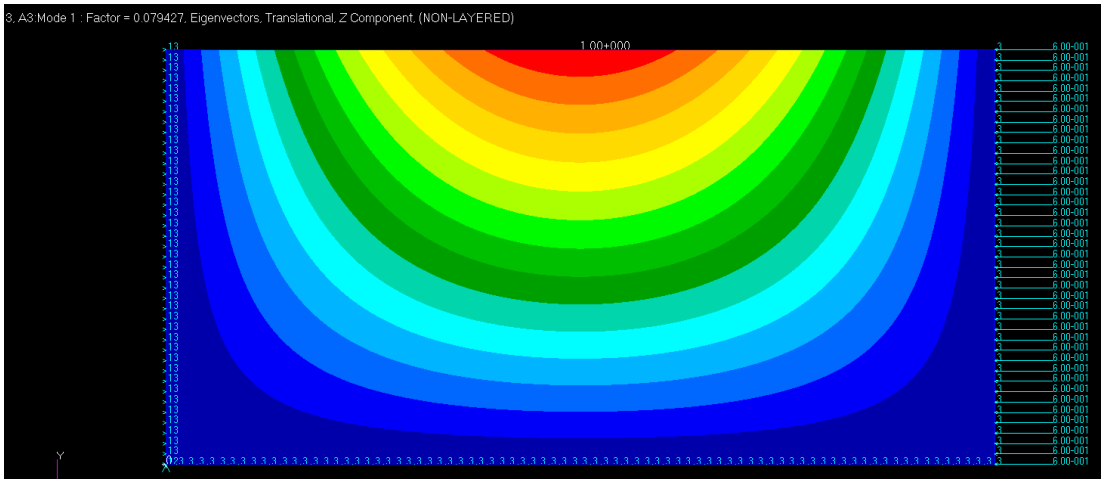

Figure 5-22 Finite Element Solution Results for Loaded Edges *Simply Supported* and Unloaded Edges *Simply Supported/Free*

First five modes are listed in Table 5-8. The first mode has a buckling factor of 0.079427, which fits with 0.078 that is previously calculated. Therefore, the edge restraints of this configuration can provide *simply supported* and *free* boundary conditions for the plate.

Table 5-8 List of Factors (Loaded and Edges *Simply Supported* / Unloaded Edges *Simply Supported* and *Free*)

Mode 1	Factor = 0.079427
Mode 2	Factor = 0.16756
Mode 3	Factor = 0.31501
Mode 4	Factor = 0.52172
Mode 5	Factor = 0.7874

So far, the boundary conditions for a panel without any stiffener elements have been verified. The effects of one-dimensional elements have not been examined yet. At

this point, stiffener elements on the unloaded edges are added to the model to see how much they provide support to the panel.

5.3.4.1.4 Loaded Edges Simply Supported / Beams at Unloaded Edges Type 1

In this section, instead of restraining the unloaded edges in the Z (3) direction, one-dimensional beam elements with axial, bending, and torsional stiffness are modeled with the same material. This type of element property is called as CBAR elements in NASTRAN. Figure 5-23 show the current configuration.

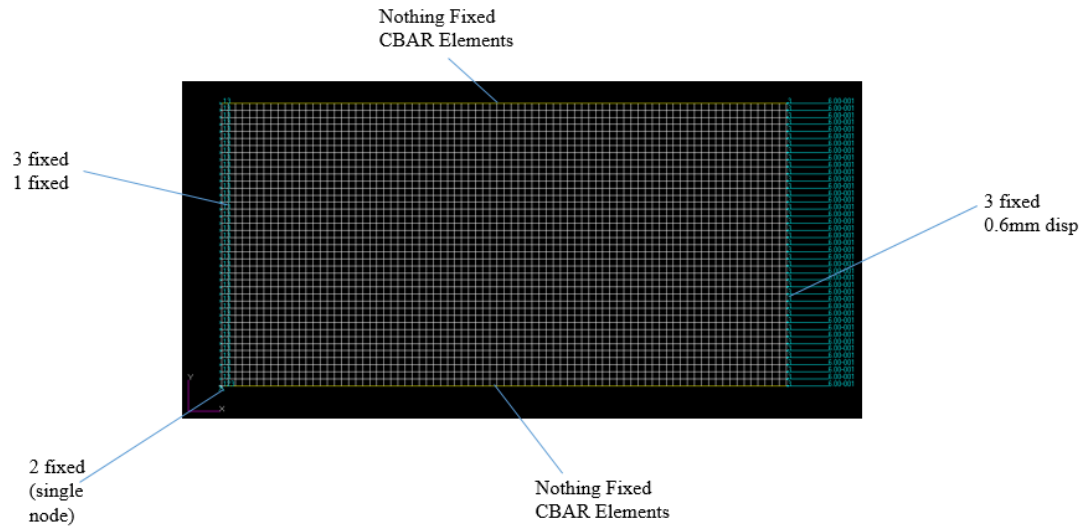

Figure 5-23 Loaded Edges Simply Supported / Beam Elements at the Unloaded Edges

Cross sections of the beam elements are all 10mm x 10mm squares. Figure 5-24 is the isometric view of the same plate. Yellow elements are the one-dimensional stiffeners with CBAR properties.

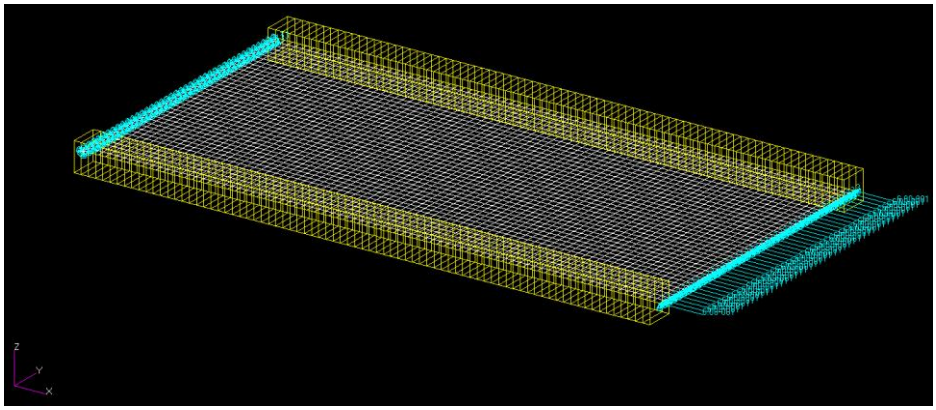

Figure 5-24 Loaded Edges Simply Supported / Beam Elements at the Unloaded Edges (Isometric View)

Finally, the cross-section properties of the stiffener elements are shown in Figure 5-25.

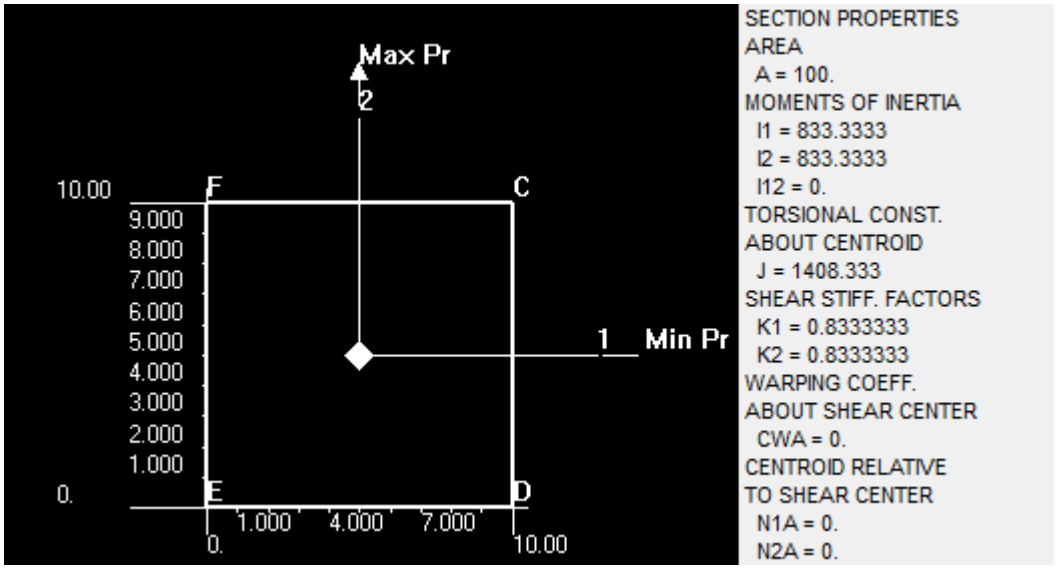

Figure 5-25 Cross Section Properties (10x10 Square Section)

Using the panel with stiffeners, initial buckling mode is obtained using MSC NASTRAN's linear buckling solution sequence SOL105. The resulting buckling mode and the first five factors are shown in Figure 5-26 and Table 5-9, respectively.

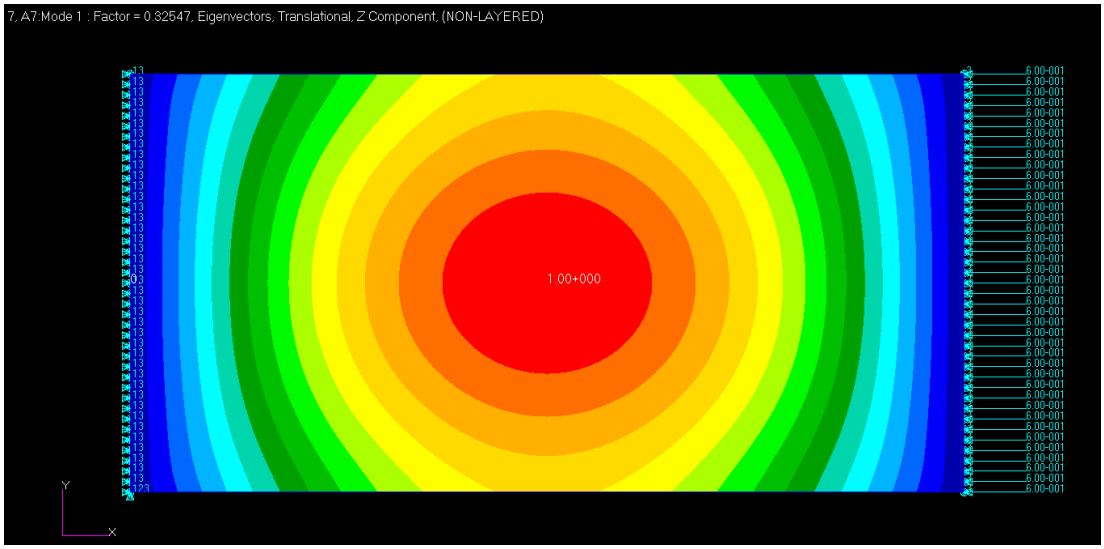

Figure 5-26 Finite Element Solution Results (Loaded Edges *Simply Supported* / *Beam Elements* at the Unloaded Edges)

Table 5-9 List of Factors (Loaded Edges *Simply Supported* / *Beam Elements* at Unloaded Edges)

Mode 1	Factor = 0.32547
Mode 2	Factor = 0.62003
Mode 3	Factor = 0.70385
Mode 4	Factor = 0.73096
Mode 5	Factor = 0.88782

The first mode has a buckling factor of 0.32547. It must be recalled that the bifurcation point was found to be 0.48 of the total load and 0.84 of the total load for *simply supported* and *clamped* unloaded edges, respectively. Therefore, the addition of beams with 10x10 cross sections are found to provide less support when compared to simply supported edge restraints. This result is going to be more meaningful when compared to a section with higher moment of inertia in the following section.

5.3.4.1.5 Loaded Edges Simply Supported / Beams at Unloaded Edges Type 2

This time, cross section of the beam elements are 5mm x 20mm rectangles as can be seen from Figure 5-27. It should be noted that all support and loading conditions are the same as the one shown in Figure 5-23. The only difference is the cross section properties of one-dimensional elements. Type 2 cross section properties are provided in Figure 5-28.

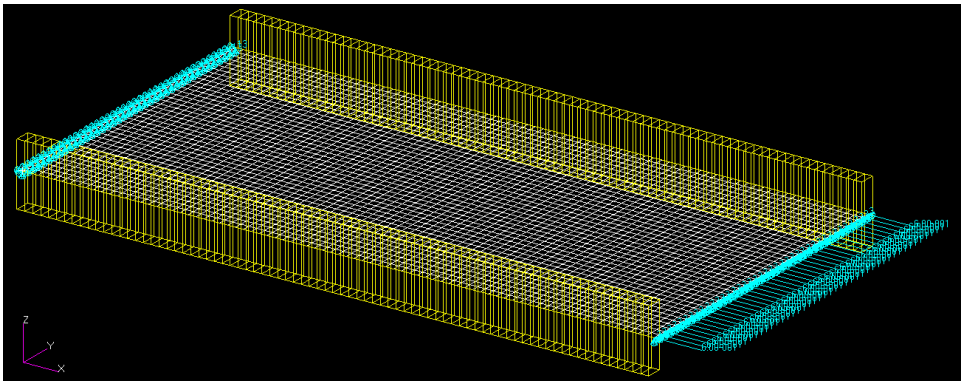

Figure 5-27 Loaded Edges Simply Supported / Beams at Unloaded Edges (Type 2)

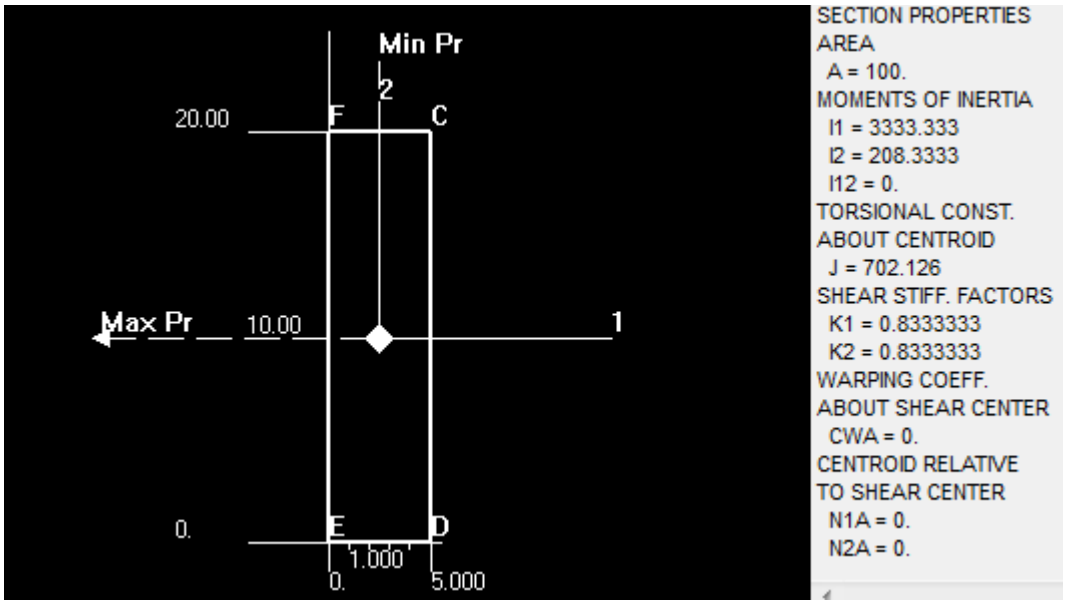

Figure 5-28 Cross Section Properties (5x20 Rectangular Section)

Initial buckling mode is obtained using MSC NASTRAN's linear buckling solution sequence SOL105. The resulting first buckling mode and the first five factors are provided in Figure 5-29 and Table 5-10, respectively.

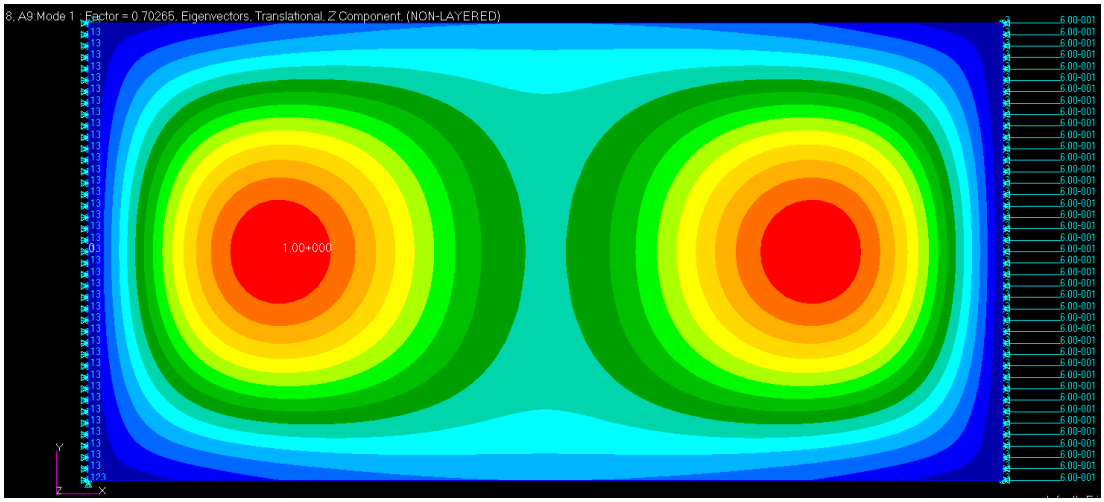

Figure 5-29 Finite Element Solution Results for Loaded Edges *Simply Supported* / *Beam Elements* at the Unloaded Edges – Type 2

Table 5-10 List of Factors (Loaded Edges *Simply Supported* / *Beam Elements* at Unloaded Edges – Type 2)

Mode 1	Factor = 0.70265
Mode 2	Factor = 0.76859
Mode 3	Factor = 0.85376
Mode 4	Factor = 0.89347
Mode 5	Factor = 1.1099

The first mode has a buckling factor of 0.70265. It must be recalled that the bifurcation point was found to be 0.48 of the total load for *simply supported* and 0.84 of the total load for *clamped* conditions, respectively. Therefore, beams with 5x20 cross sections are found to provide more support when compared to simply supported edge restraints and less support than clamped edges. It must be recalled that beams with 10x10 cross sections provided a bifurcation level of 32% of the total

load, which is a lot lower than the level provided by the beams with 5x20 rectangular sections. Consequently, it is seen that the stiffeners modeled with beam elements and CBAR properties provide a support that is dependent on their cross sections, although the cross-sectional areas of the stiffeners are the same.

In the examples of Sections 5.3.4.1.4 and 5.3.4.1.5, the beam elements are perfectly bonded to shell elements. In other words, the stiffness and restraints provided by the rivets fastening the panels to stiffeners are neglected. It can be concluded that it is not easy to achieve simply supported boundaries using one-dimensional beam elements unless the fasteners are modeled.

5.3.4.1.6 Loaded Edges Simply Supported / Shell Elements at Unloaded Edges

In this last study, the same panel is examined by modeling the stringers with two-dimensional general-purpose quadrilateral shell elements. Stiffener area is the same as the beam areas of previous two cases. It should be noted that the stiffeners are perfectly bonded to the panel, i.e. no fasteners exist in the model. Figure 5-30 shows the current configuration.

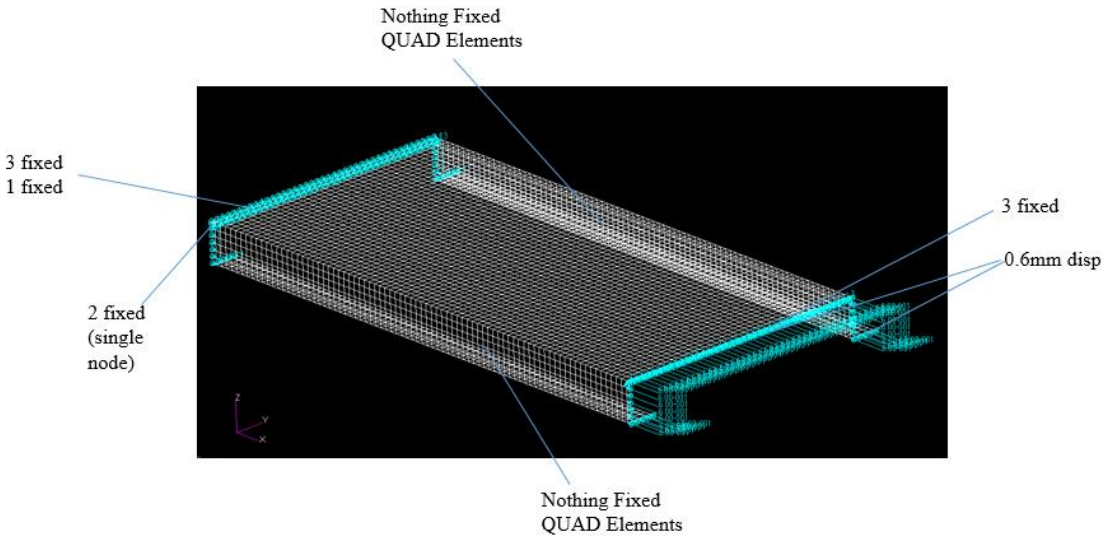

Figure 5-30 Loaded Edges Simply Supported / Shell Elements at the Unloaded Edges

The geometry of the panel cross-section is shown in Figure 5-31.

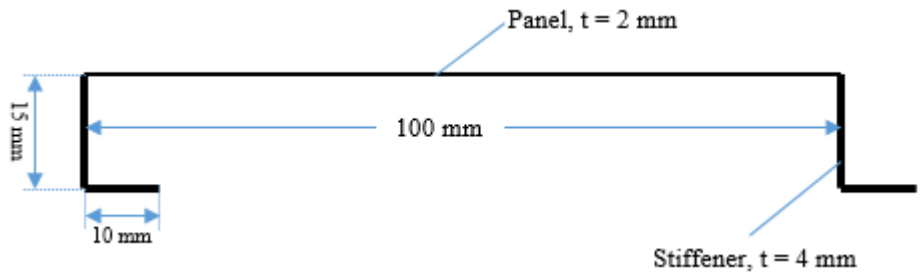

Figure 5-31 Dimensions of the stiffener shell elements

Initial buckling mode is obtained using MSC NASTRAN's linear buckling solution sequence SOL105. The first buckling mode is shown in Figure 5-32.

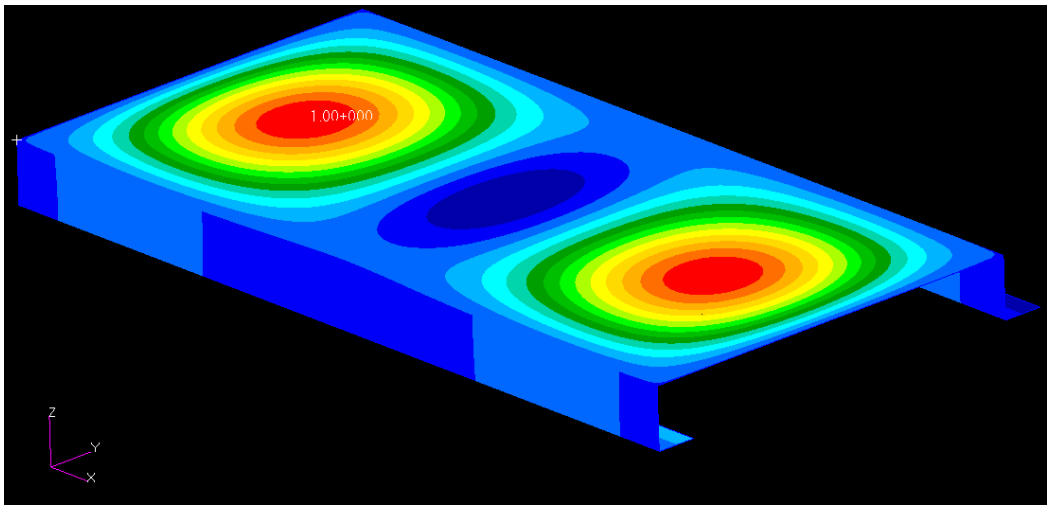

Figure 5-32 Finite Element Solution Results (Loaded Edges *Simply Supported* / *Shell Elements* at the Unloaded Edges)

The first mode has a buckling factor of 0.71745 as shown in Table 5-11. It must be recalled that the bifurcation point was found to be 0.48 of the total load and 0.84 of the total load for *simply supported* and *clamped* conditions, respectively. Thus,

stringers with shell elements provide more support when compared to simply supported edge restraints and less support than clamped edges.

Table 5-11 List of Factors (Loaded Edges *Simply Supported* / *Shell Elements* at Unloaded Edges)

Mode 1	Factor = 0.71745
Mode 2	Factor = 0.74683
Mode 3	Factor = 0.88777
Mode 4	Factor = 1.0611
Mode 5	Factor = 1.1495

Just like for the studies carried out with bar elements, the support provided the shell stiffeners is somewhere in between the simply supported and clamped conditions.

In conclusion, with the help of the buckling factor verification study, it is observed that the best way to model simply supported boundary conditions is the one examined in Chapter 5.3.4.1.1, in which the support conditions are provided by single point constraints in the 3 direction for all edges. The boundary conditions shown in Figure 5-15 can be used to model simply supported boundaries for illustrative purposes. One-dimensional bar elements *with* bending stiffness provide a support that is dependent to their cross sections. However, one-dimensional bar elements *without* bending stiffness (CROD elements) do not introduce any additional support to the panel because they do not have bending stiffness by definition. Therefore, the application of one-dimensional CROD elements together with the single point constraints along Z (3) direction makes it possible to obtain simply supported boundary conditions.

5.3.4.2 Result Comparison

Nonlinear finite element solution clearly exhibits the post buckling behavior of the stiffened panel. The load-displacement curve, which is useful to represent post-buckling, is provided in Figure 5-33.

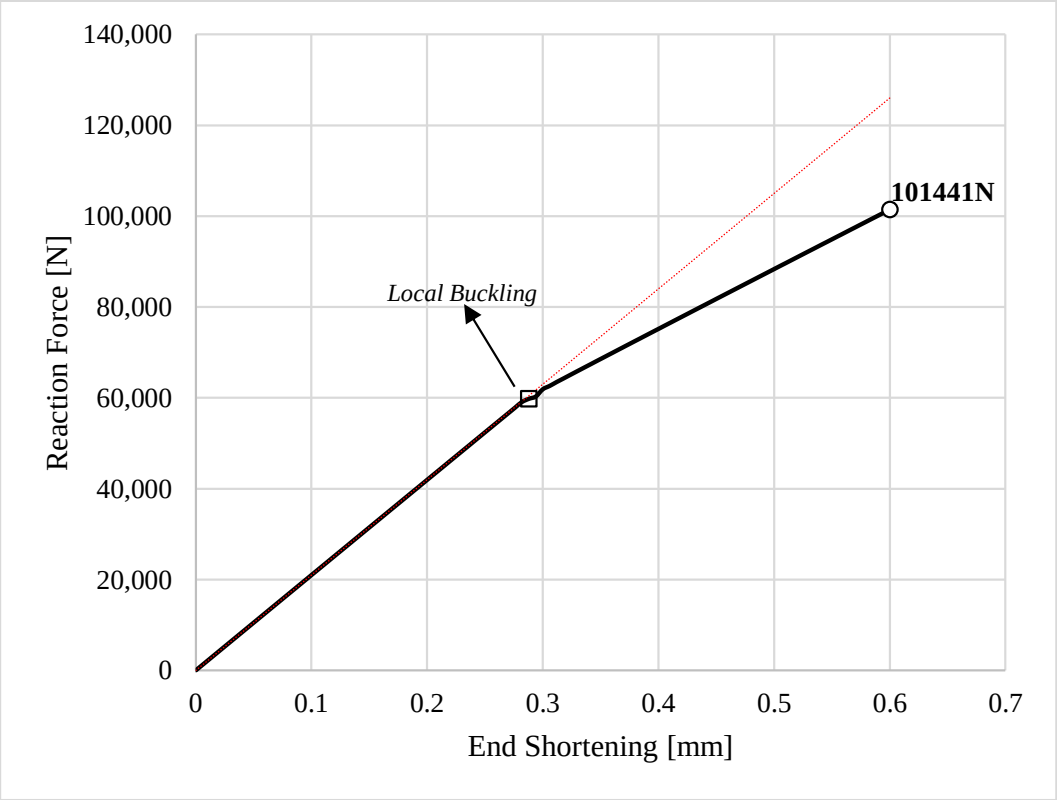

Figure 5-33 Force-Displacement Curve from Nonlinear Finite Element Analysis

First important outcome is the bifurcation point, which shows correlation with both hand calculation and linear buckling analysis. The stiffened panel has a 101441 N post buckling load carrying capacity under 0.6 mm uniform end shortening. In addition, the average stress on each stiffener is 208.4 MPa. The total load carrying capacity and the average stress are the two parameters to be compared to the ones obtained from the load redistribution results of the developed method.

For the comparison study, linear static finite element solution on the coarse model is performed using the boundary conditions provided in Figure 5-15a.

Reaction force of 101441 N, which was obtained from nonlinear finite element solution, is applied to the right end of the panel through the RBE2 element shown in Figure 5-14a. The iteration method reached the convergence in effective width and

stiffener stresses after 8 iterations. The parameters do not change significantly after the fifth iteration but the convergence criteria were kept a little tight for this illustrative study. Change in the effective width of the panel and change in the stiffener stresses within consecutive finite element analyses can be seen in Figure 5-34.

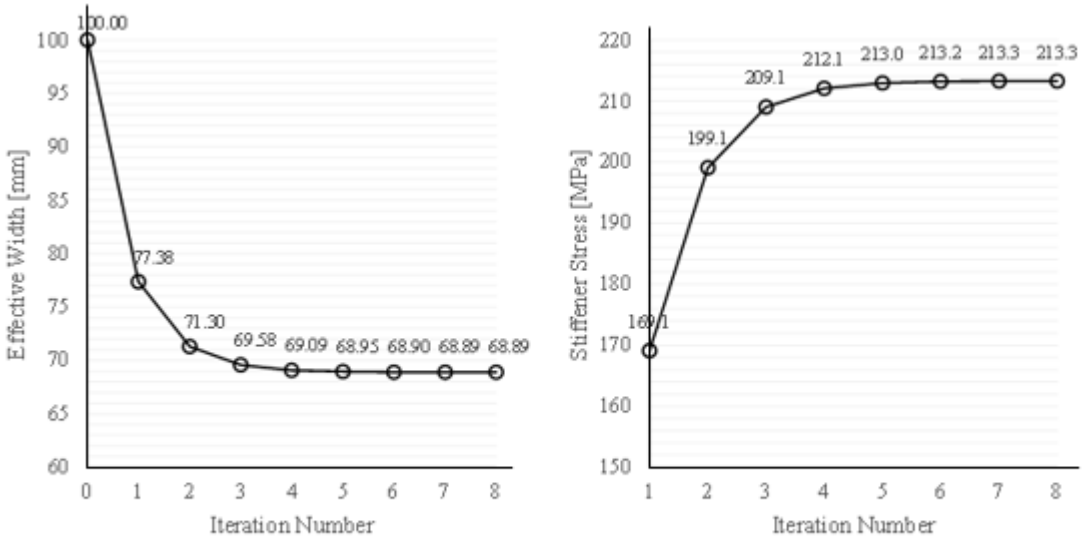

a) Change in Effective Width of Panel

b) Change in Stiffener Stress

Figure 5-34 Iteration History of the Effective Width and Stiffener Stress

It should be noted that the stiffener stress in converged the state is 213.3 MPa. This is 2.4% higher than that of the nonlinear solution (208.4 MPa). A more important comparison is to be made between the resulting load carrying capacities of the two techniques. End shortening that corresponds to the applied load is 0.609 mm in converged state according to the developed method. This is 1.5% greater than nonlinear finite element result. The obtained value is plotted onto the force-displacement curve of nonlinear finite element analysis in Figure 5-35.

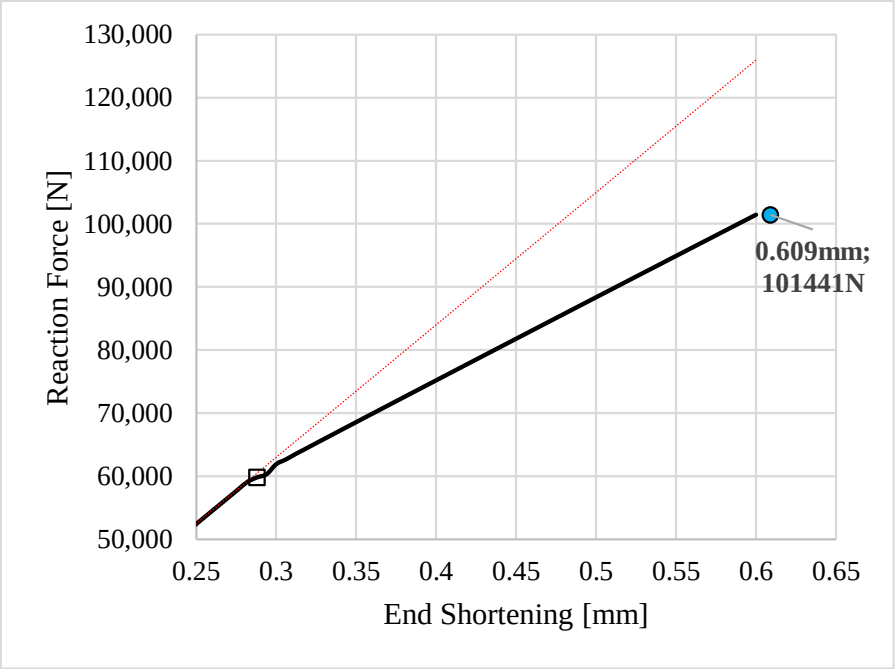

Figure 5-35 Result of the Developed Method Plotted on Nonlinear FEA Results

It is obvious that the result of the developed method, which uses the flow chart given in Figure 5-8, shows good correlation with nonlinear finite element analysis.

5.4 Application of the Post Buckling Study to the Developed Tool

Post buckling load redistribution study is implemented to the tool developed for this thesis by allowing the user to set the initial buckling load level to a certain percentage, i.e. 50%, of the limit load. If the buckling of the skins before the limit load is allowed by the user, the tool calculates the effective widths and equivalent thicknesses to obtain post buckling stresses. Effective width and equivalent thickness calculations are carried out according to Sections 5.3.2.2 and 5.3.2.3 of this chapter. The overall flow chart of stress calculations is shown in Figure 3-7.

5.5 Sample Study on the Post-Buckling Failure Checks

In this section, column buckling of a stringer is examined as a reference. In this thesis, the stiffeners have been regarded as booms that have areas but no cross-sectional properties. However, the cross-sectional properties of the stiffeners are actually very important for the instability checks. The stiffeners are only checked for the material failure in this thesis but column buckling can be more critical for the compressive side. A future improvement may be the addition of the stiffener cross-sectional properties and buckling checks.

Crippling check of an assumed cross-section is carried out to show the significance of column failure checks in this section.

Column failure can be caused by [28]:

- Flexural instability, which is the general buckling of a column and depends on the end fixity, material, and cross-section,
- Crippling, which depends on the material and cross-sectional dimensions,
- Torsional instability.

It is important to note that the interaction between flexural instability and local crippling should also be examined for the failure. Another thing to note is that the torsional instability is not very possible for the common cross-sections used in aircraft wings [28].

Considering the wingbox examined in section 4.1 and 4.2 again, the upper stringer shown with a red point in Figure 5-36 is analyzed.

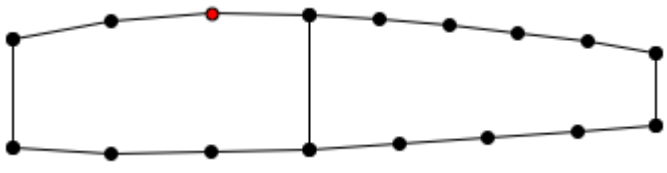

Figure 5-36 Selected Upper Stringer for Column Failure Checks

The sizing result for the shown stringer area was 101.8 mm^2 at wing section 10 in the Tucano example with buckling resistant panels (Section 4.1). Assuming a Z-type stringer like the one shown in Figure 5-37, crippling check is performed according to the method outlined by Niu [28]. The cross-section is divided into segments as shown in in Figure 5-37. Segments have widths *b* and thicknesses *t*.

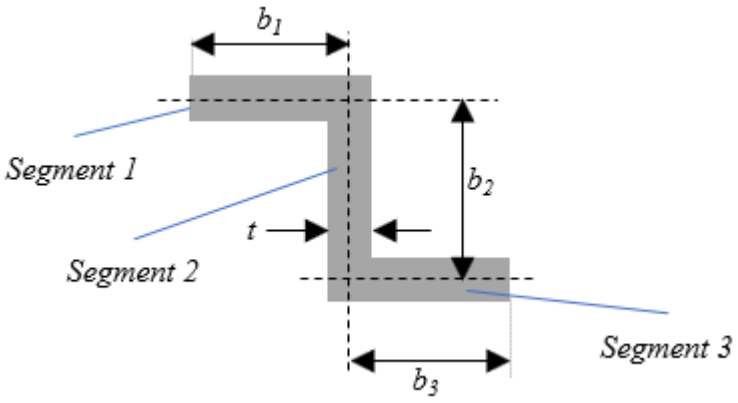

Figure 5-37 Stringer Segments

The crippling stress for the section is obtained by a weighted average of segment allowable stresses as shown in Equation (5.8).

$$F_{cc} = \frac{(b_1 t_1 F_{cc1} + b_2 t_2 F_{cc2} + \ldots)}{(b_1 t_1 + b_2 t_2 + \ldots)}$$

$$F_{cc} = \frac{\sum b_n t_n F_{ccn}}{\sum b_n t_n} \tag{5.8}$$

where F_{ccn} terms stand for the individual segment crippling allowable.

Segment 1 and 3 have one edge free and Segment 2 has no edge free. This is very important while determining the segment allowable stresses.

Crippling calculations are performed with the help of test data and empirical approaches. Niu [28] uses the following chart in order to obtain the segment

allowable stresses. This chart is only applicable to certain aluminum alloys. There are other methods for the general solution of sections. For the purposes of this study, the chart given in Figure 5-38 is sufficient.

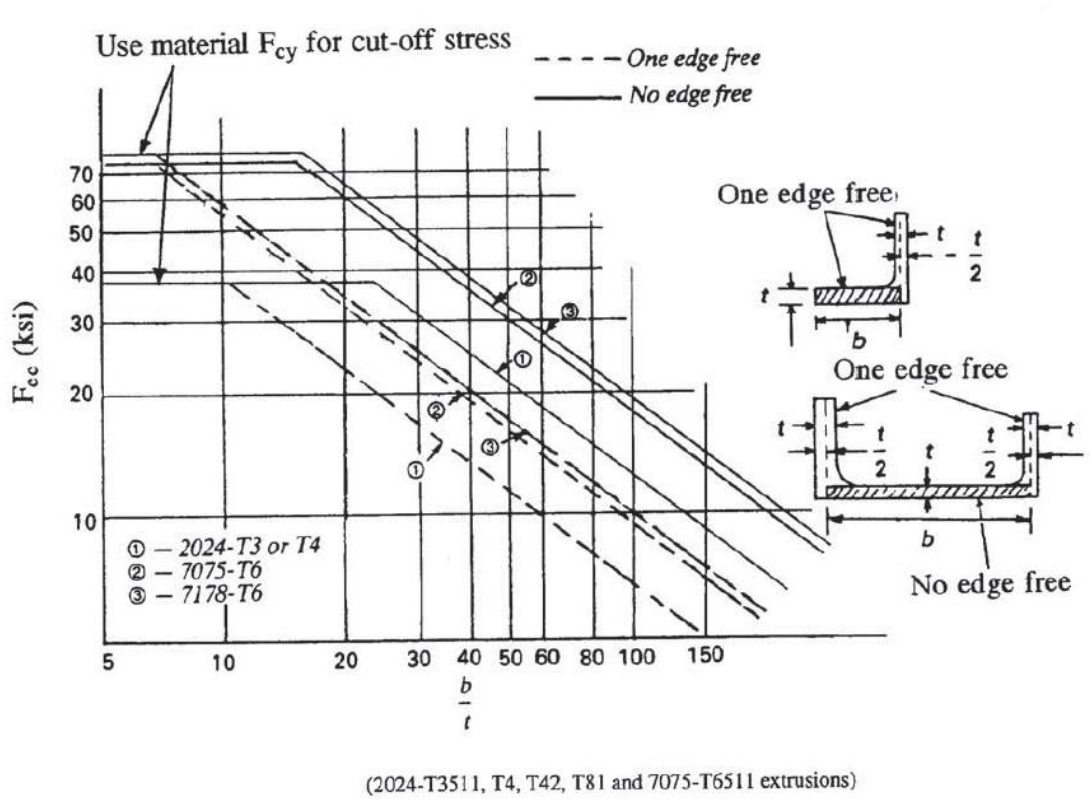

Figure 5-38 Crippling Stress of Extruded Sections [28]

The following calculation for the segments of the stringer gives the crippling stress of the entire stringer section.

Segment	Free edges	b_n	t_n	b_n/t_n	$b_n t_n$	F_{ccn}	$t_n b_n F_{ccn}$
1	1	25.5	1	25.5	25.5	28	714
2	0	51	1	51	51	29	1479
3	1	25.5	1	25.5	25.5	28	714
				Totals:	102	85	2907

The unit of the allowable stresses (F_{ccn} values) is ksi in the above calculations. Using Equation (5.8), the crippling allowable of the entire section is 28.5 ksi (196.5 MPa) for the 7075 T6 material. The segment dimensions of this example are deliberately adjusted to have large b_n/t_n values. In the end, an allowable value much smaller than the material F_{cy} is obtained. This result is sufficient to understand the significance of the cross-sectional properties of the stiffeners. Same approach would also be valid for the spar flanges. Thus, it is obvious that the addition of the cross-sectional properties to the tool as a future work would be very beneficial.

Up to this point, the structural failure check is carried out using the stresses and geometry of the case in which the skins are buckling resistant. If the buckling of skins is allowed before the limit load, there should be some extra treatments for the crippling checks. The tool developed for this thesis can calculate all the stiffener stresses in the post-buckling regime. Therefore, the stresses under ultimate loads can be obtained using the tool. However, the cross-section of the column should be modified such that the effective skin width around the attachment lines are added to the cross section. Hence, a composite cross-section shape is obtained as shown in Figure 5-39.

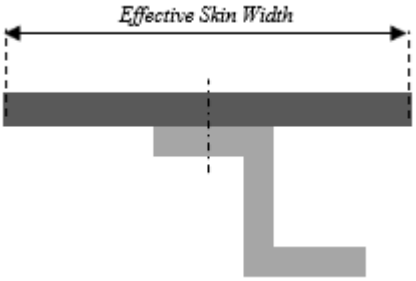

Figure 5-39 Modified Cross-Section Shape

The crippling allowable of the modified cross-section can be calculated using the approach outlined in this section with the addition of the upper skin segments to the calculation. In other words, a column formed by the stringer and the effective skins is

to be checked. It is important to recall that the margin of safety for the crippling must be calculated using the applied stress under the ultimate loading conditions for the post-buckling regime.

CHAPTER 6

CONCLUSION AND FUTURE WORK

6.1 Concluding Remarks

This thesis proposes a tool for minimum weight wingbox structural design. The developed tool can be very useful especially at the early stages of the aircraft design. As stated in Chapter 1, major aerospace companies make huge investments on their preliminary design platforms. They seek to own a complex multidisciplinary engineering environment in order to achieve reasonable designs while considering the concerns of different disciplines. This thesis is based on simpler approaches and the main goal is to have a rapid tool that can be used to compare the design candidates. The tool can be utilized to compare different layouts to select for the lightest and the most feasible configuration.

The developed tool calculates the wing loading automatically. Chapter 2 outlines the methods to obtain the load cases that can be used at the early design stages. For subsonic wings, ESDUpac A9510 computer program is used for external load calculations. The tool developed for this thesis executes the program in a fully automated way. The tool creates the A9510 input file by extracting and formatting the necessary information from the main input file. After the execution of the A9510 program, the tool reads the necessary outputs and uses them for the calculation of the internal loads. The tool calculates the internal loads and stores them for the rest of the design process. For supersonic wings, A9510 program is not used because it is limited to subsonic flows. Therefore, a geometry-based lift distribution method,

which is called as the Schrenk's approximation, is utilized. This approximate method makes use of the planform shape and ideal elliptical distribution to calculate the wing loading. Schrenk method is encoded into the code of the tool. The tool can calculate the supersonic external loads and then obtain the internal loads by means of some certain mathematical operations.

Wingbox idealization, design assumptions and strategies, strength and stability methods, and failure checks are all outlined in Chapter 3. Essential approximation techniques for the preliminary design of structural members are also explained. The scientific background of the post buckling effects after the skin local buckling is first explained in this chapter. The design strategy of the tool developed for this thesis is also provided in Chapter 3.

Three sample cases are selected to show how the tool handles the preliminary design. One supersonic wing and one subsonic wing with and without post buckling load redistribution are sized for illustration purposes. Resulting thicknesses and the overall wing weights are provided in Chapter 4. The exploration and optimization processes for achieving the minimum weight by the selection of the most feasible design variables are also outlined in Chapter 4.

Chapter 5 is allocated to the post-buckling load redistribution phenomenon. Detailed explanation about the issue is provided. Additionally, a method, which uses iterative linear finite element analyses and achieves a good correlation with the geometric nonlinear finite element analysis, is presented. Chapter 5 also shows the results of the effort to satisfy various edge conditions provided by different finite element techniques. Effective width and equivalent thickness calculations explained in Chapter 5 is used for the developed tool during the post buckling iterations.

In order to emphasize the most important results obtained in the thesis, the minimum weights obtained for the three wingbox configurations are summarized once again in the following tables.

Table 6-1 Summary of the Results Obtained for a Subsonic Turboprop Trainer Wing with Buckling Resistant Skins

Number of Internal Grids for Each Coefficient	5
Number of Repetitive Cycles	4
Lower Bound for the Variables	0.5
Upper Bound for the Variables	5.0
Minimum Wingbox Weight (Half Wing) [kg]	132.5
Coefficients @ the Minimum Weight	(1.344, 0.7813)

Table 6-2 Summary of the Results Obtained for a Subsonic Turboprop Trainer Wing for the Buckling Level of 50% Limit Load

Number of Internal Grids for Each Coefficient	5
Number of Repetitive Cycles	4
Lower Bound for the Variables	0.2
Upper Bound for the Variables	2.0
Minimum Wingbox Weight (Half Wing) [kg]	113.9 kg
Coefficients @ the Minimum Weight	(0.9875, 0.7625)

Table 6-3 Summary of the Results Obtained for a Supersonic Fighter

Number of Internal Grids for Each Coefficient	5
Number of Repetitive Cycles	4
Lower Bound for the Variables	0.5
Upper Bound for the Variables	5.0
Minimum Wingbox Weight (Half Wing) [kg]	1008.0 kg
Coefficients @ the Minimum Weight	(2.188, 0.9219)

It is important to recall that the tool developed for this thesis searches for the minimum possible wingbox weight by the help of a design exploration. Best set of design variables that return the optimum objective function is obtained after the exploration. The design variables are the thickness coefficients for the upper and lower skins. The entire interval specified for the coefficients are explored with a step

size specified by the user. The tool can perform consecutive exploration cycles around the most feasible region with smaller step sizes in order to reach the global minimum.

Figure 6-1 shows the final weight obtained for the subsonic turboprop trainer wing with buckling resistant skins, which was examined in Section 4.1. The steps getting smaller around the most feasible point can be seen in the figure.

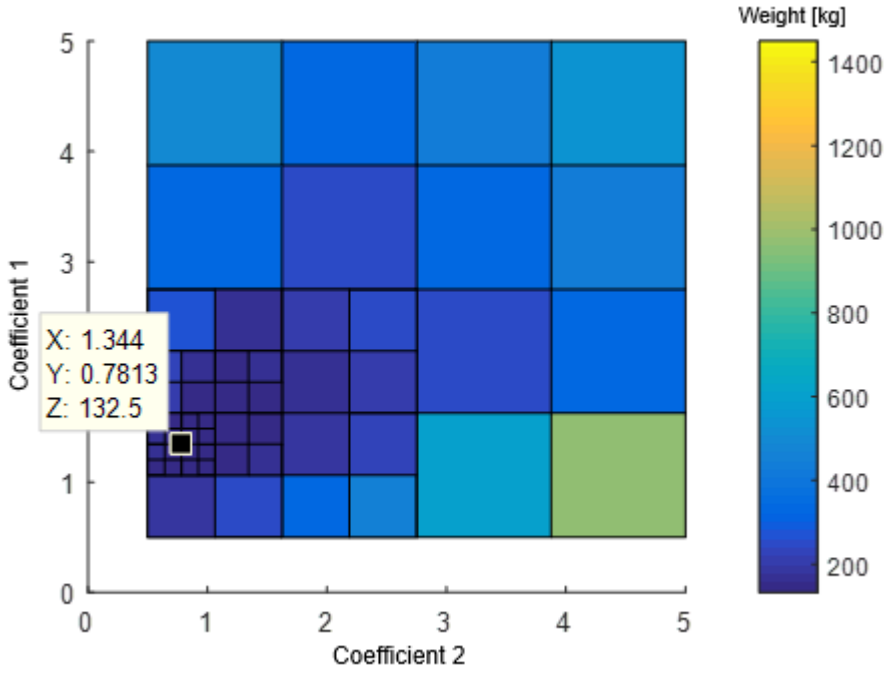

Figure 6-1 Result of the Exploration for a Subsonic Turboprop Trainer Wing with Buckling Resistant Skins

Similarly, the exploration region of the turboprop wing with buckled skins can be seen in Figure 6-2.

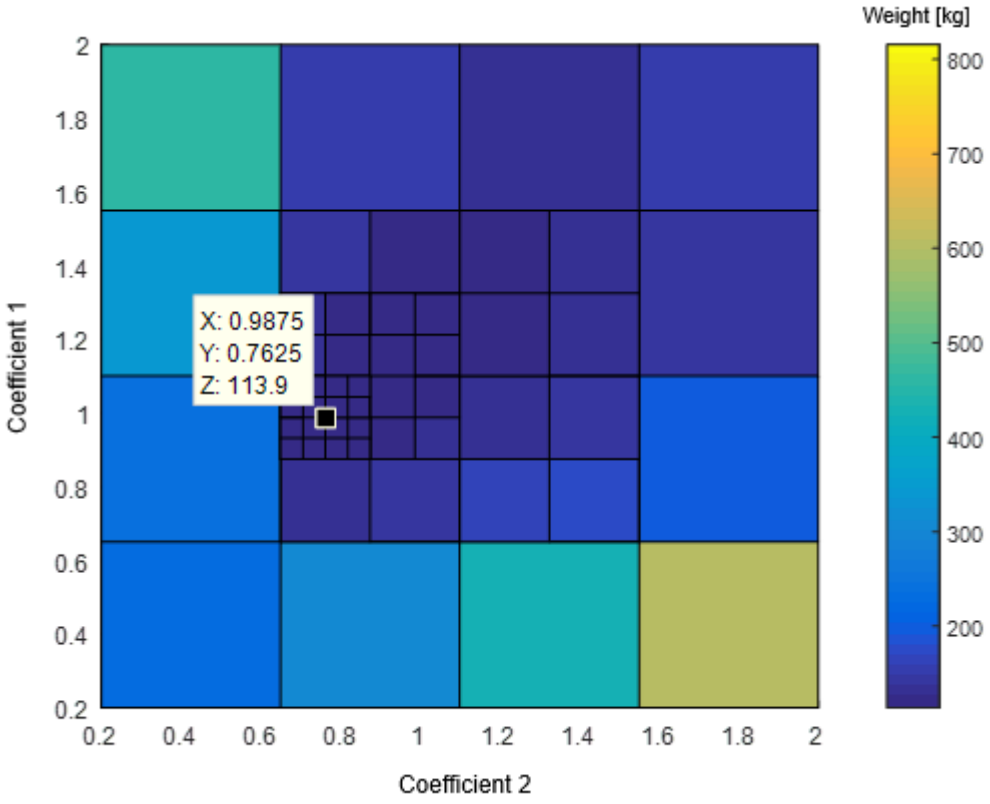

Figure 6-2 Design Space after the Exploration for the Buckling Level of 50% Limit Load

It is seen that a weight reduction of 15% has been attained by the help of allowing the elastic buckling at 50% limit load. Post-buckling load redistribution is one of the essential subjects investigated within this thesis and the clearest outcome of the post buckling study is the weight reduction achieved.

6.2 Future Work

The tool developed for this thesis may be strengthened by certain future additions. For instance, the load cases used for the study can be extended to cover more maneuvers. Moreover, dynamic effects and aeroelastic concerns may be included to the framework. The methods and failure theories in this thesis are generally applicable to metallic structures. In a possible future upgrade, this work can be extended to composites. Finally, a big improvement to this work, which is limited to

airfoil structures at the moment, may be the extension of the content to fuselage structures. By doing so, the framework can be used for the initial sizing and the weight estimation for an entire aircraft.

There are some enhancement opportunities for the failure criteria of the stiffeners (spar flanges and stringers). The stiffeners have been regarded as booms that have areas but no cross-sectional properties. However, the cross-sectional properties of the stiffeners are actually very important for the instability checks. The stiffeners are only checked for the material failure in this thesis but column buckling can be more critical for the compressive side. A future improvement may be the addition of the stiffener cross-sectional properties and buckling checks, which are already introduced in Section 5.5.

After the cross-section information is added to the tool, another important parameter can be checked. The stringer inertia requirement that comes from the panel breaking function of the stringer is essential. The stringers must have enough inertia to divide the skin into panels. Melcon and Ensrud [29] state that the moment of inertia I_{st} of the stiffener required to divide the shell into panels is expressed by:

$$I_{st} = \left(\frac{bt^3}{5}\right)\left(\frac{a}{b}\right)^{8/3} \tag{6.1}$$

where t is thickness of the panel, a is the rib spacing (unloaded edge of the compressive panel) and b is the stiffener spacing as shown in Figure 6-3.

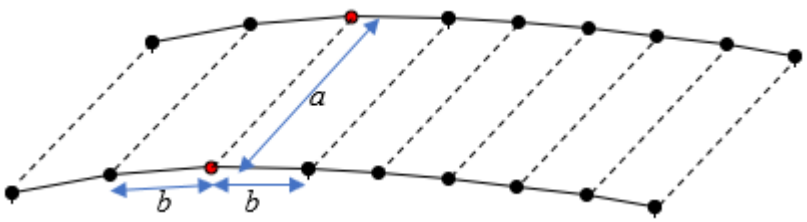

Figure 6-3 Dimensions for the Stringer Inertia Check

It should be noted that Z type stringers generally do not have any problems with the inertia requirement. However, it can be an issue with L type stringers. Therefore, the addition of the inertia check would also be a good improvement for the tool.

REFERENCES

[1] Sobieszczanski-Sobieski, J. (1999). Multidisciplinary design optimisation (MDO) methods: Their synergy with computer technology in the design process. *Aeronautical Journal*, *103*(1026), 373–382. https://doi.org/10.1017/S0001924000064599

[2] Etheridge, T. (2005). *A structural design process for a next generation aerospace design environment*.

[3] Chen, D., & Britt, R. T. (2010). Practical Application of Multidisciplinary Optimization to Structural Design of Next Generation Supersonic Transport, (September), 1–12.

[4] Eldred, L. B., Padula, S. L., & Li, W. (2015). Enabling Rapid and Robust Structural Analysis During Conceptual Design, (February 2015).

[5] A, M. K., & Mariayyah, R. (2011). Multidisciplinary design optimization (MDO) of a typical low aspect ratio wing using Isight.

[6] Ainsworth, J., Collier, C., Yarrington, P., Lucking, R., & Locke, J. (2010). Airframe Wingbox Preliminary Design and Weight Prediction. *69th Annual Conference, Virginia Beach, Virginia*, 41. Retrieved from http://www.sawe.org/store/product_info.php?products_id=45169

[7] Ko, W. L., & Jackson, R. H. (1991). Compressive Buckling Analysis of Hat-Stiffened Panel. *NASA TM-4310*. Retrieved from http://www1gtm.nasa.gov.speedera.net/centers/dryden/pdf/88235main_H-1724.pdf

[8] Ko, W. L., & Jackson, R. H. (1994). Shear Buckling Analysis of a Hat-Stiffened Panel. *NASA TM-4644*, (November 1994).

[9] Lynch, C. J., & Sterling, S. G. (1998). A finite element study of the

postbuckling behaviour of a flat stiffened panel. In *International Council of the Aeronautical Sciences Congress*.

[10] Heitmann, M., & Horst, P. (2006). A new analysis model for the effective stiffness of stiffened metallic panels under combined compression and shear stress. *Aerospace Science and Technology*, *10*, 316–326. https://doi.org/10.1016/j.ast.2005.12.008

[11] van der Veen, S., & Coatta, D. (2004). STIFFENED PANELS IN COMPRESSION REDIRECTING LOADS TOWARD HIGH-STRENGTH STIFFENERS. In *45th AIAA/ASME/ASCE/AHS/ASC Structures, Structural Dynamics & Materials Conference* (pp. 1–11).

[12] Collier, C., Yarrington, P., Gustafson, P., & Bednarcyk, B. (2009). Local Post Buckling: An Efficient Analysis Approach for Industry Use. *50th AIAA/ASME/ASCE/AHS/ASC Structures, Structural Dynamics, and Materials Conference*, (May), 1–23. https://doi.org/10.2514/6.2009-2507

[13] ESDU. (1999). *Computer program for estimation of spanwise loading of wings with camber and twist in subsonic attached flow*.

[14] Multhopp, H. (1955). Methods for Calculating the Lift Distribution of Wings (Subsonic Lifting-Surface Theory). *Aeronautical Research Council*, *2884*(2884). Retrieved from http://repository.tudelft.nl/view/aereports/uuid:06d93da1-0801-4c99-80ca-06fac0b0c11d/

[15] ESDU. (1983). *Method for the rapid estimation of spanwise loading of wings with camber and twist in subsonic attached flow*.

[16] Pilatus. (n.d.). PC-21 The 21st Century Trainer. Retrieved from https://www.pilatus-aircraft.com/data/document/Pilatus-Aircraft-Ltd-PC-21-Brochure.pdf

[17] Weissberg, V., Green, A., and Mey-Paz, H., “Towards a fastenerless all composite wing,” *27th Congress of the International Council of the Aeronautical Sciences 2010, ICAS 2010*, vol. 3, 2010, pp. 2443–2452.

[18] Megson, T. H. G. (1999). *Aircraft Structures for Engineering Students.*

[19] Bruhn, E. F. (1973). *Analysis and Design of Flight Vehicle Structures*.

[20] Battelle Memorial Institute. (2016). *Metallic Materials Properties Development and Standardization (MMPDS) Handbook – 11.*

[21] Niu, M. (1988). *Airframe Structural Design: Practical Design Information and Data on Aircraft Structures*.

[22] Kan, H. P., Cordero, R., & Whitehead, R. S. (1997). *DOT/FAA/AR-96/111 Advanced Certification Methodology for Composite Structures*.

[23] Eurofighter Jagdflugzeug GmbH. (2013). Eurofighrer Technical Guide. Retrieved from https://www.eurofighter.com/files/pdf/EF_TecGuide_2013.pdf

[24] Kuhn, P., Peterson, J., & Levin, L. (1952). A Summary of Diagonal Tension: Part 1-Methods and Analysis. *Naca Tn-2661*.

[25] MSC Software Corporation. (2011). *MSC Nastran 2012 Linear Static Analysis User's Guide*.

[26] Flabel, J. (1997). *Practical Stress Analysis for Design Engineers.*

[27] MSC Software Corporation. (2007). *MSC Nastran 2007 r1 Implicit Nonlinear (SOL600) User's Guide*.

[28] Niu, M. C.-Y. (1999). *Airframe Stress Analysis and Sizing*.

[29] Melcon, M. A., & Ensrud, A. F. (1953). Analysis of Stiffened Curved Panels Under Shear and Compression. *Journal of the Aeronautical Sciences*, *20*(2), 111–126. https://doi.org/10.2514/8.2551

APPENDIX A

ESDUpac A9510 PROGRAM OUTPUT FILE

Complete output file of A9510 program for the PC-21 wing example is provided here in order to better see the amount of data the program provides to the user.

```
**************************************************************************

ESDU International plc

Program           A9510

ESDUpac Number:   A9510V12
ESDUpac Title:    Computer program for estimation of spanwise
                  loading of wings with camber and twist in
                  subsonic attached flow.
Data Item Number: 95010
Data Item Title:  Computer program for estimation of spanwise
                  loading of wings with camber and twist in
                  subsonic attached flow.
ESDUpac Version:  1.2    Issued January 1997.

(See Data Item for full input/output specification and interpretation.)

**************************************************************************

                        S T A R T   O F   R U N
                        -----------------------
--------------------------------------------------------------------------
                           INPUT DATA CHECK
                           ================
--------------------------------------------------------------------------

RUN TITLE
---------
TEXT1 ESDU 95010
TEXT2 Sample Load Generation Study
TEXT3 PC21 Aircraft with NACA 2412 Airfoil

INPUT DATA WARNINGS AND ERRORS
------------------------------
```

```
      No warning message

      No error detected


INPUT DATA
----------

Number of spanwise Multhopp stations, NMs                      =   33
Number of chordwise Multhopp stations, NMc                     =    5

Number of loading types, NL                                    =    2
 Loading type numbers:
 Lm =      1          Loading due to incidence
           3          Loading due to camber

Number of Mach numbers, NM                                     =    1
 Mach number value:
 M  =   .7200

Number of dimensionless spanwise positions for output, Nyo     =   22
 Spanwise positions:
 yo/s =   .0000   .0500   .1000   .1500   .2000   .2500   .3000   .3500
          .4000   .4500   .5000   .5500   .6000   .6500   .7000   .7500
          .8000   .8500   .9000   .9500   .9800   .9999

Selector for calculation mode, P            =  2  Additional calculation
                                                  for specified overall
                                                  lift coefficient

Number of specified values of CLsp, Nsp     =  1

 Specified overall lift coefficient for loading calculation:
 CLsp =    .4355

Number of cranks in wing, Nk                =  0 (straight-tapered wing)

Aspect ratio, ASPECT                                    =   5.4500
Taper ratio, TAPER                                      =    .4800
Sweepback of n-chord line, ELN                          =   12.00
Fraction of chord, n                                    =    .0000

Camber data for Eta =     1.0000
-------------------------------------
       x/c                z/c
-------------------------------------
     .0000              .0000
     .0125              .0025
     .0250              .0036
     .0500              .0056
     .0750              .0075
     .1000              .0094
     .1500              .0126
     .2000              .0152
     .2500              .0172
     .3000              .0188
     .4000              .0200
     .5000              .0195
     .6000              .0180
     .7000              .0152
     .8000              .0113
```

```
     .9000              .0063
     .9500              .0033
    1.0000              .0000
-------------------------------------

Camber data for Eta =      .0000
-------------------------------------
       x/c                z/c
-------------------------------------
     .0000              .0000
     .0125              .0025
     .0250              .0036
     .0500              .0056
     .0750              .0075
     .1000              .0094
     .1500              .0126
     .2000              .0152
     .2500              .0172
     .3000              .0188
     .4000              .0200
     .5000              .0195
     .6000              .0180
     .7000              .0152
     .8000              .0113
     .9000              .0063
     .9500              .0033
    1.0000              .0000
-------------------------------------

------------------------------------------------------------------------------
                                RESULTS
                                =======
------------------------------------------------------------------------------

PLANFORM GEOMETRY
-----------------

Number of cranks in wing, Nk                =  0 (straight-tapered wing)

Aspect ratio, ASPECT                                        =   5.4500
Taper ratio, TAPER                                          =    .4800
Sweepback of n-chord line, ELN                              =   12.00
Fraction of chord, n                                        =    .0000

AERODYNAMIC LOADING DUE TO INCIDENCE
------------------------------------

                      Mach number, M     =   .7200
                      ----------------------------

WARNING: This program incorporates ESDUpac A7011 as a subroutine
         for the evaluation of lift-curve slope.  See Section 2
         of Item No. 95010.  This imposes some restrictions on
         planform, see Section 5.2 of Item No. 95010. Warnings
         on accuracy are also output for certain cases.

WARNING: High free-stream Mach number.  Item No. 70011 neither
         predicts nor caters for cases where the wing flow is
         supercritical, and if this is likely the results for
         lift-curve slope may be unreliable.  See also discussions
         in Section 4 and Appendix A of Item No. 70011.
```

Lift-curve slope a1 calculated from ESDUpac A7011 (per rad) = 5.2044

Dimensionless spanwise position of half-wing centre of pressure from centre line: tip-up moment = .4268

Dimensionless distance of wing centre of pressure behind apex based on cbar = .4981

Spanwise position Eta	Normalised local lift coefficient CLL.c/CL.cbar	Local centre of pressure position aft of leading edge as fraction of c
.0000	1.2677	.2606
.0500	1.2656	.2566
.1000	1.2600	.2511
.1500	1.2509	.2474
.2000	1.2386	.2446
.2500	1.2231	.2426
.3000	1.2043	.2410
.3500	1.1824	.2397
.4000	1.1570	.2385
.4500	1.1282	.2373
.5000	1.0955	.2360
.5500	1.0587	.2345
.6000	1.0173	.2327
.6500	.9704	.2305
.7000	.9169	.2276
.7500	.8552	.2238
.8000	.7826	.2185
.8500	.6946	.2112
.9000	.5821	.2008
.9500	.4245	.1849
.9800	.2750	.1714
.9999	.0253	.1632

AERODYNAMIC LOADING AT ZERO INCIDENCE DUE TO CAMBER

Mach number, M = .7200

Lift coefficient of wing, CL = .1997

Dimensionless spanwise position of half-wing centre of pressure from centre line: tip-up moment = .4280

Dimensionless distance of wing centre of pressure behind apex based on cbar = .8639

Spanwise position Eta	Local lift coefficient CLL.c/cbar	Local pitching moment CmL.c/cbar about local quarter chord
.0000	.2551	-.0909
.0500	.2544	-.0905
.1000	.2528	-.0892
.1500	.2503	-.0871

.2000	.2472	-.0847
.2500	.2434	-.0824
.3000	.2391	-.0800
.3500	.2342	-.0775
.4000	.2288	-.0750
.4500	.2228	-.0724
.5000	.2161	-.0698
.5500	.2088	-.0671
.6000	.2008	-.0644
.6500	.1919	-.0615
.7000	.1820	-.0585
.7500	.1707	-.0552
.8000	.1575	-.0515
.8500	.1415	-.0472
.9000	.1208	-.0415
.9500	.0906	-.0326
.9800	.0602	-.0227
.9999	.0056	-.0022

CALCULATIONS AT SPECIFIED OVERALL CL

TOTAL LOADING AT CLsp = .4355

Mach number, M = .7200

Incidence (degrees) at specified CL = 2.5959

Lift coefficient of wing at specified incidence = .4355

Dimensionless spanwise position of half-wing centre of pressure from centre line: tip-up moment = .4274

Dimensionless distance of wing centre of pressure behind apex based on cbar = .6659

Spanwise position Eta	Local overall lift coefficient CLL.c/cbar	Local overall pitching moment CmL.c/cbar about local quarter chord
.0000	.5540	-.0940
.0500	.5529	-.0924
.1000	.5499	-.0896
.1500	.5453	-.0863
.2000	.5392	-.0831
.2500	.5318	-.0802
.3000	.5231	-.0774
.3500	.5130	-.0746
.4000	.5016	-.0718
.4500	.4888	-.0691
.5000	.4745	-.0662
.5500	.4585	-.0633
.6000	.4407	-.0602
.6500	.4208	-.0571
.7000	.3982	-.0536

```
        .7500                   .3723                   -.0499
        .8000                   .3420                   -.0457
        .8500                   .3053                   -.0408
        .9000                   .2580                   -.0347
        .9500                   .1907                   -.0261
        .9800                   .1250                   -.0176
        .9999                   .0116                   -.0017
-------------------------------------------------------------------------

***  RUN COMPLETED

END OF OUTPUT  ---------------------------------------------------------
```

APPENDIX B

MATLAB CODE TO EXECUTE A9510 PROGRAM

This portion of the tool creates ESDUpac A9510 input, executes A9510 program, and stores the necessary output.

```
% Write the run.bat batch file
inputFileName = 'ESDUi.txt';
outputFileName = 'ESDUo.txt';
fid = fopen('run.bat','w');
fprintf(fid, '%s\r\n', ['A9510V12 <', inputFileName, '>',
outputFileName]);
fprintf(fid, 'exit\r\n');
fclose(fid);

%Set the files to read and write
MainInputFileName = 'main_input.dat';
esduInputFileName = inputFileName;
esduOutputFileName = outputFileName;
ribLocations =
generate_esdu_input_file(MainInputFileName,esduInputFileName);

fid = fopen('run.bat','w');
fprintf(fid,['A9510V12 <' esduInputFileName '>'
esduOutputFileName]);
fprintf(fid,[13 10 'exit']);
fclose(fid);
currDir = cd;
dos(['"C:\Program Files (x86)\DOSBox-0.74\DOSBox.exe" ', currDir,
'\run.bat']);
% system('run_script.bat')

% Read the ESDU output and store the necessary data

data2FileName = MainInputFileName;%'main_input.dat';

% 1.1. Read the Mach number from the main input file
```

```
fid = fopen(data2FileName,'r');
while true
    tline = fgetl(fid);
    if isempty(strfind(tline, 'Value of Mach number'))
        % continue until the line is found
        continue
    else
        % line is found. read next line
        tline = fgetl(fid);
        % exit
        break
    end
end
machNumber = str2double(tline);
fclose(fid);
% Unit: mm//s
velocity = machNumber*340*1000;

locOfRibs = ribLocations;

% 1.3. Density of air
rho = 1.225e-09;

% 2. linked cells
% Read the coefficients at ESDU output
fid = fopen(outputFileName);
flag1 = false;
flag2 = false;
data = [];
while true
    tline = fgetl(fid);
    % check for the first flag
    if isempty(strfind(tline, 'Spanwise position       Local
overall lift      Local overall pitching'))
        % flag not read yet
    else
        flag1 = true;
        continue
    end
    % If the first flag is found, look for the second flag
    if flag1
        if all(tline=='-')
            flag2 = true;
            continue
        end
    end
    % start reading if flag2 is set
    if flag2
        % unset flag2 if all -'s
        if all(tline=='-')
            flag2 = false;
            % end of reading
            break
        end
```

```
        try
            data(end+1,:) = str2num(tline);
        catch
            break
        end
    end
end
spanWisePos = data(:,1);
localLiftCoeff = data(:,2);
localPitchingMoment = data(:,3);

fclose(fid);
% read the root chord from the main input
fid = fopen(data2FileName,'r');
while true
    tline = fgetl(fid);
    if isempty(strfind(tline, 'root chord length (RootChord)
[mm]'))
        % continue
        continue
    else
        % read the next line
        tline = fgetl(fid);
        % exit
        break
    end
end
rootChord = str2double(tline);
fclose(fid);


% read the tip chord from the main input
fid = fopen(data2FileName,'r');
while true
    tline = fgetl(fid);
    if isempty(strfind(tline, 'tip chord length (TipChord) [mm]'))
        % continue
        continue
    else
        % read the next line
        tline = fgetl(fid);
        % exit
        break
    end
end
tipChord = str2double(tline);
fclose(fid);

cbar = (rootChord + tipChord) / 2;
chord = (rootChord - tipChord) * (1-spanWisePos) + tipChord;
c_cbar = chord ./ cbar;

% read the half span from the main input
```

```
fid = fopen(data2FileName,'r');
while true
    tline = fgetl(fid);
    if isempty(strfind(tline, 'Wing Half Span (HalfSpan) [mm]'))
        % continue
        continue
    else
        % read the next line
        tline = fgetl(fid);
        % exit
        break
    end
end
halfSpan = str2double(tline);
fclose(fid);


cll                         = localLiftCoeff ./ c_cbar;
cmc                         = localPitchingMoment ./ c_cbar;
lift_unitSpan               = 1/2 * rho * velocity^2 * chord .*
cll;
pitchingMoment_unitSpan     = 1/2 * rho * velocity^2 * chord.^2 .*
cmc;
avgRunningLoad              = ...
    1/2 * (lift_unitSpan(1:end-1) + lift_unitSpan(2:end));
distanceBtwStations         = (spanWisePos(2:end) -
spanWisePos(1:end-1)) * ...
    halfSpan / 1000;
avgStripLoad                = avgRunningLoad .*
distanceBtwStations;
centroidOfTheTrapzLoad      = ...
    lift_unitSpan(2:end) .* distanceBtwStations ./ ...
    (lift_unitSpan(1:end-1)+lift_unitSpan(2:end));

% Last three columns
% Set the vectors
n = length(lift_unitSpan);
shearForce                  = zeros(n,1);
totalBendingMoment          = zeros(n,1);
totalPitchingMoment         = zeros(n,1);
% shear force at stations
for i = n-1:-1:1
    shearForce(i) = shearForce(i+1) + avgStripLoad(i);
end
% Bending Moment of the Shear Force [Nm]
bendingMoment = distanceBtwStations .* shearForce(2:end);
% Bending Moment of the Av Strip Force [Nm]
bendingMomentOfAvStripForce = avgStripLoad .*
centroidOfTheTrapzLoad;
% Total Bending Moment at Each Station [Nm]
for i = n-1:-1:1
    totalBendingMoment(i) = totalBendingMoment(i+1) + ...
         + bendingMoment(i)...
         + bendingMomentOfAvStripForce(i);
```

```
end
% Average Running Pitching Moment Load [N.mm/m]
avgRunningPitchingMoment = 1/2 * ...
    (pitchingMoment_unitSpan(1:end-1) +
pitchingMoment_unitSpan(2:end));
% Average Pitching Moment  load  in each section [Nm]
avgPitchingMoment = distanceBtwStations .*
avgRunningPitchingMoment / 1000;
% Total Pitching Moment at Each Station [Nm]
for i = n-1:-1:1
    totalPitchingMoment(i) = totalPitchingMoment(i+1) +
avgPitchingMoment(i);
end
```

Function that creates ESDUpac A9510 input text file:

```
function ribLocations =
generate_esdu_input_file(MainInputFileName,esduInputFileName)
% MainInputFileName = 'main_input.dat';

% Open the file to write.
fidW = fopen(esduInputFileName,'w');

% TEXT inputs for the first three lines
rows=textread(MainInputFileName,'%s','delimiter','\n');
text1=rows{2};
text2 = rows{3};
text3 = rows{4};
fprintf(fidW,[text1 ' \r\n']);
fprintf(fidW,[text2 ' \r\n']);
fprintf(fidW,[text3 ' \r\n']);

fprintf(fidW,'\r\n');

% NMs, NMc: 33 3/5
fprintf(fidW,'33 ');
ar = stringCellArray2Mat(getFieldValue(MainInputFileName,'Aspect
ratio of the wing'));
m = stringCellArray2Mat(getFieldValue(MainInputFileName,'Value of
Mach number'));
beta = sqrt(1-m^2);
if (beta * ar) > 2
    % if greater than 2, NMc should be increased to 5
    NMc = 5;
else
    NMc = 3;
end
fprintf(fidW,'%d\r\n',NMc);
fprintf(fidW,'\r\n');
```

```
% Restrictions check
% 1. 0<beta*ar<12
ar = stringCellArray2Mat(getFieldValue(MainInputFileName,'Aspect
ratio of the wing'));
m = stringCellArray2Mat(getFieldValue(MainInputFileName,'Value of
Mach number'));
beta = sqrt(1-m^2);
if ((beta*ar) < 0) || ((beta*ar) > 12)
    warndlg('Restriction 1 (0<beta*ar<12) failed.');
end

% 2. ar * tan(Lmid) <= 6
ar = stringCellArray2Mat(getFieldValue(MainInputFileName,'Aspect
ratio of the wing'));
Lmid = stringCellArray2Mat(getFieldValue(MainInputFileName,'Sweep
of the mid chord line'));
if (ar*tand(Lmid)) >6
    warndlg('Restriction 2 (ar * tan(Lmid) <= 6) failed.');
end

% 3. 0<=lambda<=1
lambda = stringCellArray2Mat(getFieldValue(MainInputFileName,'Taper
Ratio (Taper)'));
if (lambda<0 || lambda>1)
    warndlg('Restriction 3 (0 <= lambda <= 1) failed');
end

 % 4. -2*(1-lambda)/(1+lambda) <= ar*tand(Lmid)
 if (-2*(1-lambda)/(1+lambda) <= ar*tand(Lmid))
 else
     warndlg('Restriction 4 (-2*(1-lambda)/(1+lambda) <=
ar*tand(Lmid)) failed.');
 end

% 5. (180 / pi * atan((ar*tand(Lmid))/(beta*ar)) >= -20)
if (180 / pi * atan((ar*tand(Lmid))/(beta*ar)) >= -20)
else
    warndlg('Restriction 5 ((180 / pi *
atan((ar*tand(Lmid))/(beta*ar)) >= -20)) failed.');
end

% 6. (1/beta * tand(L0) < 4)
L0 = stringCellArray2Mat(getFieldValue(MainInputFileName,'Sweep of
0th chord line'));
if (1/beta * tand(L0) < 4)
else
    warndlg('Restriction 6 (1/beta * tand(L0) < 4) failed.');
end

% NL: 2
fprintf(fidW,'2\r\n');
fprintf(fidW,'\r\n');

% Lm: 1   3
```

```
fprintf(fidW,'1 3\r\n');
fprintf(fidW,'\r\n');

% NM: 1 (number of Mach numbers)
fprintf(fidW,'1\r\n');
% fprintf(fidW,'\r\n');

% Ml: 0.XXXX (values of Mach numbers- if more than one written side
by side)
valStr = getFieldValue(MainInputFileName,'Value of Mach number');
fprintf(fidW,[valStr{1} '\r\n']);
fprintf(fidW,'\r\n');

% number of spanwise stations (No: 13 (number of spanwise stations-
less than equal to 40))
valStr = getFieldValue(MainInputFileName,'Number of Ribs
(NumOfRibs)');
% fprintf(fidW,[valStr{1} '\r\n']);

% dimensionless values of spanwise stations for output; leave one
or more space between the numbers
valStr = getFieldValue(MainInputFileName,'Location of Ribs from
Root (LocOfRibs) (% half span)');
ribLocs = zeros(1,length(valStr));
for i = 1:length(ribLocs)
    ribLocs(i) = str2double(valStr{i});
end
ribLocsStr = [];
% ribLocs are the percetange locations read from airfoil file
ribLocs = union(ribLocs, [0:5:100, 98]);
% loc %100 will be replaced by 0.9999
for i = 1:length(ribLocs)
    if ribLocs(i) == 100
        ribLocsStr = [ribLocsStr, '0.9999'];
    else
        ribLocsStr = [ribLocsStr, num2str(ribLocs(i)/100) ' '];
    end
end
ribLocations = str2num(ribLocsStr);
fprintf(fidW,[num2str(length(ribLocations)) '\r\n']); % number of
rib locations
fprintf(fidW,[ribLocsStr  '\r\n']);
fprintf(fidW,'\r\n');

% P, calculation mode
fprintf(fidW,'2\r\n');
fprintf(fidW,'1\r\n');

% Specified CL
valStr = getFieldValue(MainInputFileName,'Specified CL');
fprintf(fidW,[valStr{1} '\r\n']);

% Nk: 0 (number of cranks in the wing is given, 0 in this example.
0 implies straight tapred wing)
```

```
fprintf(fidW,'0\r\n');

% A: X.XX ( aspect ratio of the wing)
valStr = getFieldValue(MainInputFileName,'Aspect ratio of the
wing');
fprintf(fidW,[valStr{1} '\r\n']);

% lambda (taper ratio of the wing; 1 for rectangular wing)
valStr = getFieldValue(MainInputFileName,'Taper Ratio (Taper)');
fprintf(fidW,[valStr{1} '\r\n']);

% Sweep of 0th chord line
valStr = getFieldValue(MainInputFileName,'Sweep of 0th chord
line');
fprintf(fidW,[valStr{1} '\r\n']);

% n: 0 (chord line identifier- Sketch 3.1 on page 6)
fprintf(fidW,'0\r\n');
fprintf(fidW,'\r\n');

% NsC: 2
fprintf(fidW,'2\r\n');
fprintf(fidW,'\r\n');

% find the number of stations
upperAirfoilData =
stringCellArray2Mat(getFieldValue(MainInputFileName, 'Upper Airfoil
Data (UpAFData)'));
% lowerAirfoilData =
stringCellArray2Mat(getFieldValue(MainInputFileName, 'Lower Airfoil
Data (LoAFData)'));
nStationLocs = length(upperAirfoilData);
mcCell = getFieldValue(MainInputFileName, 'Max Camber, MC (%)');
mc = str2double(mcCell{1})/100;
mcpCell = getFieldValue(MainInputFileName, 'Max Camber Position,
MCP (%)');
mcp = str2double(mcpCell{1})/100;

% calculate camber y coords
% upper and lower airfoil x coords are assumed to be equal
camberY = zeros(nStationLocs,1);
for i = 1:nStationLocs
    x = upperAirfoilData(i,1);
    if (x>=0 && x<mcp)
        y = mc / (mcp^2) * (2*mcp*x-x^2);
    elseif (x>=mcp && x<=1)
        y = (mc / (1-mcp)^2) * (1-2*mcp+2*mcp*x-x^2);
    else
        error('Undefined xposition');
    end
    camberY(i) = y;
end
```

```
% write
for i = 0:1
    % dimensionless value of spanwise stations for camber input
from tip to root; 1 is the wing tip
    fprintf(fidW,[num2str(i) '\r\n']);
    % number of chordwise stations for camber input
    fprintf(fidW,'%d \r\n', nStationLocs);
    for j = 1:nStationLocs
        x = upperAirfoilData(j,1);
        y = camberY(j);
        fprintf(fidW,'%f %f\r\n',x,y);
    end
    fprintf(fidW,'\r\n');
end

fclose(fidW);
end

function ret = getFieldValue(fileName,fieldName)
fid = fopen(fileName,'r');
ret = {};
tline = fgetl(fid);
while ~isequal(tline,-1)
    if strcmp(tline,fieldName)
        tline = fgetl(fid);
        while ~(isempty(tline) || isequal(tline,-1))
            ret{end+1} = tline;
            tline = fgetl(fid);
        end
        fclose(fid);
        return
    end
    tline = fgetl(fid);
end

fclose(fid);
error('cannot find field named %s in %s',fieldName,fileName)
end

function ret = stringCellArray2Mat(inp)
ret = [];
for i = 1:length(inp)
    ret(end+1,:) = str2num(inp{i});
end
end
```

APPENDIX C

DATA FILE FOR BUCKLING COEFFICIENT CURVES

First 80 entries of 500+ data points for the compressive buckling coefficient (both loaded and unloaded edges simply supported):

```
a/b      kc
0.474248 7.12439
0.474287 7.13545
0.479155 7.00262
0.479231 7.02475
0.479347 7.05793
0.483908 6.8366
0.484023 6.86979
0.4841 6.89191
0.484176 6.91404
0.484253 6.93616
0.48433 6.95829
0.484714 7.06891
0.484752 7.07997
0.48916 6.81439
0.494297 6.75899
0.494412 6.79218
0.499242 6.64829
0.49928 6.65935
0.499318 6.67041
0.499395 6.69253
0.49951 6.72572
0.504378 6.59289
0.509554 6.54855
0.509707 6.5928
0.514768 6.51528
0.514883 6.54847
0.51496 6.57059
0.52508 6.41555
0.525272 6.47086
0.530217 6.36015
0.535392 6.31582
0.540376 6.21617
0.540414 6.22724
0.540683 6.30467
0.545512 6.16078
0.550649 6.10538
0.550688 6.11644
0.550765 6.13857
0.555825 6.06105
```

```
0.561039 6.02777
0.566252 5.9945
0.566329 6.01663
0.57112 5.86167
0.571159 5.87273
0.571428 5.95017
0.576411 5.85052
0.576526 5.88371
0.586493 5.68442
0.586608 5.7176
0.586646 5.72867
0.586762 5.76185
0.586762 5.76185
0.5868 5.77292
0.597074 5.66212
0.602057 5.56248
0.602173 5.59566
0.602249 5.61779
0.617699 5.46266
0.617814 5.49585
0.617852 5.50691
0.622951 5.44045
0.628241 5.4293
0.633263 5.34072
0.63334 5.36284
0.643883 5.32949
0.648712 5.18559
0.648828 5.21878
0.648904 5.2409
0.648981 5.26303
0.649058 5.28515
0.649135 5.30728
0.654118 5.20763
0.659293 5.1633
0.664469 5.11896
0.664546 5.14109
0.669683 5.08569
0.674973 5.07454
0.685324 4.98587
0.685401 5.008
0.701004 4.89712
```

APPENDIX D

THE MAIN INPUT FILES SENT TO THE TOOL

Entire input file of the subsonic turboprop trainer examined in Section 4.1 is provided below.

```
Definition of the study (Three Lines)
TEXT1 Wing Preliminary Design Study
TEXT2 PC-21 Aircraft Wing Planform
TEXT3 TUCANO Layout, NACA Airfoil

Upper Airfoil Data (UpAFData)
0      0
0.0125 0.0215
0.025  0.0299
0.05   0.0413
0.075  0.0496
0.1    0.0563
0.15   0.0661
0.2    0.0726
0.25   0.0767
0.3    0.0788
0.4    0.078
0.5    0.0724
0.6    0.0636
0.7    0.0518
0.8    0.0375
0.9    0.0208
0.95   0.0114
1      0.0013

Lower Airfoil Data (LoAFData)
0      0
0.0125 -0.0165
0.025  -0.0227
0.05   -0.0301
0.075  -0.0346
0.1    -0.0375
0.15   -0.041
0.2    -0.0423
0.25   -0.0422
0.3    -0.0412
```

```
0.4    -0.038
0.5    -0.0334
0.6    -0.0276
0.7    -0.0214
0.8    -0.015
0.9    -0.0082
0.95   -0.0048
1      -0.0013

Root chord length (RootChord) [mm]
2258

Tip chord length (TipChord) [mm]
1085

Taper Ratio (Taper)
0.48

Wing Half Span (HalfSpan) [mm]
4555

Number of Spars (NumOfSpars)
3

Locations of Spars from L.E. (LocOfSpars) (% chord)
10
40
75

Number of Upper Stringers (NumOfUpStr)
6

Location of Upper Stringers from L.E. (LocOfUpStr) (% chord)
20
30
47
54
61
68

Number of Lower Stringers (NumOfLoStr)
5

Location of Lower Stringers from L.E. (LocOfLoStr) (% chord)
20
30
49
58
67

Number of Ribs (NumOfRibs)
17

Location of Ribs from Root (LocOfRibs) (% half span)
0
5
10
15
20
25
30
```

```
35
40
47
54
61
68
75
83
91
100

Load Factor (LoadFactor) (g)
8.0

A/C Weight (ACweight) [kg]
3100.0

Value of Mach number
0.72

Upper Skin Material
2024 T851

Upper Skin Ftu [MPa]
486.8

Upper Skin Fcy [MPa]
399.9

Upper Skin E [MPa]
72397

Upper Skin v
0.33

Upper Skin Density [kg/mm3]
2767.99e-9

Lower Skin Material
7475 T7651

Lower Skin Ftu [MPa]
482.6

Lower Skin Fcy [MPa]
413.7

Lower Skin E [MPa]
70329

Lower Skin v
0.33

Lower Skin Density [kg/mm3]
2795.67e-9

Spar Material
7050 T7451

Spar Ftu [MPa]
510.2
```

```
Spar Fcy [MPa]
434.3

Spar E [MPa]
71018

Spar v
0.33

Spar Density [kg/mm3]
2823.35e-9

Stringer Material
7050 T7451

Stringer Ftu [MPa]
510.2

Stringer Fcy [MPa]
434.3

Stringer E [MPa]
71018

Stringer v
0.33

Stringer Density [kg/mm3]
2823.35e-9

Rib Material
7050 T7451

Rib Ftu [MPa]
510.2

Rib Fcy [MPa]
434.3

Rib E [MPa]
71018

Rib v
0.33

Rib Density [kg/mm3]
2823.35e-9

Initial Buckling Stage (for Subsonic Wings) [%]
100


REST OF THE INPUT FILE IS FOR SUBSONIC VEHICLES ONLY (ESDU Inputs)

Wing Area (m2)
15.22

Aspect ratio of the wing
5.45
```

```
Sweep of 0th chord line
12

Sweep of the mid chord line
5

Max Camber, MC (%)
2

Max Camber Position, MCP (%)
40
```

Entire input file of the supersonic fighter examined in Section 4.3 is provided below.

```
Definition of the study (Three Lines)
TEXT1 Wing Preliminary Design Study
TEXT2 Eurofighter Wing Planform
TEXT3 Airfoil NACA 64-206

Upper Airfoil Data (UpAFData)
0.00000      0.00000
0.00459      0.00542
0.00704      0.00664
0.01198      0.00859
0.02440      0.01208
0.04934      0.01719
0.07432      0.02115
0.09933      0.02444
0.14937      0.02970
0.19943      0.03367
0.24952      0.03667
0.29961      0.03879
0.34971      0.04011
0.39981      0.04066
0.44991      0.04014
0.50000      0.03878
0.55008      0.03670
0.60015      0.03402
0.65020      0.03080
0.70023      0.02712
0.75025      0.02307
0.80024      0.01868
0.85020      0.01410
0.90015      0.00940
0.95007      0.00473
1.00000      0.00000

Lower Airfoil Data (LoAFData)
0.00000     0.00000
0.00541     -0.00442
0.00796     -0.00524
0.01302     -0.00645
0.02560     -0.00836
0.05066     -0.01087
0.07568     -0.01267
0.10067     -0.01410
0.15063     -0.01624
0.20057     -0.01775
```

```
0.25048     -0.01877
0.30039     -0.01935
0.35029     -0.01951
0.40019     -0.01924
0.45009     -0.01824
0.50000     -0.01672
0.54992     -0.01480
0.59985     -0.01260
0.64980     -0.01020
0.69977     -0.00768
0.74975     -0.00517
0.79976     -0.00276
0.84980     -0.00064
0.89985     0.00094
0.94993     0.00159
1.00000     0.00000

Root chord length (RootChord) [mm]
7200

Tip chord length (TipChord) [mm]
1200

Taper Ratio (Taper)
0.1667

Wing Half Span (HalfSpan) [mm]
5475

Number of Spars (NumOfSpars)
15

Locations of Spars from L.E. (LocOfSpars) (% chord)
12
17
22
27
32
37
42
47
52
57
62
67
72
77
82

Number of Upper Stringers (NumOfUpStr)
0

Location of Upper Stringers from L.E. (LocOfUpStr) (% chord)


Number of Lower Stringers (NumOfLoStr)
0

Location of Lower Stringers from L.E. (LocOfLoStr) (% chord)
```

```
Number of Ribs (NumOfRibs)
7

Location of Ribs from Root (LocOfRibs) (% half span)
0
10
20
35
60
80
100

Load Factor (LoadFactor) (g)
9.0

A/C Weight (ACweight) [kg]
16000.0

Value of Mach number
2.0

Upper Skin Material
2024 T851

Upper Skin Ftu [MPa]
486.8

Upper Skin Fcy [MPa]
399.9

Upper Skin E [MPa]
72397

Upper Skin v
0.33

Upper Skin Density [kg/mm3]
2767.99e-9

Lower Skin Material
7475 T7651

Lower Skin Ftu [MPa]
482.6

Lower Skin Fcy [MPa]
413.7

Lower Skin E [MPa]
70329

Lower Skin v
0.33

Lower Skin Density [kg/mm3]
2795.67e-9

Spar Material
7050 T7451

Spar Ftu [MPa]
```

```
510.2

Spar Fcy [MPa]
434.3

Spar E [MPa]
71018

Spar v
0.33

Spar Density [kg/mm3]
2823.35e-9

Stringer Material


Stringer Ftu [MPa]


Stringer Fcy [MPa]


Stringer E [MPa]


Stringer v


Stringer Density [kg/mm3]
0

Rib Material
7050 T7451

Rib Ftu [MPa]
510.2

Rib Fcy [MPa]
434.3

Rib E [MPa]
71018

Rib v
0.33

Rib Density [kg/mm3]
2823.35e-9

Initial Buckling Stage (for Subsonic Wings) [%]
100


REST OF THE INPUT FILE IS FOR SUBSONIC VEHICLES ONLY (ESDU Inputs)

Wing Area (m2)


Aspect ratio of the wing
```

```
Sweep of 0th chord line

Sweep of the mid chord line

Max Camber, MC (%)

Max Camber Position, MCP (%)
```

APPENDIX E

OPTIMIZATION STEPS OF THE *fminsearch* FUNCTION

Entire output of the *fminsearch* function for the example of Section 4.2 is provided.

```
weight: 143.54, exp1: 0.5, exp2: 0.5, 7.14484

 Iteration   Func-count     min f(x)         Procedure
     0           1           143.54
weight: 139.656, exp1: 0.525, exp2: 0.5, 6.62819
weight: 144.999, exp1: 0.5, exp2: 0.525, 5.99856
     1           3           139.656         initial simplex
weight: 138.232, exp1: 0.525, exp2: 0.475, 6.07127
weight: 135.376, exp1: 0.5375, exp2: 0.45, 5.85297
     2           5           135.376         expand
weight: 132.307, exp1: 0.5625, exp2: 0.45, 5.73117
weight: 133.434, exp1: 0.59375, exp2: 0.425, 5.81319
     3           7           132.307         reflect
weight: 137.358, exp1: 0.575, exp2: 0.4, 5.81463
weight: 131.998, exp1: 0.5625, exp2: 0.425, 5.81182
     4           9           131.998         contract outside
weight: 133.233, exp1: 0.5875, exp2: 0.425, 5.83054
weight: 131.536, exp1: 0.575, exp2: 0.43125, 5.86924
     5           11          131.536         contract outside
weight: 136.047, exp1: 0.575, exp2: 0.40625, 6.12236
weight: 131.509, exp1: 0.565625, exp2: 0.439062, 5.85842
     6           13          131.509         contract inside
weight: 130.367, exp1: 0.578125, exp2: 0.445312, 5.73063
weight: 129.865, exp1: 0.585938, exp2: 0.455469, 5.71613
     7           15          129.865         expand
weight: 131.19, exp1: 0.576562, exp2: 0.463281, 5.79299
     8           16          129.865         reflect
weight: 129.652, exp1: 0.596875, exp2: 0.479687, 5.66358
weight: 128.9, exp1: 0.6125, exp2: 0.5, 5.59794
     9           18            128.9         expand
weight: 127.608, exp1: 0.621875, exp2: 0.492187, 5.59788
weight: 125.989, exp1: 0.644531, exp2: 0.506641, 5.5198
    10           20          125.989         expand
weight: 125.304, exp1: 0.671094, exp2: 0.551172, 5.38095
weight: 123.43, exp1: 0.713672, exp2: 0.599023, 5.20724
    11           22           123.43         expand
weight: 121.293, exp1: 0.745703, exp2: 0.605664, 5.10817
weight: 118.691, exp1: 0.812305, exp2: 0.658496, 5.10955
```

```
    12           24          118.691         expand
weight: 117.884, exp1: 0.881445, exp2: 0.750879, 4.74343
weight: 116.86, exp1: 0.999902, exp2: 0.872998, 4.48957
    13           26           116.86         expand
weight: 116.576, exp1: 1.09854, exp2: 0.932471, 4.437
weight: 122.858, exp1: 1.29097, exp2: 1.09919, 4.18932
    14           28          116.576         reflect
weight: 124.601, exp1: 1.28613, exp2: 1.14697, 4.20722
weight: 116.635, exp1: 0.930762, exp2: 0.780615, 4.6487
    15           30          116.576         contract inside
weight: 114.964, exp1: 1.02939, exp2: 0.840088, 4.46473
weight: 114.045, exp1: 1.04414, exp2: 0.823633, 4.42585
    16           32          114.045         expand
weight: 117.322, exp1: 1.21191, exp2: 0.975488, 4.30174
weight: 115.518, exp1: 1.00105, exp2: 0.829333, 4.54586
    17           34          114.045         contract inside
weight: 114.175, exp1: 0.946655, exp2: 0.720496, 4.65677
    18           35          114.045         reflect
weight: 116.008, exp1: 0.989746, exp2: 0.714795, 4.58784
weight: 114.643, exp1: 0.998224, exp2: 0.800699, 4.51959
    19           37          114.045         contract inside
weight: 114.12, exp1: 0.992572, exp2: 0.74343, 4.57361
    20           38          114.045         reflect
weight: 113.84, exp1: 1.09006, exp2: 0.846567, 4.40109
weight: 115.366, exp1: 1.16176, exp2: 0.909602, 4.26534
    21           40           113.84         reflect
weight: 115.988, exp1: 1.14163, exp2: 0.92677, 4.30936
weight: 113.387, exp1: 1.02984, exp2: 0.789265, 4.45733
    22           42          113.387         contract inside
weight: 113.443, exp1: 1.07575, exp2: 0.812199, 4.36881
    23           43          113.387         reflect
weight: 114.165, exp1: 1.01553, exp2: 0.754897, 4.51554
weight: 113.602, exp1: 1.07143, exp2: 0.823649, 4.5375
    24           45          113.387         contract inside
weight: 113.521, exp1: 1.03416, exp2: 0.777814, 4.46241
weight: 113.355, exp1: 1.04348, exp2: 0.789273, 4.48985
    25           47          113.355         contract outside
weight: 113.642, exp1: 0.997561, exp2: 0.766339, 4.42355
weight: 113.184, exp1: 1.0562, exp2: 0.800734, 4.29047
    26           49          113.184         contract inside
weight: 113.569, exp1: 1.06985, exp2: 0.800742, 4.25109
weight: 113.202, exp1: 1.03984, exp2: 0.792134, 4.33372
    27           51          113.184         contract inside
weight: 113.211, exp1: 1.05256, exp2: 0.803595, 4.27165
weight: 113.218, exp1: 1.05029, exp2: 0.800014, 4.33144
weight: 113.177, exp1: 1.04802, exp2: 0.796434, 4.32832
weight: 113.211, exp1: 1.04984, exp2: 0.795003, 4.30527
    28           55          113.177         shrink
weight: 113.151, exp1: 1.05438, exp2: 0.802164, 4.2791
weight: 113.243, exp1: 1.05666, exp2: 0.805745, 4.28967
    29           57          113.151         reflect
weight: 113.144, exp1: 1.0462, exp2: 0.797864, 4.31669
weight: 113.301, exp1: 1.0412, exp2: 0.79643, 4.33636
    30           59          113.144         reflect
weight: 113.211, exp1: 1.05256, exp2: 0.803595, 4.38342
weight: 113.204, exp1: 1.04916, exp2: 0.798224, 4.31543
weight: 113.218, exp1: 1.05029, exp2: 0.800014, 4.27041
weight: 113.16, exp1: 1.04711, exp2: 0.797149, 4.28558
    31           63          113.144         shrink
weight: 113.241, exp1: 1.04302, exp2: 0.794999, 4.3324
weight: 113.192, exp1: 1.04847, exp2: 0.798761, 4.31652
```

```
    32           65          113.144         contract inside
weight: 113.195, exp1: 1.04484, exp2: 0.796253, 4.36143
weight: 113.197, exp1: 1.04757, exp2: 0.798134, 4.28849
weight: 113.152, exp1: 1.04666, exp2: 0.797507, 4.29193
weight: 113.193, exp1: 1.04734, exp2: 0.798312, 4.32131
    33           69          113.144         shrink
weight: 113.23, exp1: 1.04552, exp2: 0.797059, 4.39423
weight: 113.192, exp1: 1.04688, exp2: 0.797999, 4.45605
    34           71          113.144         contract inside
weight: 113.216, exp1: 1.04597, exp2: 0.797372, 4.4602
weight: 113.17, exp1: 1.04666, exp2: 0.797842, 4.32767
    35           73          113.144         contract inside
weight: 113.126, exp1: 1.0462, exp2: 0.797529, 4.48909
weight: 113.216, exp1: 1.04597, exp2: 0.797372, 4.54096
    36           75          113.126         reflect
weight: 113.23, exp1: 1.04575, exp2: 0.797886, 4.44861
weight: 113.143, exp1: 1.04643, exp2: 0.797602, 4.50084
    37           77          113.126         contract inside
weight: 113.125, exp1: 1.04643, exp2: 0.797266, 4.56918
weight: 113.116, exp1: 1.04654, exp2: 0.796967, 4.40911
    38           79          113.116         expand
weight: 113.167, exp1: 1.04632, exp2: 0.796894, 4.39654
weight: 113.132, exp1: 1.0464, exp2: 0.797425, 4.47039
    39           81          113.116         contract inside
weight: 113.11, exp1: 1.04634, exp2: 0.797071, 4.41233
weight: 113.167, exp1: 1.04632, exp2: 0.796894, 4.4795
    40           83           113.11         reflect
weight: 113.1, exp1: 1.04669, exp2: 0.796509, 4.50518
weight: 113.088, exp1: 1.04693, exp2: 0.795999, 4.35339
    41           85          113.088         expand
weight: 113.081, exp1: 1.04673, exp2: 0.796103, 4.36562
weight: 113.064, exp1: 1.04682, exp2: 0.795672, 4.39133
    42           87          113.064         expand
weight: 113.154, exp1: 1.0474, exp2: 0.7946, 4.31669
weight: 113.093, exp1: 1.04661, exp2: 0.796453, 4.41238
    43           89          113.064         contract inside
weight: 113.059, exp1: 1.04714, exp2: 0.795218, 4.39583
weight: 113.154, exp1: 1.0474, exp2: 0.7946, 4.4079
    44           91          113.059         reflect
weight: 113.147, exp1: 1.04703, exp2: 0.79489, 4.33489
weight: 113.074, exp1: 1.04695, exp2: 0.795722, 4.39419
    45           93          113.059         contract inside
weight: 113.048, exp1: 1.04701, exp2: 0.795167, 4.42323
weight: 113.147, exp1: 1.04703, exp2: 0.79489, 4.36654
    46           95          113.048         reflect
weight: 113.155, exp1: 1.04732, exp2: 0.794714, 4.34924
weight: 113.059, exp1: 1.04695, exp2: 0.795432, 4.55022
    47           97          113.048         contract inside
weight: 113.048, exp1: 1.04681, exp2: 0.795382, 4.27154
weight: 113.11, exp1: 1.04665, exp2: 0.795464, 4.491
    48           99          113.048         reflect
weight: 113.105, exp1: 1.04687, exp2: 0.795117, 4.53755
weight: 113.053, exp1: 1.04693, exp2: 0.795353, 4.53927
    49          101          113.048         contract inside
weight: 113.043, exp1: 1.04689, exp2: 0.795196, 4.37577
weight: 113.105, exp1: 1.04687, exp2: 0.795117, 4.39959
    50          103          113.043         reflect
weight: 113.11, exp1: 1.0467, exp2: 0.79541, 4.49286
weight: 113.047, exp1: 1.04693, exp2: 0.795228, 4.34208
    51          105          113.043         contract inside
weight: 113.041, exp1: 1.04701, exp2: 0.795042, 4.38015
```

```
weight: 113.15, exp1: 1.0471, exp2: 0.794872, 4.42451
    52          107          113.041         reflect
weight: 113.037, exp1: 1.04697, exp2: 0.79501, 4.49946
weight: 113.145, exp1: 1.04699, exp2: 0.794901, 4.29375
    53          109          113.037         reflect
weight: 113.148, exp1: 1.04709, exp2: 0.794856, 4.39306
weight: 113.041, exp1: 1.04694, exp2: 0.795111, 4.30663
    54          111          113.037         contract inside
weight: 113.037, exp1: 1.0469, exp2: 0.795079, 4.378
weight: 113.103, exp1: 1.04685, exp2: 0.795097, 4.28631
    55          113          113.037         reflect
weight: 113.033, exp1: 1.04693, exp2: 0.794978, 4.36523
weight: 113.142, exp1: 1.04693, exp2: 0.794911, 4.33073
    56          115          113.033         reflect
weight: 113.101, exp1: 1.04686, exp2: 0.795046, 4.28486
weight: 113.036, exp1: 1.04694, exp2: 0.795019, 4.30024
    57          117          113.033         contract inside
weight: 113.077, exp1: 1.04697, exp2: 0.794918, 4.3637
weight: 113.036, exp1: 1.04692, exp2: 0.795038, 4.33212
    58          119          113.033         contract inside
weight: 113.101, exp1: 1.04691, exp2: 0.794997, 4.31043
weight: 113.035, exp1: 1.04693, exp2: 0.795013, 4.3117
    59          121          113.033         contract inside
weight: 113.077, exp1: 1.04695, exp2: 0.794953, 4.32365
weight: 113.035, exp1: 1.04693, exp2: 0.795017, 4.28357
    60          123          113.033         contract inside
weight: 113.033, exp1: 1.04692, exp2: 0.794981, 4.31544
weight: 113.144, exp1: 1.04692, exp2: 0.794965, 4.26837
    61          125          113.033         reflect
weight: 113.076, exp1: 1.04693, exp2: 0.794942, 4.37953
weight: 113.034, exp1: 1.04693, exp2: 0.794998, 4.28095
    62          127          113.033         contract inside
weight: 113.077, exp1: 1.04693, exp2: 0.79496, 4.28712
weight: 113.034, exp1: 1.04693, exp2: 0.794989, 4.29997
    63          129          113.033         contract inside
weight: 113.077, exp1: 1.04693, exp2: 0.79497, 4.32087
weight: 113.033, exp1: 1.04693, exp2: 0.794984, 4.33933
    64          131          113.033         contract inside
weight: 113.077, exp1: 1.04693, exp2: 0.794975, 4.36904
weight: 113.033, exp1: 1.04693, exp2: 0.794982, 4.31193
    65          133          113.033         contract inside
weight: 113.033, exp1: 1.04692, exp2: 0.794985, 4.25505
weight: 113.033, exp1: 1.04691, exp2: 0.794989, 4.35647
    66          135          113.033         expand
weight: 113.1, exp1: 1.04691, exp2: 0.794988, 4.35573
weight: 113.033, exp1: 1.04692, exp2: 0.794983, 4.27659
    67          137          113.033         contract inside
weight: 113.033, exp1: 1.04691, exp2: 0.794987, 4.3596
weight: 113.1, exp1: 1.04691, exp2: 0.794988, 4.3552
    68          139          113.033         reflect
weight: 113.1, exp1: 1.0469, exp2: 0.794995, 4.30123
weight: 113.033, exp1: 1.04692, exp2: 0.794984, 4.32063
    69          141          113.033         contract inside
weight: 113.101, exp1: 1.04691, exp2: 0.794991, 4.30795
weight: 113.033, exp1: 1.04692, exp2: 0.794986, 4.35024
    70          143          113.033         contract inside
weight: 113.101, exp1: 1.04691, exp2: 0.794989, 4.34119
weight: 113.033, exp1: 1.04692, exp2: 0.794987, 4.29707
    71          145          113.033         contract inside

Optimization terminated:
```

```
 the current x satisfies the termination criteria using OPTIONS.TolX of
1.000000e-04
 and F(X) satisfies the convergence criteria using OPTIONS.TolFun of
1.000000e-04

K>>
```